Asadollah Kariman

Electrochemical wastewater treatment at nanostructured anodes

Doctoral thesis

For the degree of Doctor of Philosophy

Christchurch, August 2019

University of Canterbury

Department of Chemical and Process Engineering

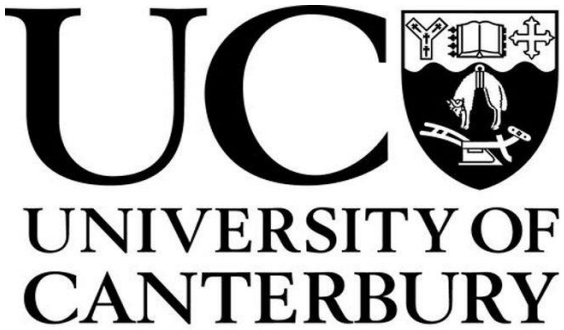

Acknowledgments

It is a pleasure to thank those who made this thesis possible, First and foremost, my supervisor Dr Aaron Marshall for his generous support, invaluable guidance and constant availability throughout this project. Aaron's advice and encouragement helped me to be an independent researcher in the best possible way.

The CAPE staff who supported me through their advice and technical skills, specially Stephen Beuzenberg, Graham Furniss, Tim Moore, Michael Sandridge and Glenn Wilson, Rayleen Fredericks, Graham Mitchell and Leigh Richardson. I would like to thank Ranee Hearst and Joanne Pollard for helping me with the all paperwork.

To technical staff outside CAPE, specially Mike Flaws and Shaun Mucalo at Mechanical Engineering, for helping with SEM/EDX imaging and analysis. Matthew Polson at Chemistry for his help with XRD.

To my officemate for engaging discussions over tea, especially Dr Jared Steven, late Dr Calvin and Navid. To all my friend who their company made this journey easy and fruitful, especially Ali , Marzieh and Ali Sepidan.

Finally, I would like to thank my parents and my siblings, who gave considerable support and love during my years of study.

Thanks,

Asadollah Kariman

Abstract

Water pollution is one of the greatest challenges of the twenty-first century; therefore, there has been a high demand to find a suitable eco-friendly technology to treat wastewater. Advanced oxidation processes (AOPs) are an effective solution for treating various organic pollutants. Among AOPs, electrochemical oxidation is a promising way to treat a wide range of organic compounds with high chemical toxicity and non-biodegradability.

The main objectives of this thesis work were: 1) to understand the mechanism of electrochemical organic oxidation, 2) to investigate the possibility of anode properties improvement for the organic oxidation by addition of nanoparticles into the oxide layer of anode, 3) to study the effect of pulsed and constant electrolysis on the current efficiency of the organic oxidation using numerical simulation.

The IrO_2-Sb_2O_5-SnO_2/Ti anode was prepared via standard thermal decomposition method and 4-nitrophenol (4-NP) chosen as the model organic compound. It is confirmed that this anode does follow the “active” anode mechanism, with the rate of 4-NP oxidation being dependent on the coverage adsorbed oxygen on the surface of the anode. This surface coverage is estimated by fitting steady-state polarisation curves with a micro-kinetic model describing the oxygen evolution behaviour of the anode. The rate of oxidation is dependent on the surface coverage at relatively low overpotentials where mass transport limitation is avoided, and this rate is controlled by mass transport of 4-NP to the anode surface at high overpotential. It is also shown that the assumption in the literature that the rate of organic oxidation is much larger than the oxygen evolution reaction is not valid at all the times provided that mass transfer does not limit the process.

The incorporation of nanoparticles into a thermally prepared IrO_2 anode as a way of improving its service lifetime was investigated. The results show that incorporation of up to 25 wt% antinomy-doped tin oxide nanoparticles into the coating formed crack-free structure during the thermal decomposition process and thus enhanced the service lifetime of modified electrode dramatically by up to 10x compared to the pure IrO_2 anode. Importantly, these nanoparticle additions have minimal effect on the performance of the anode towards the oxygen evolution reaction. It is proposed that adding the right quantity of nanoparticles into the IrO_2 layer improved the anodes lifetime by minimising electrolyte penetration to the substrate while increasing the mechanical strength of the layer.

The incorporation effect of antimony-doped tin oxide (ATO) nanoparticles on DSA electrode and oxidation pathway of 4-NP was investigated. Due to high energy consumption of “non-active” anode such as BDD, combinition of anode material with high activity towards organic oxidation and low activity towards OER at low potentials is chosen. The result indicates that an increase in nanoparticles weight percentage leads to increase in the electrochemical active surface area (EASA), in which anode with 5 wt% ATO nanoparticles has the highest electrochemical active surface area. The complete oxidation of intermediate and products occurs at anodes with the incorporation of ATO nanoparticles, while partial oxidisation of 4-NP occurs at pure IrO_2 anode with high accumulation of 2-hydroxy-benzoquinone (HBQ).

The electrochemical oxidation of organic species using pulsed and constant potential electrolysis is investigated through numerical simulations on “non-active” anode. By comparing the pulsed potential organic oxidation with constant potential organic oxidation over a range of electrolysis, it can be concluded that the current efficiency of pulse potential organic oxidation is improved over a range of potentials compare to constant potential electrolysis. Both models validated by comparing the simulation against the experimental data recorded at the pulsed and constant potential at BDD electrode.

UNIVERSITY OF CANTERBURY
Te Whare Wānanga o Waitaha
CHRISTCHURCH NEW ZEALAND

Deputy Vice-Chancellor's Office
Postgraduate Research Office

Co-Authorship Form

This form is to accompany the submission of any thesis that contains research reported in co-authored work that has been published, accepted for publication, or submitted for publication. A copy of this form should be included for each co-authored work that is included in the thesis. Completed forms should be included at the front (after the thesis abstract) of each copy of the thesis submitted for examination and library deposit.

Please indicate the chapter/section/pages of this thesis that are extracted from co-authored work and provide details of the publication or submission from the extract comes:

Chapter 3

Kariman, Asadollah, and Aaron T. Marshall. "Investigating the Kinetics and Mechanism of Organic Oxidation in Parallel with the Oxygen Evolution Reaction." Electrocatalysis 9.1 (2018): 31-39.

Please detail the nature and extent (%) of contribution by the candidate:
Asad:60%
Aaron:40%

Certification by Co-authors:
If there is more than one co-author then a single co-author can sign on behalf of all

The undersigned certifies that:

- The above statement correctly reflects the nature and extent of the PhD candidate's contribution to this co-authored work
- In cases where the candidate was the lead author of the co-authored work he or she wrote the text

Name: *Aaron Marshall* Signature:  Date: *16/8/2019*

UNIVERSITY OF CANTERBURY
Te Whare Wānanga o Waitaha
CHRISTCHURCH NEW ZEALAND

Deputy Vice-Chancellor's Office
Postgraduate Research Office

Co-Authorship Form

This form is to accompany the submission of any thesis that contains research reported in co-authored work that has been published, accepted for publication, or submitted for publication. A copy of this form should be included for each co-authored work that is included in the thesis. Completed forms should be included at the front (after the thesis abstract) of each copy of the thesis submitted for examination and library deposit.

Please indicate the chapter/section/pages of this thesis that are extracted from co-authored work and provide details of the publication or submission from the extract comes:

Chapter 4

Kariman, Asadollah, and Aaron T. Marshall. "Improving the Stability of DSA Electrodes by the Addition of TiO_2 Nanoparticles." Journal of The Electrochemical Society 166.8 (2019): E248-E251.

Please detail the nature and extent (%) of contribution by the candidate:
Asad:70%
Aaron:30%

Certification by Co-authors:
If there is more than one co-author then a single co-author can sign on behalf of all
The undersigned certifies that:

- The above statement correctly reflects the nature and extent of the PhD candidate's contribution to this co-authored work

- In cases where the candidate was the lead author of the co-authored work he or she wrote the text

Name: *Aaron Marshall* Signature:  Date: *16/8/2019*

Contents

Abbreviation

4-NP	4-nitrophenol
AOP	Advanced oxidation process
ATO	Antimony-doped tin oxide
BDD	Boron-doped diamond
COD	Chemical oxygen demand
CV	Cyclic voltammetry
DSA	Dimensionally stable anode
EASA	Electrochemical active surface area
EO	Electrochemical oxidation
EOI	Electrochemical oxidation index
GC	Gas chromatography
GCE	General current efficiency
HER	hydrogen evolution reaction
HPLC	High-pressure liquid chromatography
ICE	Instantaneous current efficiency
MCE	Mineralisation current efficiency
OER	Oxygen evolution reaction
SCE	Standard Calomel electrode
SEM	scanning electron microscope
SHE	Standard hydrogen electrode
TOC	Total organic carbon
XRD	X-ray powder diffraction

Chapter 1

Introduction

1.1 The need for wastewater treatment

The awareness of environmental protection has been increasing in recent years due to the severe damage caused by wastewater on the ecosystem and human health. This has led to wastewater discharge being increasingly regulated, to the point where existing treatment methods are unsuitable, and thus, new methods for treatment must be developed [4-6]. Sources of wastewater can generally be divided into three groups; domestic wastewater which mainly includes organic waste such as sewage, household chemicals and stormwater, etc.; Agricultural and horticultural wastewater such as pesticide and fertilizer runoff, animal effluent; industrial wastewater which usually concentrated and specific to the each industry such as dairy, pharmaceuticals, paints and dyes, petrochemicals, detergents, plastics, paper and pulp industries, etc.[7-13].

1.2 Wastewater treatment methods

To meet regulatory requirements, most wastewater streams need to be treated in some way before their discharge to the environment [14]. Generally, the treatment processes for

wastewater can be consist of any of these three methods physical, biological and advanced oxidation processes (AOPs) [6, 14].

1.2.1 Physical treatment

Physical treatment includes processes where physically substances are removed from the wastewater by the use of physical barriers or natural forces such as gravity and electromagnetic force [14]. Physical methods include screening, filtering, floatation and adsorption can only partially treat the waste streams and quite often use with the other technique to complete the treatment. The good example of the ineffectiveness of this method is when the wastewater includes dissolved organic or microbiological substances that cannot be easily separated from the wastewater.

1.2.2 Biological treatment

Biological treatment is considered as the leading technique to treat the vast majority of the wastewater due to it is low capital and operating costs [15]. These biological processes can be either aerobic or anaerobic depending on the type of wastewater to be treated, and thus, the type of microorganisms used [13]. While these methods are applicable to a wide range of waste streams, they are ineffective against bio-toxic or bio-refractory substances present in the waste stream [16].

1.2.3 Chemical and advanced oxidation processes

Chemical and advanced oxidation processes are alternatives to the biological treatment processes when these are not capable of degradation of refractory organic and toxic compounds [17]. These methods typically involve in the generation or use of strong oxidising species or highly active radicals. Examples of these species include ozone, hydrogen peroxide and hydroxyl radicals. These active species oxidise organic compounds and oxidise them into carbon dioxide, water and other smaller molecules (which can be oxidised further by the

biological process) [18, 19]. Some examples of chemical oxidation processes include the use of hydrogen peroxide, ozone, wet air oxidation and chlorine whereas advanced oxidation processes (AOPs) include the electrochemical oxidation, Fenton process, photocatalysis, O_3 / UV radiation, and cavitation [20]. While these methods are very robust and effective, they are not perfect and have some major shortcomings. The chemical oxidation processes have low processing capacity, require the storage of dangerous reactants and environmental problem due to accumulation of large amount of oxidants, whereas the advanced oxidation processes require a pre-treatment in some cases and require high capital and operating costs. In general, the application of these methods is when either dangerous or toxic compounds are present in the waste stream or when water must be treated for use as drinking water. Therefore it is necessary to select more efficient methods than those selected for conventional treatment processes [5, 21].

1.3 Electrochemistry and electrochemical oxidation

Electrochemistry offers an exciting approach to the industrial wastewater treatment: in particular, electrochemical oxidation is a promising method for the complete elimination of the organic pollutants and remediation of wastewater. This method can be apply for the wastewater containing chemical oxygen demand (COD) less than 5 g L^{-1} [22, 23]. The main characteristics associated with electrochemical wastewater are:

- versatility; it can treat a wide range of effluent volumes and contamination concentrations and compounds which are normally difficult to treat with conventional methods.
- environmentally compatible; it uses electrical energy and electron to operate which is clean, and very effective reagent.
- ease of operation; automation and control of process is easy and can be quickly started-up and shut-down [5, 21].

However, despite the low capital and maintenance costs, the operating costs can be high because of the low current efficiency of the process (i.e. the proportion of the current used

for organic oxidation). In most cases, it is the oxygen evolution reaction which occurs in parallel to the organic oxidation reaction, which lowers the current efficiency of electrochemical wastewater treatment processes [1, 22].

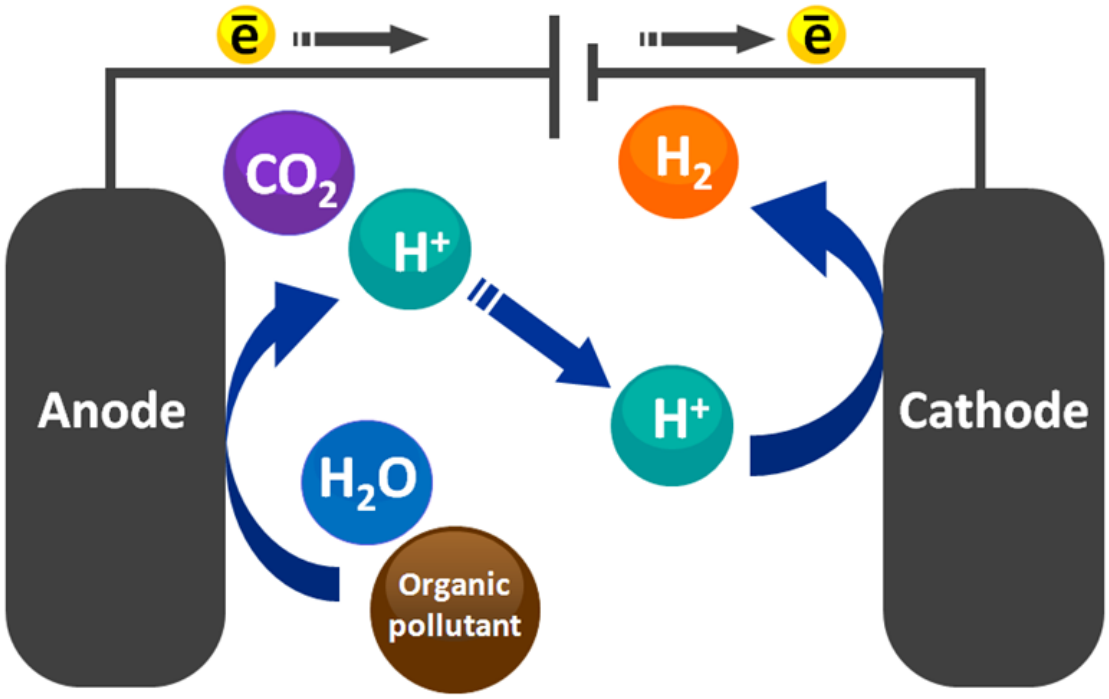

Figure 1-1 Conceptual diagram of an electrochemical cell for oxidation of wastewater

1.4 Thesis scope and structure

The focus of this work is to evaluate ways to improve dimensionally stable anode (DSA) electrode for the electrochemical oxidation of organic pollutants. As this process can have high operational costs due to low current efficiency, this research will aim to discover more efficient processes and materials for the remediation of wastewater via electrochemical methods both in batch and continuous process. This thesis therefore has the following objectives:

- Understanding the mechanism of organic oxidation
- Preparation of mixed metal oxide anodes by addition of nanoparticles

- Characterisation of mixed metal oxide anodes by electrochemical methods
- Investigation on the effect of nanoparticles in anodes on organic oxidation
- Modelling of pulsed and constant electrolysis on electrochemical oxidation

The structure of chapters in this thesis follows a research paper style, including dedicated introduction, experimental and concluding sections. Therefore, some introduction and experimental details is unavoidably repeated. Note that chapters 4 and 5 have been published in a peer-review journal, therefore they are presented in their original form with minor adjustment to fit the style of this work. The first chapter is presented to cover larger overview of the relevant literature and theory.

Chapter 2

Literature Review

Over the past few decades, the intensive investigation has been carried out to improve the electrochemical stability and electrocatalytic activity of the electrode materials. Also, much work has been carried out to determine the efficiency of various anodes materials on wide range wastewater, and the factors influencing on the performance of the process including developing models of the mechanism and kinetics of electrochemical wastewater treatment [6, 24]. Electrochemical oxidation of pollutants is commonly divided into two oxidation mechanisms depending on the place where the overall oxidation occurs. When the oxidation occurs at or on the electrode surface the process is known as direct oxidation whereas, indirect oxidation occurs when the electrode produces a reactant which then reacts with the wastewater within the aqueous solution away from the electrode surface [25].

2.1 Direct oxidation

Direct oxidation, which also known as anodic oxidation, pollutants are oxidised directly after adsorption on the anode surface, which indicate a significant role of the anode materials in the efficiency and selectivity of the oxidation process. Also as the pollutants must reach the electrode surface before reacting, mass transfer becomes an imperative process [26]. Depends on the anode materials, anodic oxidation takes place in two different pathways

- Electrochemical conversion. If the anode materials are “active” or have low oxygen evolution overpotential, organic pollutants are partially oxidised. In the case of the “active” anode, first a chemisorbed hydroxyl radical is generated on the electrode surface, then oxidation process completed through higher oxide by a direct transfer of electrons from the electrode surface. This leads to the production of polymers and many refractory organics as final products of the oxidation process. Thus, biological treatment is required as secondary treatment.

- Electrochemical combustion. If the anode materials are “non-active” or consider as high oxygen evolution overpotential, the complete oxidation of the organic pollutant occurs, which leads to the formation of water, carbon dioxide. In the case of “non-active” anode materials, the weak interaction between the electrode surface and hydroxyl radicals -physiosorbed-, result in complete oxidation of organic compounds [27] (Table 2-1).

Table 2-1 Potential for oxygen evolution reaction on various anodes

Anode material	Anode category	Oxidation Potential / V vs SHE
RuO_2	active	1.47
IrO_2	active	1.52
Pt	active	1.6
Graphite	active	1.7
SnO_2	non-active	1.9
PbO_2	non-active	1.9
Ti/BDD	non-active	2.7

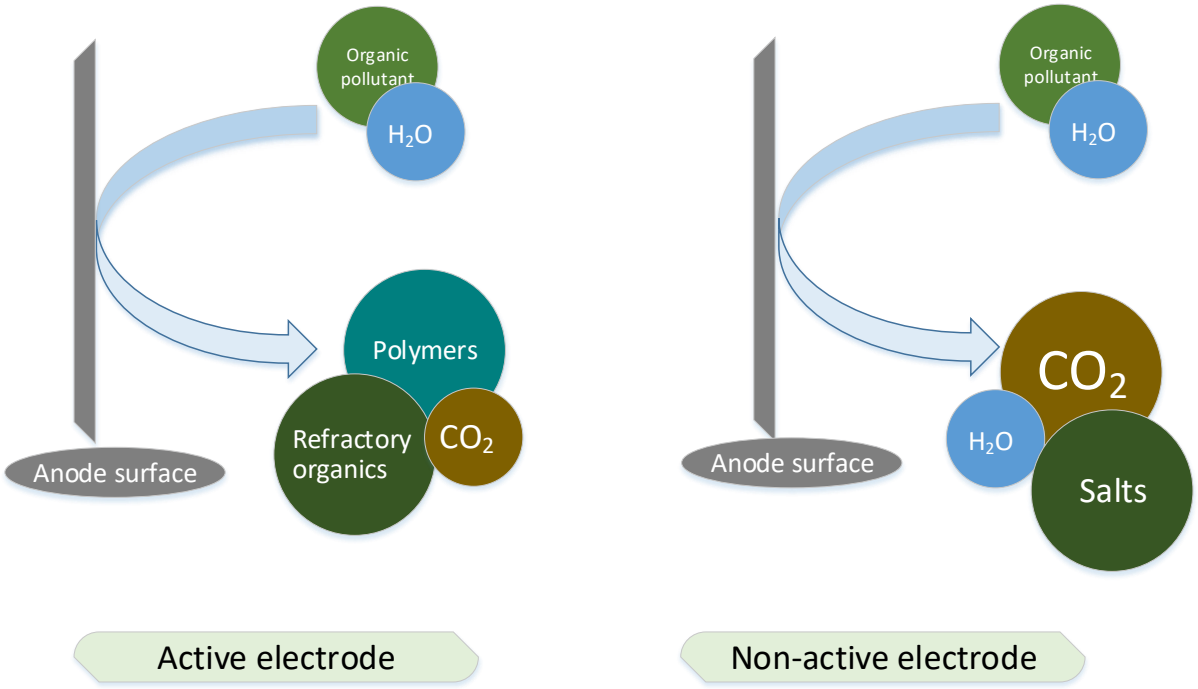

Figure 2-1 Schemes for direct oxidation of organic pollutants

Comninellis et al. [1] proposed a comprehensive model for the direct oxidation of organic pollutants in acidic medium, including the competition with parallel reactions of oxygen evolution in both cases of “active” and “non-active” anodes.

The generalised scheme of the electrochemical oxidation of organic pollutants on the metal oxide anode (MO_x) is illustrated in the in **Error! Reference source not found.**. The first step o f the reaction is the discharge of H_2O molecules at the anode to form an adsorbed hydroxyl radical (Equation 2-1).

$$MO_x + H_2O \longrightarrow M_x(^{\bullet}OH) + H^+ + e^- \qquad (2\text{-}1)$$

The following steps based on the anode materials can be distinguished into two mechanism pathways; In the case of the “active” anode, the adsorbed hydroxyl radicals further oxidises on the anode, forming the so-called” higher oxide” (MO_{x+1}) (Equation 2-2).

$$MO_x\ (\ ^{\bullet}OH\ )\ \ MO_{x+1}\ \ +\ H^+ + e^- \qquad (2\text{-}2)$$

The higher oxide (MO_{x+1}) acts as a mediator in the oxidation process of organic compounds (Equation 2-3). The side reaction of oxygen evolution (Equation 2-4) is in competition with the conversion of the organic compounds (Equation 2-3).

Conversion of organic compounds:

$$R\ +\ MO_{x+1} \longrightarrow RO\ + MO_x \qquad (2\text{-}3)$$

Parallel oxygen evolution reaction:

$$MO_{x+1} \longrightarrow MO_x + \frac{1}{2}O_2 \qquad (2\text{-}4)$$

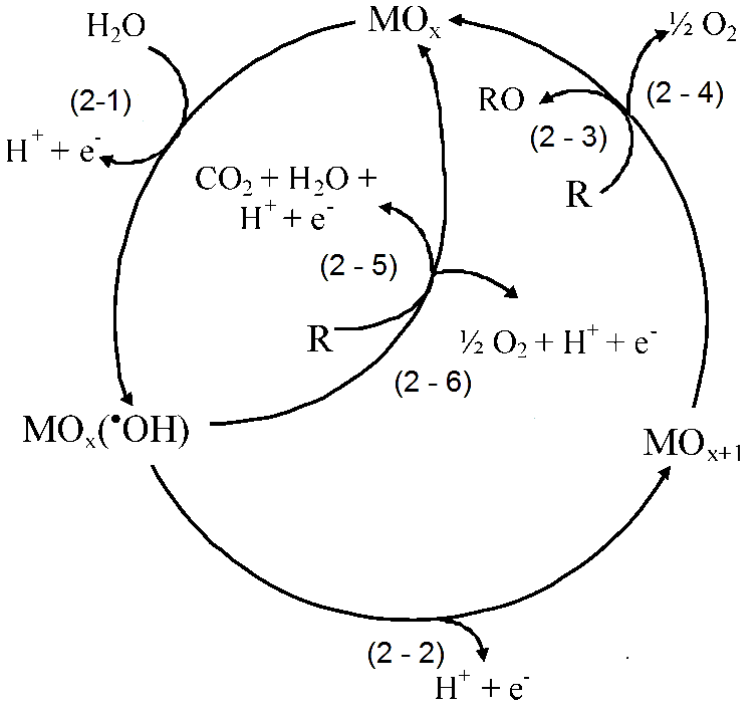

Figure 2-2 Generalised scheme of the electrochemical conversion and combustion of organics with simultaneous oxygen evolution at the lattice of the oxide anode (Reproduced with permission from Electrochim. Acta, 1994, 39, 1857. Copyright 1994, Elsevier.[1])

In the case of the “non-active” anode, oxidation of organics is mediated by hydroxyl radicals directly, which leads to complete combustion of organic compounds (Equation 2-5). This reaction competes with the side reaction of hydroxyl radicals to oxygen evolution (Equation 2-6) without any interaction with the “non-active” anode surface.

Complete combustion:

$$R + MO_x\ (^{\bullet}OH) \longrightarrow H_2O + CO_2 + H^+ + e^- + MO_X \quad (2\text{-}5)$$

Parallel oxygen evolution reaction:

$$MO_x(^{\bullet}OH) \longrightarrow MO_x + \frac{1}{2}O_2 + H^+ + e^- \quad (2\text{-}6)$$

The most common reaction occurs at the cathode during the oxidation is hydrogen evolution (Equation 2-7)

The reaction at the cathode:

$$2H^+ + 2e^- \longrightarrow H_2 \quad (2\text{-}7)$$

2.2 Indirect oxidation

During indirect oxidation, the oxidation of wastewater of species occurs in the bulk solution via the electrochemical generation of a mediator such as peroxide, chlorine, Fenton’s reagent, hypochlorite, peroxodisulfate and ozone [28]. These oxidants can be produced either in the anodic or cathodic process, which can lead to the complete combustion to carbon dioxide, water. The most used electrochemical oxidants are chlorine and hydrogen peroxide, due to their effectiveness in dealing with the organic pollutants [15].

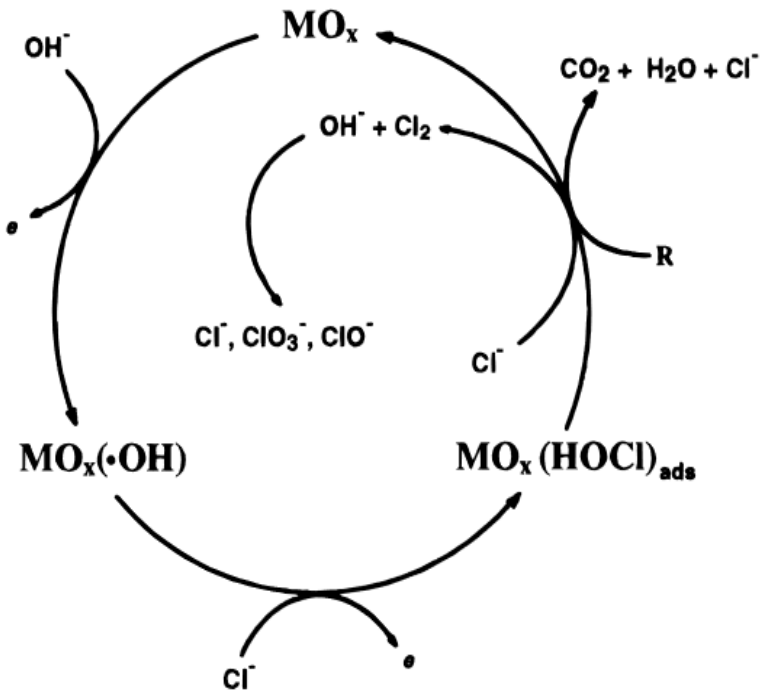

Figure 2-3 *Extension of the reaction pattern proposed by Comninellis* [1] *for the electrochemical incineration of organics, to the case of active chlorine mediated electrochemical incineration. Reprinted with permission from J. Electrochem. Soc., 2000, 147, 592.* [3] *Copyright 2000,* The Electrochemical Society.

The key factor in obtaining high removal efficiency of wastewater in indirect electrolytic processes are the following:

- High generation rate of intermediate
- Low overpotential
- The reaction rate of the pollutant and intermediate species must be higher than the rate of any competing reactions.
- Zero or minimum absorption of organic pollutants

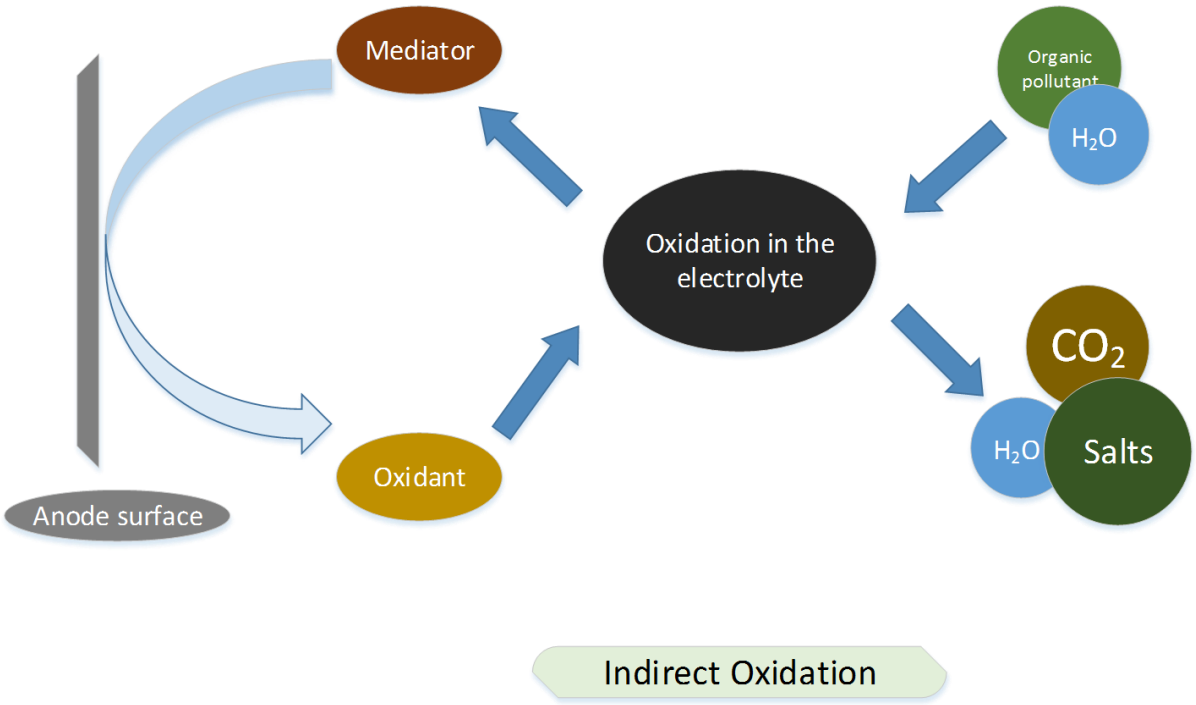

Figure 2-4 Scheme for indirect oxidation of organic pollutants

2.3 Example of electrochemical wastewater treatment

The pioneering studies on the electrochemical oxidation of wastewater have carried out by Dabrowski in the ’70s, Kirk, Stucki, Kotz, Chettiar and Watkinson in the ’80s, and later in the early ’90s by Comninellis. In these studies to reach the optimal condition, some suggested the oxidation of organic pollutants at two-dimensional electrodes or planar electrodes and for more complexed pollutants the use of three-dimensional multi-phase electrode or nonplanar electrodes [29]. Also, various compounds have been investigated, including phenolic groups [30-36], herbicides and pharmaceutical drugs [34, 37-40], Textile Dyes[41-44] etc.

2.3.1 Dye wastewater

The discharge of the natural or synthetic dyes in the environment lead to serious health problems and endanger the aquatic species. The azoic dyes are found to be carcinogenic and highly poisonous to the ecosystem [45].

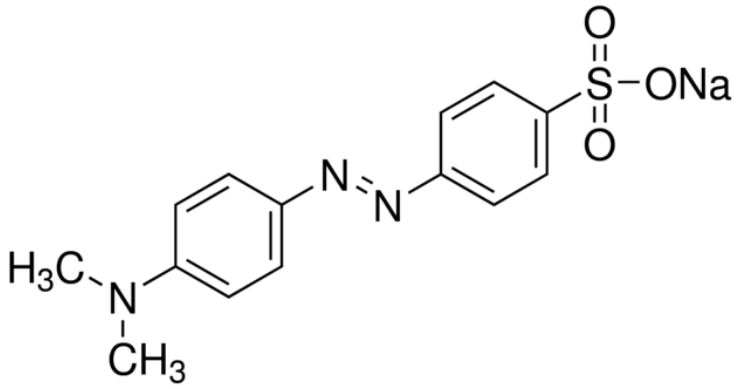

Figure 2-5 Example of azodic dyes, Methyl orange

Canizares et al.[46] conducted experiments to investigate the effect of BBD anode on the oxidation of Eriochrome Black T, Methyl orange , and Congo red. The results revealed that complete chemical oxygen demand (COD) and colour removal was attained for all azoic dyes. The current efficiency of the process seems to be unaffected by the dye molecule, but it depends on the dye concentration range. The energy requirement initially increases linearly up to 80% removal, followed by exponential increment, which makes this technique suitable for pre-treatment of the waste, but not for the complete removal as the energy cost is high.
Yi and Chen [47, 48] investigated the alizarin red S dye oxidation using an activated carbon fibre electrode. The results indicated that an activated carbon fibre anode is more active in the removal of colour than the carbon fibre anode. The higher electrochemical degradation of the dye is possible when the activated carbon fibre anodes have high specific surface area and high absorption capacity. The chemical oxygen demand (COD) result revealed that removal efficiency of the aqueous dye solution in a neutral or alkaline medium is higher than in acidic medium and was about 74% after one hour of electrolysis. Maximum colour and COD removals were about 98% and 76.5%, respectively.

2.3.2 Petroleum refinery wastewater

The petroleum effluents consist of serious environmental pollution, which contains a wide range of toxic compounds with high chemical oxygen demand (COD). The inorganic substances inside the petroleum effluents give rise to aromatic petroleum hydrocarbons, and phenolic compounds which are the main contributor to high COD [29, 49]. Some researcher studied the electro-oxidation of petroleum refinery wastewater [50-53], in particular, Yan et al. [29] studied the removal of organic and inorganic pollutants from the petroleum refinery wastewater by using two-dimensional system, three dimensional system (only Fe particle assisted) and three-dimensional multi-phase (both Fe particle and air assisted) system with graphite used as anode and cathode. The result showed the introduction of iron particles as a third electrode assisted with air lead to achieve highest COD removal efficiency of 92.8% and low salinity of 84 μS cm^{-1}. The applied conditions of this experiment, such as pH and cell voltage were 6.5 and 12 V, respectively, while fine iron particles were in use through the experiment. The overall result showed that using this type of electrochemical system is a promising way to treat refinery wastewater.

2.3.3 Naphthalene sulfonates

The naphthalene sulfonate compounds have low toxicity in the environment, but due to their high solubility in water and slow rate or non-biodegradability are considered as a potential risk for the ecosystem. The main usage of naphthalene sulfonate compounds in the industry is for the production of dispersants, detergents and azo dye [54]. Panizza et al.[55] investigated the electrochemical oxidation feasibility of an industrial wastewater containing mixture of naphthalene sulfonates and some other refractory organic pollutants. A biofilm airlift suspension (BAS) reactor employed along with an undivided electrochemical cell equipped with a BDD anode.

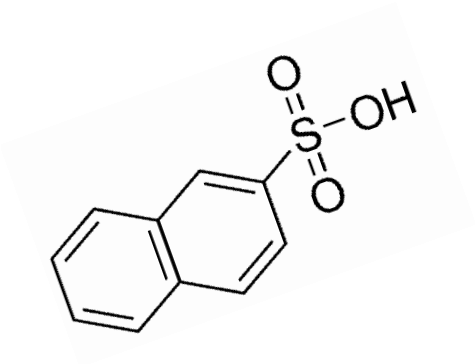

Figure 2-6 Example of naphthalene sulfonate compounds, 2-Naphthalenesulfonic acid

The overall degradation efficiency of the biological process occurring in the BAS reactor was at 70% maximum based on the COD measurement. The biological process was less effective on the naphthalene sulfonates. However, these organics were completely mineralised by the secondary process of electrochemical oxidation. The results indicated that the energy consumption and time required could be reduced from 80 kWh m^{-3} and 4 h to 61 kWh m^{-3} and 3 h for complete mineralisation of raw and biologically pre-treated, respectively.

2.3.4 Pulp and paper wastewater

The pulp and paper industries discharge significant effluent with high chemical oxygen demand, toxicity and colour. Electrochemical oxidation can potentially be a solution to this problem [56]. Others [57-61] investigated the possibility of treating the pulp and paper wastewater, in particular, Wang et al. [62] studied the effect of the two-dimensional electrode of Ti/ Co/ SnO_2 on paper mill wastewater and found low degradation efficiency. The usages of active carbon particles as packed bed particle electrodes with Ti/ Co/ SnO_2 anode lead to achieving high degradation efficacy, 75% colour removal and decrease in dimensionless COD to 0.137 after 1 hour.

2.4 Example of electrochemical treatment of persistent wastewater

2.4.1 Herbicides and pharmaceutical drugs

The herbicides and pharmaceutical drugs are another pollutant that can be found in sewage effluents, surface water [40]. Some examples of these pollutants in the environments are paracetamol, antibiotics ofloxacin and lincomycin and methamidophos. The group of Brillas [40, 63-65] investigated the effect of electrochemical oxidation on herbicides and pharmaceutical drugs at BDD anode. The results showed that the electrochemical oxidation in a batch flow reactor under the steady condition is very effective for complete mineralisation of this kind of pollutants. The efficiency of the process increased with increased drug concentration, temperature, current density and liquid flow, although it is unaffected by pH in aqueous solution. They also indicated that the degradation kinetics follow a pseudo first order reaction.

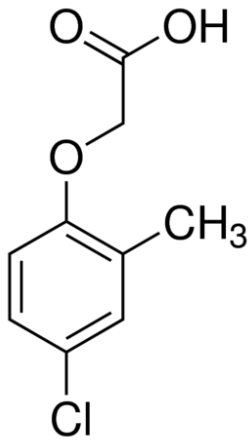

Figure 2-7 Example of herbicide, 4-Chloro-2-tolyloxyacetic acid

Jara et al. [66] investigated the mechanism and effectiveness of electro-oxidation of three different anodes of Ti/Pt, graphite and 3D activated carbon electrode on the antibiotics ofloxacin and lincomycin. The result showed that ofloxacin is oxidised efficiently in all anodes whereas, lincomycin was hardly oxidised mainly due to difficult induction of the molecules deprotonation. The COD removal of 90% achieved at Ti/Pt, graphite and 3D activated carbon in 374, 793 and 102 min respectively. The best electrode for a continuous industrial process

is 3D activated carbon electrode, but high corrosion rate at high applied potential hampered its application.

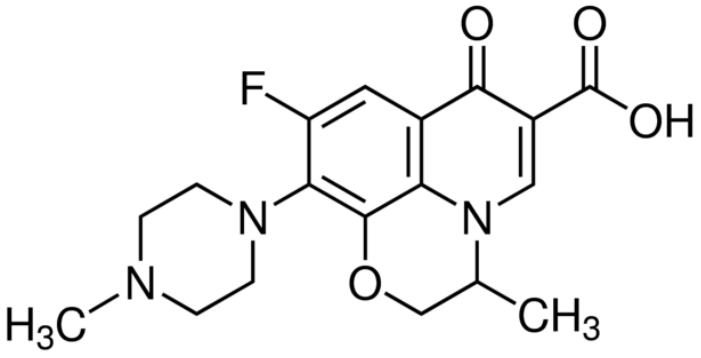

Figure 2-8 Example of pharmaceutical, ofloxacin

Huitle et al. [67] investigated the oxidation of methamidophos (MMD), a highly toxic pesticide, in a sodium sulphate aqueous solution on the three different anodes (Pb/PbO_2, Ti/SnO_2, and Si/BDD). The results showed that under the galvanostatic conditions, the performance of the anode is influenced by pH and current density. The complete combustion of MMD occurred only at a Si/BDD anode with the applied current density of 50 mA cm^{-2}. The current efficiency of the fabricated electrode for MMD removal follows the order: Si/BDD > Pb/PbO_2> Ti/SnO_2.

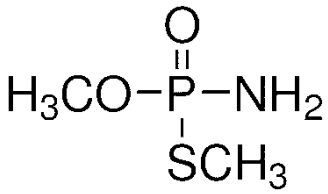

Figure 2-9 Example of pesticide, methamidophos

2.4.2 Surfactants

The wide usage of surfactant such as perfluorinated compounds (PFCs) in fire retardants [68], surfactants and protective coating for the carpets and clothing [69] is responsible for widespread contamination of this pollutants in wastewater [70], surface water [71], animal [72] and human body [73]. Others [74-82] investigated the possibility of treating the surfactant compounds wastewater, in particular, Zhuo et al. [83] investigated the electrolysis of persistent organic pollutant of perfluorooctane sulfonate (PFOS) at Ti/PbO_2, Ti/TiO_2-NTs/PbO_2 and Ti/TiO_2-$NTs/Ag_2O/PbO_2$ electrode with supporting electrolyte of 1.4 g L^{-1} $NaClO_4$. The results showed the highest removal efficiency of perfluorooctane sulfonate with the ratio of 74.87% are obtained at the Ti/TiO_2-$NTs/Ag_2O/PbO_2$ anode after 3 hours of electrolysis at a constant current density of 30 mA cm^{-2} with a pseudo-first-order kinetic constant of 0.0165 min^{-1}. In general, the anode stability and electrocatalytic activity towards removal of the PFOS followed the sequence: Ti/TiO_2-$NTs/Ag_2O/PbO_2$ > Ti/TiO_2-NTs/PbO_2 > Ti/PbO_2.

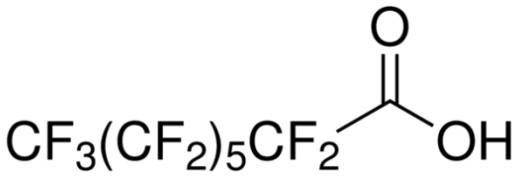

Figure 2-10 Example of surfactant, Perfluorooctanoic acid

2.4.3 Phenolic compounds

The phenolic compounds are increasingly often found in industrial effluents, urban and agricultural wastes. The high stability, solubility and toxicity of these compounds induce a dramatic problem for the drinking-water reservoir as well as the environment, and it has been classified as high priority pollutants by the United States EPA [84].

Adam et al.[36] studied the oxidation of 2-nitrophenol, 3-nitrophenol, and 4-nitrophenol on four different SnO_2-based electrodes in 0.5 M Na_2SO_4 supported electrolyte adjusted to pH 2.

The degradation of the nitrophenols revealed that the rate constant for the electrochemical oxidation of the nitrophenols decreases in the order: 2-NP > 4-NP > 3-NP. The lifetime tests exhibited that doping different metal oxide into SnO_2-based electrode, increase the service life significantly. In particular, the lifetime of Ti/SnO_2-Sb_2O_5 electrode under 160 mA cm^{-2} current density was 12 h while Ti/SnO_2 -Sb_2O_5-IrO_2 electrode with the same condition had a very long lifetime of 155 days. The results indicated that the degradation of 4-NP at the four SnO_2-base electrodes explained by pseudo-first-order kinetics and follows in the order: Ti/SnO_2-Sb_2O_5 > Ti/SnO_2-Sb_2O_5-PtO_x > Ti/SnO_2-Sb_2O_5-IrO_2 > Ti/SnO_2-Sb_2O_5-RuO_2. Even though the first two electrodes showed higher activity towards 4-NP elimination, but due to their short service lifetimes, it is not a good option for the oxidation process. However, Ti/SnO_2-Sb_2O_5-IrO_2 anode has best performance with long lifetime service and high activity towards oxidation.

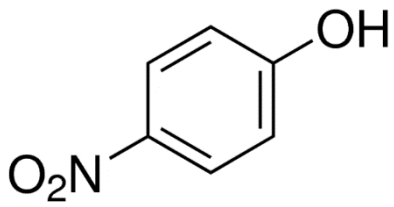

Figure 2-11 Example of phenolic compounds with nitro group, para-nitrophenol

Polcaro et al. [39, 85, 86] studied the oxidation of phenolic compounds, triazine, diuron and 3,4-dichloroaniline at BDD anodes. The result identified that the critical factor in obtaining high current efficiency during wastewater oxidation is the rate of mass transfer between an electrode surface and wastewater species. In order to achieve high mass transfer coefficient ($\sim 10^{-4}$ m s^{-1}), an impinging cell was used. The results showed that if the applied current density is low enough, the process can be carried out at the current efficiency close to 100%, resulting in the nearly complete oxidation of the organic pollutant.

In other work, Feng and Li [87, 88] examined phenol oxidation on Ti/PbO_2 and Pt electrodes and compared the results with DSA RuO_2-based anodes. The performance of phenol oxidation

on the three electrodes containing RuO_2 follows the sequence: Ti/Sb-Sn-RuO_2-Gd > Ti/Sb-Sn-RuO_2 > Ti/RuO_2. Comparing this result with Ti/PbO_2 and Pt electrodes showed that Ti/PbO_2 and Pt electrodes they are still more efficient. In case of RuO_2 anodes, phenol partially oxidised and aromatic intermediates formed, such as benzoquinone, hydroquinone, maleic acid, succinic acid, and oxalic acid, and thus wastewater still contained considerable total organic carbon (TOC). The complete removal of TOC occurred only at the Ti/PbO_2 anode after 4000 C of charge consumed.

Gattrell and Kirk [89] investigated reticulated glassy carbon anodes for oxidation of phenol in a flow-by electrochemical cell. They showed that the electrode surface could be blocked with mostly insoluble polymeric products at low anodic potentials and high phenol concentration (over the range of 5-20 mmol L^{-1}), led to a rapid decrease in the reaction rate. On the other hand, complete organic oxidation is possible at higher temperatures of 50 ^{o}C, and applied potentials (1.9 V vs SCE). These conditions led to faster electrode corrosion and reduced current efficiency as a consequence of the electrode resistance increasing.

Comninellis and Pulgarin [1, 90] discussed phenol oxidation at Pt anodes in a two-compartment cell, supported by 150 g L^{-1} Na_2SO_4 adjusted to pH 12.3 or 3. The oxidation process occurs in two parallel steps: In the first step, aromatic intermediates such as hydroquinone, catechol and benzoquinone are formed, followed by aromatic ring opening, with the formation of aliphatic acids that are stable to further oxidation. Due to the formation of these intermediates, only partial TOC removal can be attained, and current efficiency decreased during electrolysis. The electrochemical oxidation index (EOI) was uninfluenced by current density and temperature, while it depended on the pH and phenol concentration.

Polcaro et al. [91, 92] studied the electrolysis of 2-chlorophenol and 2, 6- dichlorophenol using a porous carbon felt anode, a fixed bed of carbon pellets and a dimensionally stable anode Ti/RuO_2 in a flow cell. The result showed the efficient removal of chlorophenol and their oxidation intermediate at both carbon-based anodes. The flow rate through the cell did not affect the reaction kinetics but decreasing the initial concentration of chlorophenols led to a decrease in the reaction rate. Increasing the current densities led to lower current efficiency.

In case of DSA electrode, if a divided electrochemical cell was used, the chlorophenols can be rapidly removed, but the need of a membrane in this cell design results in a more complex and expensive setup.

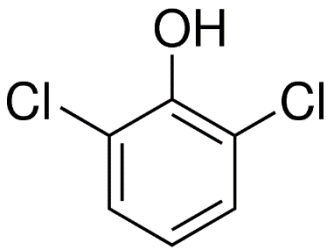

Figure 2-12 Example of phenolic compounds with chlorine atoms, 2, 6- dichlorophenol

Table 2-2 Examples of Direct electrochemical oxidation

Pollutants	Anodes	Comments	ref
Petroleum refinery wastewater	3D graphite electrode	COD removal efficiency of 92.8% and salinity of 84 μS cm^{-1}	[29]
Azoic dyes	BDD	Complete oxidation, due to high energy requirement after 80% removal its best to be used as pre-treatment	[45]
Alizarin red S dye	Activated carbon fibre	Maximum COD removal of 98% and 76.5% in neutral and alkaline medium	[48]
Naphthalene sulfonates	BDD	Achieved complete mineralisation and lower energy consumption of when Combined biological and electrochemical process used	[55]
Paper mill wastewater	Ti/ Co/ SnO_2	75% colour removal in 1 hour and dimensionless COD decrease to 0.137	[62]
Herbicides and pharmaceutical drugs	BDD	Batch reactor, complete oxidation	[40, 63]
Antibiotics ofloxacin	Ti/Pt, graphite and three-dimensional activated carbon	90% of COD removal after 374 min at Ti/Pt and 102 min at 3D activated carbon in 0.02 N of Na_2SO_4	[66]

Methamidophos	Pb/PbO2, Ti/SnO2, and Si/BDD	Complete oxidation at Si/BDD and Current efficiency as follows Si/BDD > Pb/PbO_2> Ti/SnO_2	[67]
Perfluorooctane sulfonate (PFOS)	Ti/PbO_2, Ti/TiO_2-NTs/PbO_2 and Ti/TiO_2-$NTs/Ag_2O/PbO_2$	Highest removal efficiency of 74.8% for Ti/TiO_2-$NTs/Ag_2O/PbO_2$. Electrocatalytic activity of Ti/TiO_2-$NTs/Ag_2O/PbO_2$ > Ti/TiO_2-NTs/PbO_2 > Ti/PbO_2.	[83]
Perfluorooctanoate (PFOA)	BDD	Complete degradation of Perfluorooctanoate	[93]
2-nitrophenol, 3-nitrophenol, and 4-nitrophenol	Ti/SnO_2-Sb_2O_5, Ti/SnO_2-Sb_2O_5-PtO_x, Ti/SnO_2-Sb_2O_5-IrO_2 and Ti/SnO_2-Sb_2O_5-RuO_2	Rate constant for oxidation 2-NP > 4-NP > 3-NP and Ti/SnO_2-Sb_2O_5-IrO_2 has long service life and high activity towards 4-NP	[36]
Phenolic compounds	BDD	100% current efficiency and near-complete oxidation of pollutant at low current density	[86]
Phenol	Glassy carbon	Complete oxidation achieved at temperature 50 ^{o}C and potential of 1.9 V	[89]
Phenol	Pt	Partial TOC removal, electrochemical oxidation depended on the pH and phenol concentration	[90]
Clofibric acid	Pt and BDD	Complete and partial oxidation at BDD and Pt respectively	[63]

2.5 Efficiency and energy parameters in electrochemical oxidation

2.5.1 Instantaneous current efficiency

Instantaneous current efficiency (ICE) is defined as the ratio of the electrochemical equivalent current density for the oxidation of specific compound to the total applied current density during electrolysis.

$$\mathrm{ICE} = \frac{current\ density\ comsumed\ by\ specific\ compound}{total\ applied\ current\ density} \quad (2\text{-}8)$$

Instantaneous current efficiency also can be determined based on the oxygen flow rate (OFR) method and the chemical oxygen demand (COD) method. Chemical oxygen demand is a

standard parameter in wastewater treatment terminology, which measures the amount of oxygen required to oxidise organic pollutants in aqueous solution. This parameter then provides the number of electrons needed to be removed from the solution in order to obtain full mineralisation. The oxygen flow method uses:

$$ICE = \frac{\dot{V}_0 - (\dot{V}_t)_{org}}{\dot{V}_0} \quad (2\text{-}9)$$

where $V_0$is the oxygen flow rate determined in the anodic compartment at t=0 when there is no organic pollutants present in the reaction ($cm^3\ min^{-1}$) and $\dot{V}_t$is the oxygen flow rate at desire time of t in the presence of organic pollutants ($cm^3\ min^{-1}$); or with the COD method

$$ICE = \frac{(COD_t - COD_{t+\Delta t})}{8I\Delta t} FV \quad (2\text{-}10)$$

Where $(COD)_t$ and $(COD)_{t+\Delta t}$ are the chemical oxygen demands at time t and $t + \Delta t$ ($g\ L^{-1}$), I is the current (A), F is Faraday's constant (96,485 C mol^{-1}), V is the electrolyte volume (L), and 8 is the oxygen equivalent mass ($g\ eq^{-1}$).

2.5.2 General current efficiency

The general current efficiency (GCE) is the average value of the instantaneous current efficiency during overall oxidation and is determined based on ICE.

$$GCE = \int_0^t ICE\ dt \quad (2\text{-}11)$$

2.5.3 Specific energy consumption

The specific energy consumption (E_{sp}), is typically expressed as the energy consumed in Wh g^{-1} for removal of a unit mass of COD from wastewater.

$$E_{sp} = \frac{tUI}{(COD_t - COD_{t+\Delta t})}\frac{1}{V} \quad (2\text{-}12)$$

Where U is the average cell potential (V), I is current density (A), V is the volume of the electrolyte (L), $(COD)_t$ and $(COD)_{t+\Delta t}$ are the chemical oxygen demands at time t and $t + \Delta t$ (g L^{-1}) [5].

2.5.4 Limiting mechanism of electrode reaction rate and current

The simple electrode reaction of $O + ne^- \rightleftharpoons R$, consists of two stable and soluble species of O and R in the electrolysis medium that interconvert at the surface of electrode. In general, the limiting mechanisms are as follow:

1. Electron transfer
2. Mass transfer
3. Coupled chemical reactions
4. Other surface reaction such as adsorption and phase formation

We have not discussed the effect of coupled chemical reactions, adsorption in this work, as in most cases of the electrochemical organic oxidation, to simplifying the process, these effect is neglected.

2.5.4.1 Electron transfer at the electrode surface

When the mass transfer of species from the bulk to the surface of electrode is very fast which means efficient stirring and low current applied, the oxidation reaction is controlled by kinetics of reaction and the concentration of species at the surface of electrode is equal to the concentration of species in the bulk solution.

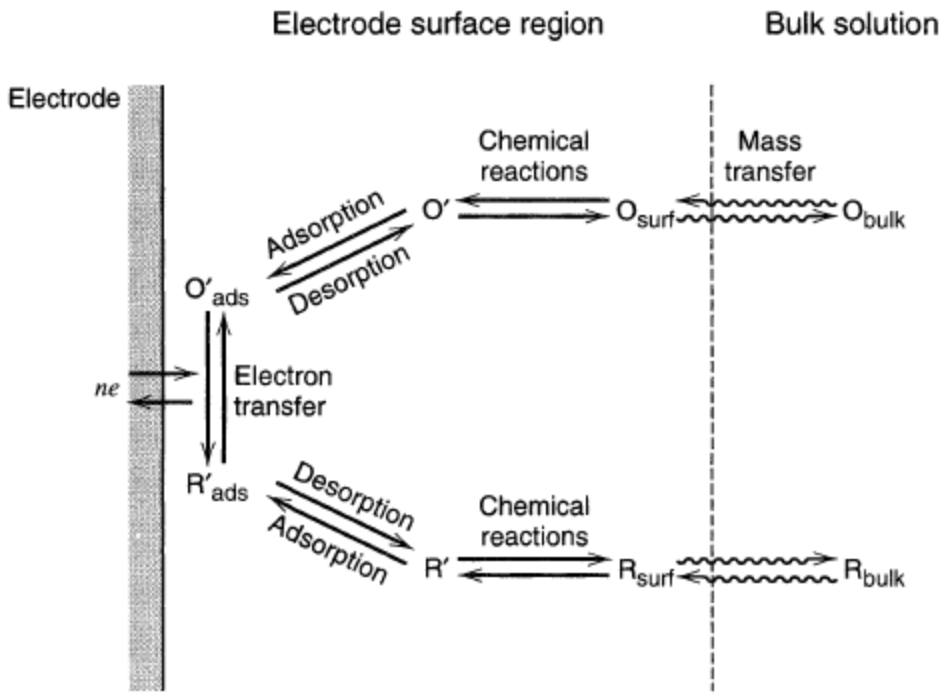

Figure 2-13 Pathway of a general electrode reaction, (Reprinted with permission from Wiley 2001 [2] *. Copyright 2001 John Wiley & Sons)*

In this case, the rates constant of reaction is potential dependent and can be expressed through Butler-Volmer equation e.g.:

$$k_f = k_f^0 exp^{\frac{\beta F}{RT}(E-E_{rev})} \quad (2\text{-}13)$$

$$k_b = k_b^0 exp^{\frac{-(1-\beta)F}{RT}(E-E_{rev})} \quad (2\text{-}14)$$

where R, T, β , F, k_f and k_b are the gas constant, temperature, symmetry factor, faraday constant, forward and backward rate constants respectively and E and E_{rev} are the anode and reversible potential. The parameter β –symmetry factor- usually has a value of approximately 0.5 for metal [94]. The difference between the rate of the forward and

backward reactions at the electrode surface is proportional to the current of the kinetic control and defined as:

$$i = nFA[k_f C_O - k_b C_R] \quad (2\text{-}15)$$

Where, A, C_O and C_R are the electrode area, surface concertation of O and R respectively.

2.5.4.2 Mass transfer controlled

When kinetics of the electrode reaction is sufficiently fast or sufficiently high current is applied, the mass transfer of the reactant from the bulk solution to the surface of electrode become insufficient, so the concentration of reactant on the surface of electrode become equal to zero. Mass transfer can occur by,

1. Migration. Movement of charge species due to the gradient of electrical potential.
2. Convection. Movement of species due to the density gradient and forced convection with bulk movement.
3. Diffusion. Movement of the species due to the concentration gradient.

The migration effects can be neglected by choosing the condition such as presence of high concentration (>0.1 M) of inert or supporting electrolyte and concertation of 10^{-3} M of electroactive species. In this condition charge can easily transfer across the electrolyte without any solution resistance. The convection effects also can be eliminated by using forced convection such as stirrer or agitator or using the continuous flow cell. Considering above condition, through this work we consider the case of only diffusion control governing the oxidation process when it is under the mass transport condition.

The maximum production rate of the electrochemical cell under mass transfer control can be estimated via limiting current density i_{lim}:

$$i_{lim} = nFk_m C_{org} \quad (2\text{-}16)$$

Where i_{lim} is the limiting current density for the electrochemical oxidation of an organic compound under specific hydrodynamic conditions (A m^{-2}), n is the number of electrons involved in the reaction, F is the Faraday constant (96485 C mol^{-1}), k_m is the mass transport coefficient (m s^{-1}) and $C_{org}$is the concentration of organic pollutants in the electrolyte (mol m^{-3}).

The specific hydrodynamic conditions for the limiting current density equation are: the adsorption of the organic compounds at the electrode surface is negligible, the global rate of electrochemical oxidation of organic compounds is a fast reaction, and it is controlled by mass transport of organic to the diffusion layer of the anode surface, which indicates that hydrodynamic parameters of the electrochemical cell are independent of the chemical nature of the organic compound present in the electrolyte .

The limiting current density can be defined based on the chemical oxygen demand (COD), which can be used when a mixture of organic compounds or the actual wastewater is treated.

$$i_{lim} = 4Fk_mCOD \quad (2\text{-}17)$$

Where 4 is the number of exchanged electrons per mole of oxygen, F is the Faraday constant (96485 C mol^{-1}), (COD) is the chemical oxygen demands (mol m^{-3}), k_m is the mass transport coefficient (m s^{-1}). k_m value should be similar for each individual organic compound in order the equation (2-17) be valid.

2.6 Anode material

The choice of anode material has a great impact on pollutants degradation of electrochemical oxidation. The anode materials control the final oxidation products and the efficiency of the process. The anode material must have the following properties [25, 94]:

- High chemical and electrochemical stability- leads to resistance to erosion, corrosion and formation of passivation layers as well as improvements in service lifetime of the electrode
- High electrical conductivity
- Catalytic activity and selectivity towards organic pollutants
- Low cost

The typical anode materials which have been investigated earlier are as follows: platinum [95, 96], carbon and graphite, boron-doped diamond (BDD) [97, 98] and metal oxides such as SnO_2 [99], PbO_2 [100], IrO_2 [101] and RuO_2 [88].

2.6.1 DSA electrode

Dimensionally stable anode known as DSA electrodes is one of the greatest technological advancement in the recent history of electrochemistry [102], developed by Henry Beer [103]. DSA electrodes are known for its high chemical and electrochemical stability, and its selective oxidation process characterised by a thin layer of conductive metal oxide (Particularly IrO_2 and RuO_2) covered on the base titanium metal. This type of anode due to its low oxygen overpotential referred to as an "active" anode [24]. The potential for oxygen evolution of RuO_2 and IrO_2 anodes are relatively low (i.e., 1.47 and 1.52 V vs SHE in 0.5 M H_2SO_4 respectively). In the industry in order to achieve a higher stability and catalytic activity towards wastewater, a combination of the metal oxide is used. There is a wide range of applications for this type of electrode, mainly chlor-alkali [104], water electrolysis [105], electrowinning [106] and organic oxidation [107-109].

2.6.2 Platinum

Platinum anodes have been investigated as electrode materials for a long time due to its good conductivity and corrosion resistance [5]. The potential for oxygen evolution reaction of the

platinum anode is relatively low (i.e., 1.6 V vs SHE in 0.5 M H_2SO_4). Due to its low overpotential, platinum behaviour follows "active" anode, which has a selective conversion of organic pollutants at low current efficiency. The wide range of organic pollutants has been treated on Pt anode such as synthetic dye [42], Phenol [88, 110], glucose [111], herbicides [112], chlorophenols [113], methanol [114].

2.6.3 Carbon and Graphite

Carbon and graphite electrode have been used in the electrochemical wastewater treatment due to their large surface area and low cost. The three-dimensional electrodes (e.g. fluidised bed, porous electrode, carbon particles, etc.) is the most used configuration at these type of electrodes for organic oxidation, which accompanies with both mechanisms of adsorption and electro-oxidation. The shortcoming of this type of electrode occurs mainly at high potentials, which leads to electrode surface corrosion over time and subsequently reduce its service lifetime. Thus, further investigation into the electrode passivation mechanism and prevention and electrode regeneration [115] require for the application of three-dimensional electrodes to used widely in the industry. Some example of wastewater treated on carbon-based electrodes are as follow: petroleum refinery [29], phenols [116, 117], chlorophenol [118-120], synthetic dye [121, 122].

2.6.4 Boron-doped diamond

The synthetic boron-doped diamond (BDD) was first introduced by Carey [123] as electrodes for organic oxidation. Since then, the use of BDD electrodes has received considerable attention due to its commercial feasibility to synthesise conductive diamond films with high-quality [124-126]. The potential for oxygen evolution reaction of BDD anode is relatively high (i.e., 2.7 V vs SHE in 0.5 M H_2SO_4). Due to its high overpotential, BDD behaviour follows "non-active" anode which leads to complete oxidation of organic pollutants, such as pesticides [85,

127], surfactant [128, 129], synthetic dye [130-134], pharmaceutical drugs [63, 135] and phenolic compounds [70, 136-140].

2.7 Anode preparation

2.7.1 Thermal decomposition of precursors

The most common method for preparation of DSA electrode is thermal decomposition method of metal precursors onto titanium substrate. The temperature programmed analysis (TPA) such as Thermogravimetric analysis (TGA) is used to investigate the effect of temperature on the DSA electrode during the decomposition stage. The thermal decomposition of $IrCl_3.3H_2O$ at atmospheric pressure showed with two overlapping stages of losing the crystal water at 100-200 °C and oxidation of IrO_2 above 600 °C and final stage of decomposition to metallic iridium above 1000 °C [141, 142]. A common example is the decomposition of hydrate iridium chloride into iridium oxide.

$$2IrCl_3.3H_2O + 2O_2 \longrightarrow 2IrO_2 + 3Cl_2 + 6H_2O \qquad (2\text{-}18)$$

The annealing condition has great impact on the structure and chemical composition of electrode coating. Introducing high annealing temperature during the thermal decomposition process leads to an increase in crystallinity structure and also has a stabilising effect on the metal oxide. However, this increase in temperature causes a decrease in surface area and also passivation of the titanium substrate, whereas lower annealing temperature cause precursors (metal salt) to be partial decomposed and lower mechanical adhesion to the substrate [94].

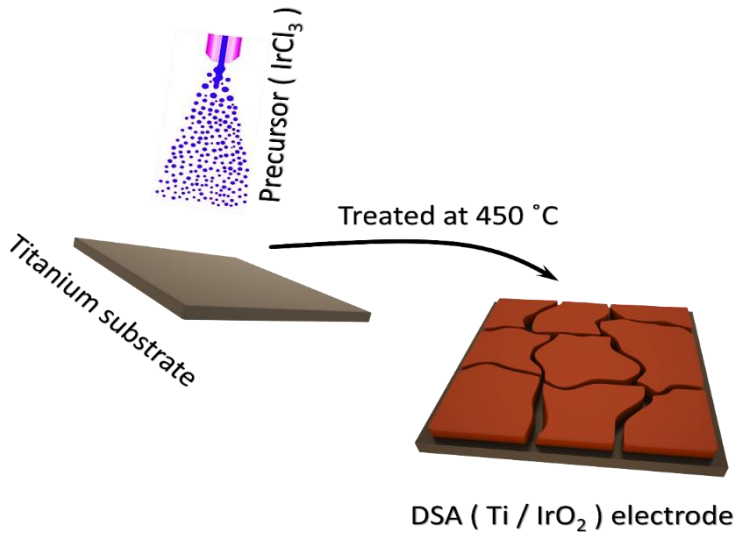

Figure 2-14 Schematic of DSA electrode preparation

2.7.1.1 The role of solvent

The preparation procedure of metal oxide has great impact on the active surface area of the anode. Trasatti et al. [94] investigated the effect of preparation procedure, nature of the solvent and also different operator to synthesise the metal oxide and concluded that by modifying any of these parameters the active surface area dependency on composition also changed dramatically.

2.7.1.2 The role of precursor

The effect of precursor also has been discussed for a better understanding of metal oxide preparation. The most used type of precursors for metal oxide preparation is the chloride form of metal. This may leave a significant quantity of chlorine on newly form oxide, which consequently might have some effect on the electrode properties. Another option is to use nitrate salts or organometallics. Ardizzone et al. [143] investigated the effect of chloride precursor and nitrate salt precursor on thermally prepared RuO_2. The results show that the volumetric charge of the prepared RuO_2 from the nitrate salts precursor was approximately

17 times larger the chloride precursor, while their volumetric curves were almost similar in shape. Further investigation revealed that the higher catalytic activity in the oxide formed from the nitrate is a result of lower crystallinity.

2.7.1.3 Coating deposition technique

Brush coating

Brush coating is one of the oldest techniques used to coat various objects. In this technique, a precursor applied by brush on the surface of the substrate, which efficiently penetrates into the subtle surface of the substrate. The main disadvantage is excess usage of precursor and uneven coating.

Dip coating

Dip coating is another method to coat the surface of the substrate and involves dipping the substrate into a precursor solution and then slowly removing the substrate from the precursor solution. Dip coating is a simple, reproducible and reliable technique and commonly used for coating continuous and curvy substrate [144]. The disadvantage is that produced coatings are inconsistent. Therefore it is not a good option for industrial scale [145].

Spray coating

In the spray coating process, a precursor solution is deposited on the surface of the substrate by using a spray gun connected to the air compressor. The substrate can be fixed at sloped or vertical configuration while the hand-held spray gun is moving along the substrate surface. To improve productivity and reproducibility, automated spray gun devices used in the industry. The coating thickness depends on the number of coating layers, a distance of the spray gun from the substrate, the concentration of the precursor and substrate temperature if equipped with a substrate heater. It is important to note that the coating layer formation

depends on how precursor droplet land on the substrate, solvent evaporation and any possible reaction [146].

2.7.1.4 Titanium substrate treatment

Sandblasting

To achieve the reproducible result from electrode coating, at first surface substrate should be treated under a systematic process. Sandblasting is a pre-treatment process in which substrate psychically smoothed and cleaned before the etching process. In this way, any castings mark or scratch on the surface of the metal is removed.

Etching

Further treatment on the titanium substrate is essential to improve surface roughness and adhesion of deposited films at the substrate surface. The etching is a chemical process that effectively treated the surface of the substrate by appropriate etching reagent. The common etching reagent is HF, HCl and oxalic acid [147, 148].

2.7.2 Electrodeposition method

Electrochemical deposition is another technique for preparation of electrode used in the industry. In this technique, metallic coating deposited on the surface of the electrode by passing an electric current through a metallic substrate that is immersed in a dissolved metallic species solution. The advantage of this technique to traditional deposition methods such as chemical vapour deposition (CVD), physical vapour deposition (PVD) and pulsed laser deposition (PLD) is that the deposition happens under atmospheric pressure and ambient temperature [149]. Due to cost-effective process and also flexibility in the control of the surface structure of oxide electrodes, electrodeposition technique finds many important

applications [150]such as supercapacitors [151, 152], solar cells [153, 154], corrosion protection coatings[155, 156] and semiconductor industry [157, 158].

2.7.3 PVD/CVD technique

Chemical vapour deposition (CVD) is a process of synthesising materials, in which a solid material from the vapour phase deposited by the decomposition of chemicals on the surface of the substrate. In contrast of CVD that relies on chemical reaction and its endothermic process, physical vapour deposition (PVD), relies on vacuum deposition and its exothermic process, in which thin films deposited by condensation of a vaporised form of a solid onto the substrate [159]. The main drawback of the CVD technique are: 1) need to prepare chemical precursors with high pressure which can be hazardous and extremely toxic, 2) toxic and corrosive by-products of the CD reactions, 3) operating at a high temperature above 600 °C which is not suitable for wide range of substrate materials, although this can be offset partially by using the metallo-organic CVD and plasma-CVD. The main disadvantage of PVD technique are operating under ultra-high vacuum and requirement of complex machines and high cost of coating [160].

Chapter 3

Investigating the kinetics and mechanism of organic oxidation in parallel with the oxygen evolution reaction

This chapter can be found published as:

Kariman, Asadollah, and Aaron T. Marshall. "Investigating the Kinetics and Mechanism of Organic Oxidation in Parallel with the Oxygen Evolution Reaction." ***Electrocatalysis*** **9.1 (2018): 31-39.**

3.1 Abstract

In this paper, the mechanism of organic oxidation in parallel with the oxygen evolution reaction at an electrode following the “active” anode mechanism is investigated. The active anode (IrO_2-Sb_2O_5-SnO_2/Ti) was prepared via standard thermal decomposition method and 4-nitrophenol (4-NP) chosen as the model organic compound. It is firstly confirmed that this anode does follow the “active” anode mechanism, with the rate of 4-NP oxidation being dependent on the coverage adsorbed oxygen on the surface of the anode. This surface coverage can be estimated by fitting steady-state polarisation curves with a micro-kinetic

model describing the oxygen evolution behaviour of the anode. This surface coverage dependent oxidation rate can only be observed at relatively low overpotentials where mass transport limitations are avoided. At high overpotentials, the rate of oxidation is completely controlled by mass transfer of 4-NP to the anode surface, with the measured and calculated rate constants agreeing closely. It is also shown that the instantaneous current efficiency can be directly calculated from the measured pseudo first order rate constant in both the kinetic and mass transport limited regimes. Using this analysis method, it was found that the instantaneous current efficiency for 4-NP oxidation is less than 100% in both regimes and only approached 100% at very low overpotentials. This finding is important as in prior literature, it is often believed that the instantaneous current efficiency of electrochemical wastewater oxidation will be 100% provided that mass transfer does not limit the process, due to an underlying assumption that the rate of organic oxidation is much larger than the OER.

3.2 Introduction

In recent years there has been expanding attention for ecological damage by industrial contamination, and as a result much research and development into new technologies for wastewater treatment is underway [20, 161-164]. Due to the variability of wastewater which is discharged by industrial activities [163], new advanced oxidation processes should be capable of treating toxic and non-biodegradable compounds [20, 165, 166].

Electrochemical wastewater treatment, where organic species are oxidized at anodes is a promising alternative to traditional processes as it has been shown to oxidise a range of compounds [5, 39, 164-177]. However, electrochemical oxidation has had limited penetration into industrial processes due to the high energy requirements for this process [169, 170]. The presence of the oxygen evolution reaction (OER) which occurs in parallel to the oxidation of organic compounds is the main cause for high energy consumption during electrochemical wastewater treatment as this lowers the current efficiency of the process [5, 169, 171]. Thus anodes with high overpotentials for the OER (known as non-active anodes [5, 169]) are

commonly used to increase current efficiency of organic reaction [5, 39, 169, 178], but this in turn increases the cell potential which again leads to high energy consumption.

In order to improve the current efficiency of the organic oxidation reaction, various metal oxides have been examined [168, 171, 179-182]. For example, SnO_2 and Sb-doped SnO_2 have been shown to be a good anodes for electrochemical wastewater treatment as they exhibit a high overpotential for the oxygen evolution reaction and are inexpensive relative to anodes which incorporate noble metal oxide coatings [171, 183]. SnO_2 based anodes are normally considered to be non-active anodes [5, 169, 171], where the organic oxidation mechanism involves the generation of hydroxyl radicals [168] which subsequently oxidise the organics at electrode interface and within the bulk of the electrolyte [184, 185]. This generally leads to the complete oxidation of organic compounds due to the high activity and low selectivity of the hydroxyl radical for organic oxidation [168, 185]. While SnO_2 or Sb-doped SnO_2 anodes exhibit good electrochemical wastewater treatment performance, by adding a small amount of IrO_2 or RuO_2 to Sb_2O_5-SnO_2 anodes, the service life and catalytic activity of the anodes can be increased dramatically [171]. However, given that both IrO_2 and RuO_2 are excellent electrocatalysts for the OER, it is unclear if these additions to SnO_2 based anodes will suppress the formation of the hydroxyl radicals in favour of oxygen gas.

As the mechanism for organic oxidation is normally suggested to involve intermediates of oxygen evolution [168, 186], it seems inevitable that oxygen evolution will occur in parallel with organic oxidation. The relative magnitude of these reactions will depend on both the inherent kinetics of the two reactions and the rate of mass transfer of the organic species into the reaction zone. The latter case means even anodes with extremely poor OER kinetics, will evolve oxygen under conditions where the applied current is larger than the rate at which organics can be transported from the bulk electrolyte into the reaction zone [39, 187]. For boron-doped diamond (non-active) anodes, it has been shown that it is possible to balance the organic mass transfer rate with rate of the organic oxidation reaction to achieve a current efficiency of 100% with almost complete oxidation of the organic species [175]. For non-active electrodes, this balance can be achieved as the inherent reaction rate between the generated hydroxyl radicals is both fast and independent of electrode potential. This balance however

is much more difficult for active anodes. Even at applied currents above the theoretical mass transfer limited organic oxidation rate, the fraction of current which goes to the OER will be dependent of the relative kinetics of the OER and the organic oxidation reactions [186]. Clearly as the organic oxidation is mediated via the higher-oxide surface species (e.g. IrO_3) for active anodes, and as the surface coverage of these species is potential dependent, balancing reaction rate and mass transfer to achieve high current efficiencies is much more challenging.

Indeed, it conceivable that the current efficiency can be close to zero if the rate constant of organic oxidation is much smaller than that for the OER [188]. Despite this, in some cases, an assumption that organic oxidation reaction is much faster than the oxygen evolution reaction has been successfully applied in models and validated by experiment [174, 189] even at electrodes which are known to be very active for oxygen evolution [182].

In the present study, we have investigated the oxidation of 4-nitrophenol (4-NP) at IrO_2-Sb_2O_5-SnO_2/Ti anodes to gain insights into the reaction mechanism and process efficiency. Firstly, given that SnO_2 is considered a non-active anode whereas IrO_2 an active anode, we have attempted to determine whether this mixed IrO_2-Sb_2O_5-SnO_2 electrode behaves as an active or non-active anode. Secondly, given that the vast amount of literature on electrochemical wastewater treatment investigates the process under mass transfer limited conditions, we have also attempted to measure the kinetics of the organic oxidation reaction in absence of any mass transfer limitations so that the dependence of reaction rate on the higher-oxide surface coverage can be established and compared to a micro-kinetic model. And finally, we develop a simple set of equations which can be used to estimate the instantaneous current efficiency from an experimentally determined rate constant.

3.3 Experimental

Dimensionally stabilized anodes were prepared by coating a titanium substrate with a IrO_2-Sb_2O_5-SnO_2 layer using the standard thermal decomposition technique [190]. Briefly, the titanium discs (Grade 2, diameter=45mm) were etched in concentrated HCl in an ultrasonic

bath for 40 minutes, then rinsed in deionized water and isopropanol, before being dried at 105. A precursor solution was prepared by dissolving 0.16 g of $IrCl_3.3H_2O$ (99.8%, Sigma-Aldrich), 1 g of $SnCl_2$ (98%, Sigma-Aldrich) and 0.1 g of $SbCl_5$ (99.99%, Sigma-Aldrich) into 9 mL of isopropanol (99.9%, ASCC) and 1 mL of concentrated HCl (37%, Fisher chemical). The precursor solution composition was chosen to achieve the an anode coating similar to that described by Adams et al. [171] of 10 wt% IrO_2 and 90 wt% Sb_2O_5-SnO_2 (Sn:Sb molar ratio 16:1). Approximately 0.2 mL of this precursor solution was sprayed on the titanium disk held at 80 °C before heating at 450 °C in air for 10 minutes to oxidise the precursor. This spray / heating process was repeated five times before the final layer was annealed for 1 hour at 450 °C. The final total oxide loading was measured gravimetrically to be approximately 1 mg cm^{-2}.

The electrochemical measurements were carried out in a parallel plate electrode flow cell connected to a continuous stirred 150 mL electrolyte reservoir via a peristaltic pump (Masterflex console drive). The electrolyte was 0.5 M Na_2SO_4 (99.4%, Labserv) acidified to pH 1.75 (using concentrated sulfuric acid) with or without the addition of 4-NP (99%, BDH) and the flow rate set at 160 mL min^{-1}. The anode in this cell was the prepared IrO_2-Sb_2O_5-SnO_2/Ti electrode, the cathode was a stainless-steel plate and a saturated calomel reference electrode (SCE) was placed in the electrolyte reservoir. The space between anode and cathode was 1 cm and the each of these electrodes had an exposed area of 12.56 cm^2. To account for the ohmic resistance between the anode and the reference electrode, electrochemical impedance spectroscopy was measured over a frequency range of 100 kHz to 10 mHz, with an AC amplitude of 10 mV and a DC potential of 0.6 V vs SCE. Typically, the resistance between the anode and the reference electrode was around 1 Ω, and was used to compensate the IR drop after the cyclic voltammetry and polarization measurements. A Gamry Interface 1000 potentiostat was used to control the electrochemical measurements. All potentials in this paper are referenced against the SCE unless otherwise stated.

As the mass transport behaviour within the electrochemical flow cell has a strong influence on the current efficiency of 4-NP oxidation, the diffusion layer thickness (δ) at the anode under the hydrodynamic conditions used in this work was measured using the Fe^{3+}/Fe^{2+} redox

couple (5 mM $NH_4Fe(SO_4)_2$ and $FeSO_4$ in 0.5 M H_2SO_4). Briefly, a gold wire (diameter 1 mm) was embedded in an acrylic disc and used in place of the anode. Then the mass transport limiting current density for the reduction of Fe^{3+} to Fe^{2+} was measured over a range of flow rates and the diffusion thickness layer calculated from:

$$\delta = \frac{nFDC_{bulk}}{i_{lim}} \tag{3-1}$$

Where i_{lim} is the limiting current density (A cm^{-2}), n is the number of electrons transferred, F the Faraday constant (96485 C mol^{-1}), D is the diffusion coefficient of Fe^{3+} (5.6×10^{-6} cm^2 s^{-1}) [191], C_{bulk} is the concentration of the Fe^{3+} in the bulk of the electrolyte (mol cm^{-3}). At the typical electrolyte flow rate of 160 mL min^{-1}, this yielded a diffusion layer thickness of 95 μm.

The potentiostatic oxidation of 4-NP was conducted between 1.2 and 1.5 V vs SCE to ensure both the kinetically and mass transport limited oxidation regimes were observed. During the oxidation, electrolyte samples were taken periodically, and the concentration of 4-NP determined spectroscopically using a UV/Vis spectrophotometer (UV-1600PC, VWR). Here, it was found that the absorbance peak at 319 nm was directly proportional to concentration of 4-NP between 0 and 0.15 mM in agreement with others [171]. It was also found that the 4-NP was stable (no observed changes in the UV/Vis spectra) in 0.5 M Na_2SO_4 at pH=1.75 for at least 5 weeks, indicating that any changes in the UV/Vis spectra during potentiostatic oxidation can be contributed to the electrochemical process.

3.4 Results and Discussion

While the anodic oxidation of organic molecules at electrodes have fairly complex reaction mechanisms, some useful insights can be gained by considering simple cases. The two most important general mechanisms for the oxidation of organics at anodes were first proposed by Comninellis [168], and are based on either “active” or “non-active” anodes. For active anodes,

the oxidation of the organic is mediated by the higher-oxide (S-O, e.g. IrO_3) formed on the anode surface at potentials above the thermodynamic OER potential, whereas on non-active anodes the organic is oxidised by hydroxyl radicals generated by anode. Given that the potential for hydroxyl radical generation is 2.74 V vs NHE [192], if the anode operates at potentials much lower than this, it seems reasonable to assume that hydroxyl generation will be negligible. This is certainly consistent with IrO_2 anodes which are known to operate at low anodic potentials (IrO_2 is an excellent electrocatalyst for the OER) and have been shown not to generate significant quantities of hydroxyl radicals [168]. Furthermore, both boron-doped diamond and SnO_2 anodes are known to generate hydroxyl radicals and are typically found to have very high overpotentials for the OER. In this work, it has been found that the IrO_2-Sb_2O_5-SnO_2/Ti anode can operate the OER at a current density of 10 mA cm^{-2} with an overpotential of only 360 mV, which is consistent with others who show that additions of as low as 0.5 mol% IrO_2 to SnO_2 anodes can dramatically lower the overpotential for the OER [193]. Thus, it is assumed that the IrO_2-Sb_2O_5-SnO_2/Ti anode is unlikely to generate the hydroxyl radical and therefore will operate via the "active" anode mechanism. To ensure that the mechanism is consistent with proposed mechanisms for the OER, here it is the higher-oxide is formed via the electrochemical oxide path [194]:

$$S + H_2O \rightleftharpoons S - OH + H^+ + e^- \quad \text{(R1)}$$

$$S - OH \rightleftharpoons S - O + H^+ + e^- \quad \text{(R2)}$$

$$S - O \rightleftharpoons S + \frac{1}{2}O_2 \quad \text{(R3)}$$

Where S is a free-surface site. The higher-oxide formed in step two of the OER mechanism can form oxygen gas via reaction R3 or oxidise an organic molecule (R) via reaction R4:

$$S - O + R \longrightarrow S + RO \quad \text{(R4)}$$

Thus, it should be expected that oxygen gas evolution will compete with the oxidation of organics within an electrochemical wastewater treatment process, when the anode potential is above 1.23 V vs RHE. However, as the thermodynamic requirements for organic oxidation

are often lower than that for oxygen evolution, it is possible that oxidation of organic compounds can occur below 1.23 V vs RHE. In this work, this possibility was assessed via cyclic voltammetry.

3.4.1 Cyclic voltammetry measurement

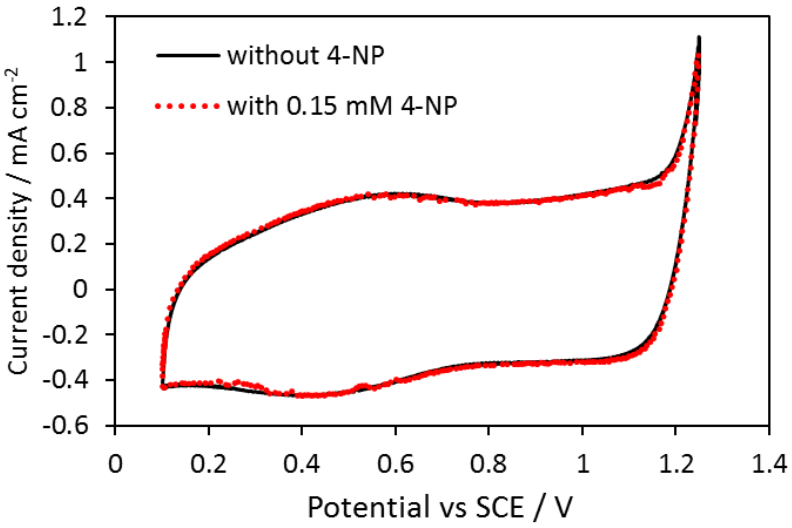

Figure 3-1 Cyclic voltammetry of the IrO_2-Sb_2O_5-SnO_2/Ti electrode in 0.5 M Na_2SO_4 and in 0.5 M Na_2SO_4 containing 0.15 mM 4-NP. Sweep rate = 50 mV/s, pH=1.75

These cyclic voltammetry measurements revealed that almost no difference between the electrochemical behaviour of the IrO_2-Sb_2O_5-SnO_2/Ti anode in 0.5 M Na_2SO_4 and 0.15 mM 4-NP in 0.5 M Na_2SO_4 solution (Figure *3-1*). The rather featureless voltammograms in 0.5 M Na_2SO_4 is consistent with the behaviour of IrO_2 and SnO_2 anodes prepared by thermal decomposition [171, 195] with only double-layer charging and pseudo-capacitive behaviour observed at potentials between 0.1 and 1.15 V. As the potential is swept above 1.15 V (1.29 V vs RHE), an anodic current most likely originating from oxygen evolution is observed in both electrolytes. Importantly, no evidence to suggest the anodic oxidation of 4-NP occurs between 0.1 and 1.1 V, and thus we conclude that the oxidation of 4-NP must occur at potentials high enough for oxygen evolution (i.e. above 1.15 V).

3.4.2 Activity of electrodes towards the electrochemical oxidation of 4-NP

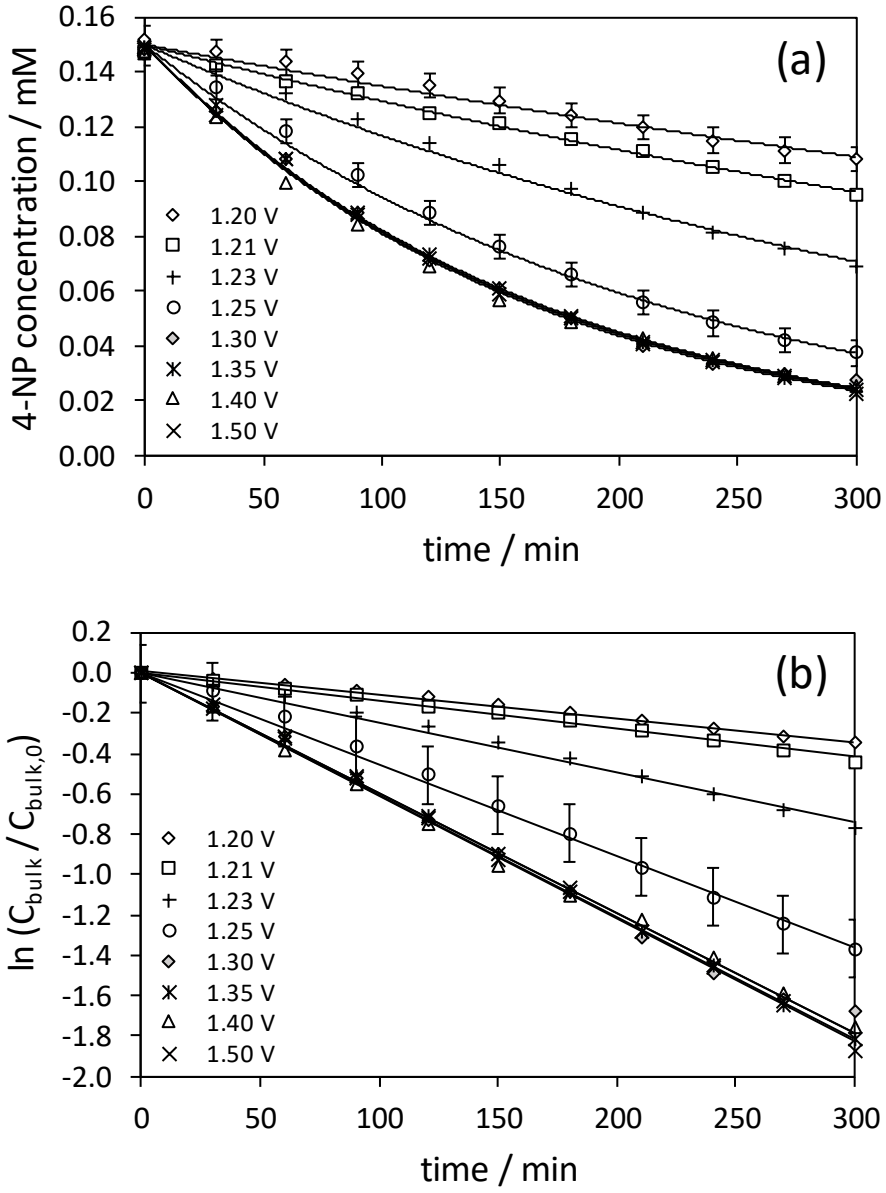

Figure 3-2: Potentiostatic electrolysis of a 0.5 M Na_2SO_4 solution (pH=1.75) initially containing 0.15 mM of 4-NP. (a) Concentration (C_{bulk}) vs time, (b) first-order plot of $ln(C_{bulk}/C_{(bulk,0)})$

At potentials above 1.2 V, the anodic oxidation of 4-NP is observed by monitoring the absorbance at 319 nm. As the potential increases from 1.2 V, the overall oxidation rate also increases until 1.3 V, after which no further changes in the 4-NP concentration vs time behaviour was observed (Figure *3-2* a). Clearly no further enhancements in the oxidation rate

of 4-NP can be achieved above 1.3 V, suggesting either electrode kinetics or mass transport begins to limit the oxidation rate above 1.3 V. The oxidation rate is to be pseudo first order in respect to the 4-NP concentration with linear $ln(C_{bulk}/C_{(bulk,0)})$ vs time behaviour found over the entire potential range examined (Figure *3-2* b). Assuming that the rate of the 4-NP oxidation (equation 4) is given by:

$$\frac{dC_{bulk}}{dt} = -k_4\theta_O C_{bulk} \quad (3\text{-}2)$$

where k_4 is the rate constant for reaction R4, θ_O is the surface coverage of the higher oxide (S-O) and C_{bulk} is the concentration of 4-NP in the electrolyte bulk. This can be simplified further to be a pseudo first order reaction, if it is assumed that the surface coverage of the higher-oxide is approximately constant throughout the electrolysis time:

$$\frac{dC_{bulk}}{dt} = -k_{4,app}C_{bulk} \quad (3\text{-}3)$$

Where the pseudo first order reaction rate constant is $k_{4,app} = k_4\theta_O$.

3.4.3 Influence of potential on the oxidation of 4-NP

As with the overall 4-NP oxidation rate, the calculated pseudo first order rate constant is clearly found to increase with potential until 1.3 V (Figure *3-3*). Above this potential, as no further increase in the pseudo first order rate constant occurs, any further additional current above that found at 1.3 V will be wasted in reactions other than 4-NP oxidation (most likely the oxygen evolution reaction).

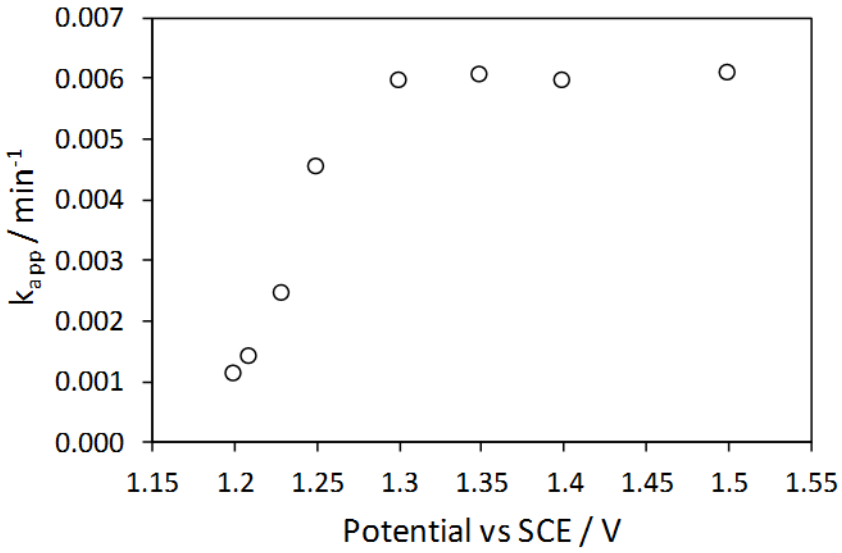

Figure 3-3: The dependence of the first order rate constant ($k_{4,app}$) on applied potential at the IrO_2-Sb_2O_5-SnO_2/Ti anode. The maximum uncertainty in the calculated rate constant (95% confidence interval) was found to be 2 $\times$ 10^{-4} min^{-1}.

3.4.4 The polarisation curve experimental and simulation

To understand why the pseudo first order rate constant is potential dependent between 1.2 and 1.3 V, first the potential dependence of the higher-oxide surface coverage (θ_O) is examined. This can be estimated by fitting the OER behaviour of the anode (i.e. a polarisation curve in absence of 4-NP) to a micro-kinetic model of the OER following the electrochemical oxide pathway [196]. Briefly, the reaction rates for each step in the OER (R1-R3) are given by:

$$r_1 = k_1 C_{H_2O}(1 - \theta_{OH} - \theta_O) - k_{-1} C_{H^+} \theta_{OH} \quad (3\text{-}4)$$

$$r_2 = k_2 \theta_{OH} - k_{-2} C_{H^+} \theta_O \quad (3\text{-}5)$$

$$r_3 = k_3 \theta_O - k_{-3} C_{O_2}^{1/2}(1 - \theta_{OH} - \theta_O) \quad (3\text{-}6)$$

where k_1 and k_{-1} etc. are forward and back rate constants and C are concentrations of protons or dissolved oxygen. θ_{OH} and θ_O are the surface coverage of OH and O respectively.

As steps R1 and R2 are electrochemical reactions, the rate constants k_1, k_{-1},k_2, and k_{-2} are potential dependent as per Butler-Volmer kinetics, e.g.:

$$k_i = k_i^0 \exp^{\frac{\beta F}{RT}(E-E_{rev})} \tag{3-7}$$

$$k_{-i} = k_{-i}^0 \exp^{\frac{-(1-\beta)F}{RT}(E-E_{rev})} \tag{3-8}$$

where, E and E_{rev} are the anode and reversible potential for the OER respectively and β, F, R and T are the symmetry factor, Faraday constant, gas constant and temperature respectively. While it is often assumed that β = 0.5, as this is know to differ from 0.5 for processes involving adsorbed species [197], β is allowed to vary during the fitting procedure. From these kinetic equations, the differential equations describing the surface coverages of S-OH and S-O can be solved at steady-state to give:

$$\theta_{\mathrm{O}} = \frac{\dfrac{k_{-3}C_{\mathrm{O_2}}^{1/2}}{k_{-3}C_{\mathrm{O_2}}^{1/2} - k_2} - \dfrac{k_1 C_{\mathrm{H_2O}}}{k_1 C_{\mathrm{H_2O}} + k_{-1}C_{\mathrm{H^+}} + k_2}}{\dfrac{k_{-2}C_{\mathrm{H^+}} - k_1 C_{\mathrm{H_2O}}}{k_1 C_{\mathrm{H_2O}} + k_{-1}C_{\mathrm{H^+}} + k_2} - \dfrac{-k_{-2}C_{\mathrm{H^+}} - k_3 - k_{-3}C_{\mathrm{O_2}}^{1/2}}{k_{-3}C_{\mathrm{O_2}}^{1/2} - k_2}} \tag{3-9}$$

$$\theta_{\mathrm{OH}} = \frac{\theta_{\mathrm{O}}\left(-k_{-2}C_{\mathrm{H^+}} - k_3 - k_{-3}C_{\mathrm{O_2}}^{1/2}\right) + k_{-3}C_{\mathrm{O_2}}^{1/2}}{k_{-3}C_{\mathrm{O_2}}^{1/2} - k_2} \tag{3-10}$$

These surface coverages are used along with the rate constants to determine the reaction rates and thus the OER current density (i_{OER}) as a function of potential at steady-state:

$$i_{\mathrm{OER}} = F(r_1 + r_2) \tag{3-11}$$

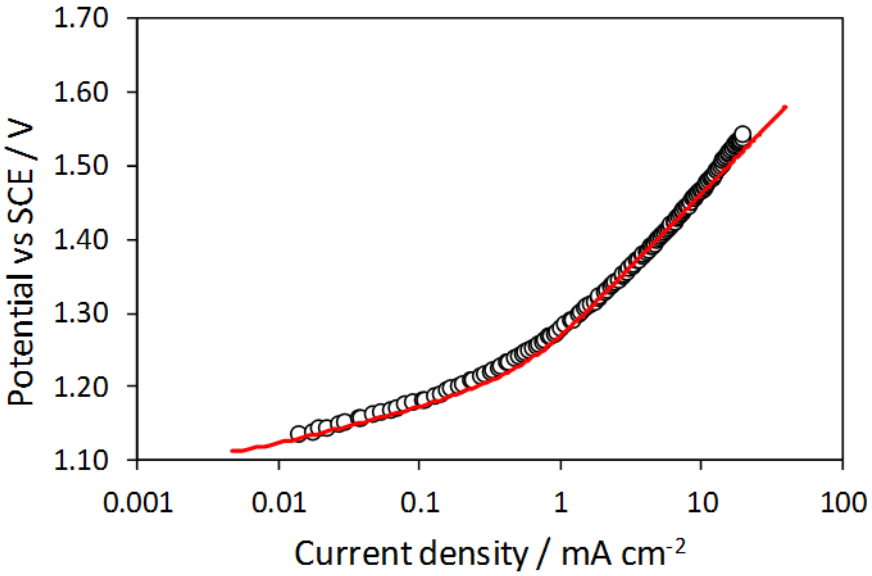

Figure 3-4: Comparison between the experimentally measured (circles) and the calculated (line) oxygen evolution reaction steady-state polarisation curves in 0.5 M Na_2SO_4 at pH=1.75.

Here is it found that this kinetic model fits the experimentally determined OER polarisation curve reasonably well (Figure *3-4*), with the high Tafel slope (≈ 140 mV) suggesting that the initial discharge of water (R1) is the rate determining step for the OER reaction on this IrO_2-Sb_2O_5-SnO_2/Ti anode. It is also found that the surface coverage of S-O increases from close to 0 to almost 1 between 1.1 and 1.3 V (Figure *3-5*). This increase in the surface coverage of S-O with potential, agrees well with the measured increase the pseudo-first order rate constant ($k_{4,app} = k_4\theta_O$) and suggest that this is the main reason for the potential dependence in the rate constant. As the surface coverage approaches 1 above 1.3 V, it is possible that this could limit the organic oxidation reaction rate. However, as that initial step in the overall reaction mechanism is that rate limiting step, in this case it is unlikely that the apparent limit in the rate constant above 1.3 V is related to inherent kinetics. Rather it seems more likely that this limit is related to the mass transport of organic from the bulk to the electrode surface.

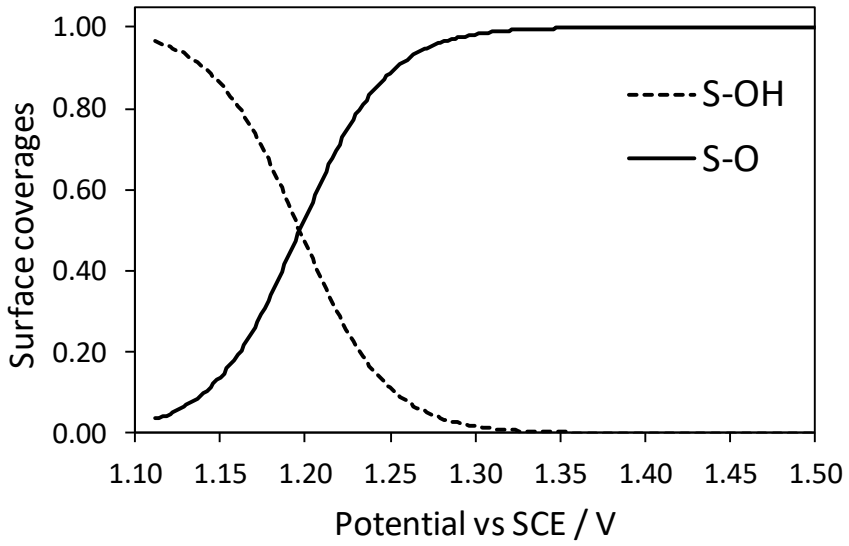

Figure 3-5: Calculated surface coverages of the surface bound intermediates during the oxygen evolution reaction at pH=1.75.

To investigate this hypothesis, the pseudo first order rate constant under mass transport control was determined. Given that the change in 4-NP concentration within the bulk of the electrolyte will be equal to the mass transport across the diffusion layer to the electrode surface, the change in 4-NP concentration (C_{bulk}) with time is described by:

$$\frac{dC_{bulk}}{dt} = -\frac{DA}{\delta V}\left(C_{bulk} - C_{surf}\right) \tag{3-12}$$

When the oxidation of 4-NP at the electrode surface is controlled by mass transfer, the surface concentration of 4-NP (C_{surf}) will be zero. With this, by comparing equations 3 and 12, the pseudo first order rate constant under mass transport control ($k_{4,app,lim}$) can be calculated by:

$$k_{4,app,lim} = \frac{DA}{\delta V} \tag{3-13}$$

Using a diffusion coefficient (D) of 0.919$\times 10^{-5}$ cm^2 s^{-1} [198], an experimentally determined diffusion layer thickness (δ) of 95 µm, an anode area (A) of 12.56 cm^2 and an electrolyte volume (V) of 150 mL, the pseudo first order rate constant for a mass transport limited process ($k_{(app,lim)}$) at our hydrodynamic conditions is calculated to be 0.0056 min^{-1}. This value

agrees closely with the observed limit in the measured pseudo first order rate constant (0.0060 min^{-1}, Figure *3-3*) which confirms that the electrochemical oxidation of 4-NP is limited by mass transport at potentials above 1.3 V.

3.4.5 Investigation on current efficiency

As the 4-NP oxidation rate is limited by mass transport above 1.3 V, it must be concluded that the instantaneous current efficiency for 4-NP oxidation must be below 100% and thus energy is wasted in the OER. This is well understood in the previous literature and many have developed models to estimate the instantaneous current efficiency under mass transport limiting rates [174, 182, 189, 199]. However, below 1.3 V, the results here suggest that the oxidation of 4-NP will not be limited by mass transport and is instead limited by the production rate of the S-O on the surface of the anode. As the 4-NP oxidation will compete with the final step of the OER reaction for these surface bound O species, it is important to estimate the instantaneous current efficiency. In previous models [174, 182, 189, 199], it has been assumed that the organic oxidation rate is must faster than the final recombination step of the OER mechanism, which results in the prediction that in absence of any mass transport limitations, the instantaneous current efficiency will be 100%. To investigate whether this is indeed the case, here the equivalent current density going to 4-NP oxidation is estimated and compared with the actual current density measured throughout the experiment.

In order to calculate the equivalent current density going to 4-NP oxidation (i_{4NP}) the following approach was used. Firstly, this current density can be directly related to the change in 4-NP concentration by:

$$\frac{dC_{bulk}}{dt} = -\frac{i_{4NP}}{nF}\frac{A}{V} \tag{3-14}$$

where n represents the number of electrons which must be transferred as part of the first two steps of the OER mechanism to oxidise a 4-NP molecule. For the oxidation of 4-NP, the minimum value for n is 2 and the maximum value is 28 [200]. The logical products formed by a $n = 2$ oxidation would be 4-nitrocatechol or hydroquinone as these have been observed

during solution phase oxidation [201]. However, we did not observe any development of UV/Vis absorbance peaks consistent with 4-nitrocatechol (309 and 345 nm [202]) or hydroquinone (288 nm [203]) and so it seems unlikely that these compounds are the final oxidation products from 4-NP. It is also possible that 1,4-benzoquinone could form via a $n = 4$ oxidation and we did observe small absorbance peaks around 245 nm which could be consistent with 1,4-benzoquinone [203], although we suspect that this just indicates that 1,4-benzoquinone is one of the intermediates of complete 4-NP oxidation as others have confirmed that complete oxidation of 4-NP to CO2, H2O and HNO3 is possible [204]. To provide an accurate measurement of the equivalent electrons used during 4-NP oxidation either total carbon analysis or complete product identification and quantification would be required. Rather, here the maximum possible instantaneous current efficiency is determined by assuming that the disappearance of 4-NP (as detected by UV/Vis spectroscopy) corresponds to complete oxidation ($n = 28$). Integrating equation 3 gives:

$$C_{bulk} = C_{bulk,0}\exp^{-k_{4,app}t} \tag{3-15}$$

and thus with equation 3:

$$\frac{dC_{bulk}}{dt} = -k_{4,app}C_{bulk,0}\exp^{-k_{4,app}t} \tag{3-16}$$

Using this with equation 14 then gives:

$$i_{4NP} = -\frac{k_{4,app}C_{bulk,0}nFV}{A}\exp^{-k_{4,app}t} \tag{3-17}$$

and then instantaneous current efficiency (ICE) for 4-NP oxidation can be determined from:

$$ICE = \frac{i_{4NP}}{i_{total}} \tag{3-18}$$

As expected, the calculated current density resulting in 4-NP oxidation is found to increase with potential until 1.3 V (Figure 3-6) after which this current becomes limited by mass transport (or possibly reaction kinetics).

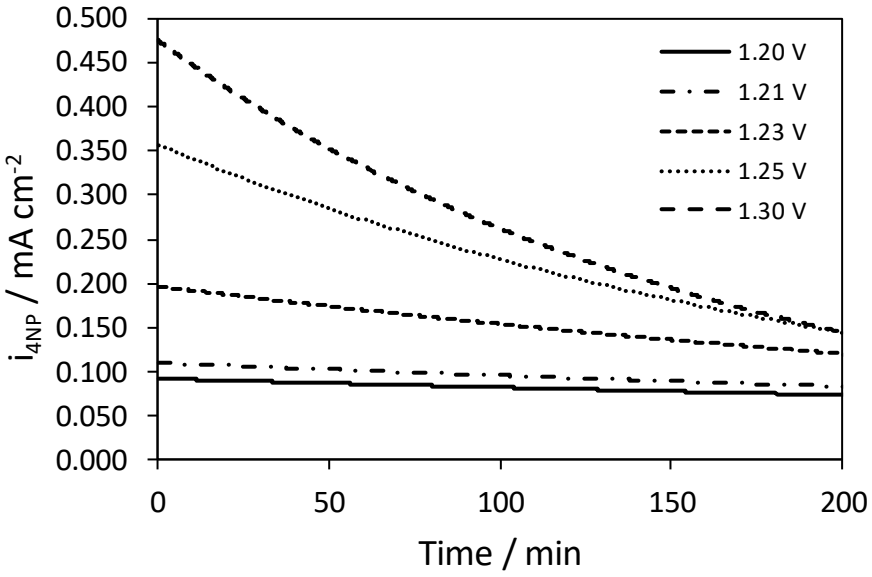

Figure 3-6 Calculated current density of 4-NP oxidation (i_{4NP}) as a function of time at potentials between 1.2 and 1.3 V vs SCE. Above 1.3 V, as the reaction rate becomes limited mass transport, the 4-NP oxidation current densities become the same

Interestingly, the ICE is seen to increase in the first 30 min of 4-NP oxidation (Figure *3-7*) which reflects the significantly higher current observed at the start of electrolysis period. It is likely that while the 4-NP oxidation current density slowly decreases over time as the 4-NP is removed, the OER may be slightly poisoned in the first 30 minutes which decreases the kinetics of the OER, and thus improves the ICE for 4-NP oxidation. This analysis clearly shows that the ICE can be less than 100% when the 4-NP oxidation reaction is limited by kinetics rather than mass transport. This finding is important as it indicates that it cannot always be assumed that the organic oxidation reactions will be much faster than the OER when using anodes known to be active for the OER.

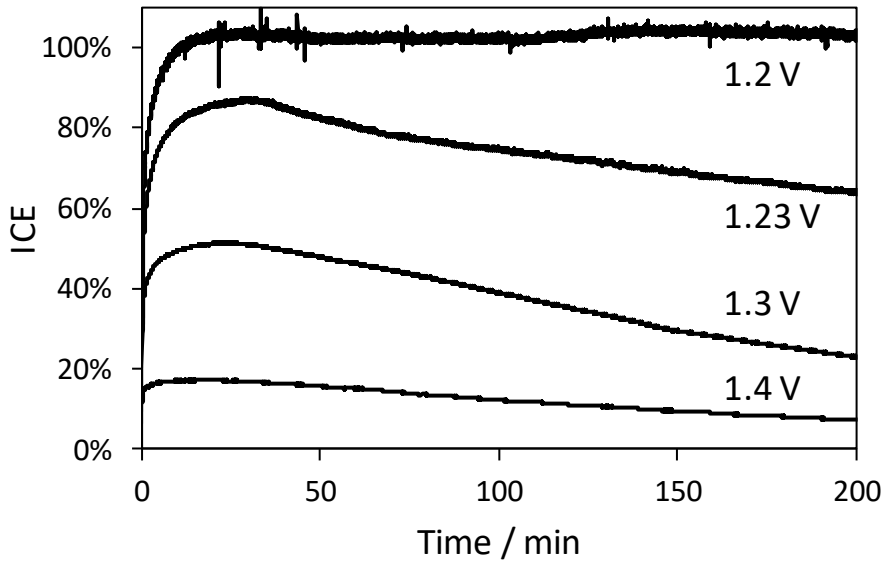

Figure 3-7 Instantaneous current efficiency over time as function of anode potential

By integrating the current going to 4-NP oxidation over 200 minutes of oxidation and comparing this with the total charge passed during this time, the general current efficiency can be determined (Figure *3-8*). As expected from the ICE results, the general current efficiency is highest at the lowest anode potentials and decreases continuously with increasing anode potential. Between 1.2 and 1.3 V, the decrease in general current efficiency is due to the increasing rate of the OER kinetics relative to the kinetics of 4-NP oxidation. In this case, the OER kinetics increase faster than the kinetics of 4-NP oxidation as the final step of the OER is proportional to the square of the S-O surface coverage, whereas the kinetics of 4-NP are directly proportional to the S-O surface coverage. Above 1.3 V, the continued decrease in the general current efficiency is dominated by the limitation in the mass transport of 4-NP from the bulk of the electrolyte to the anode surface.

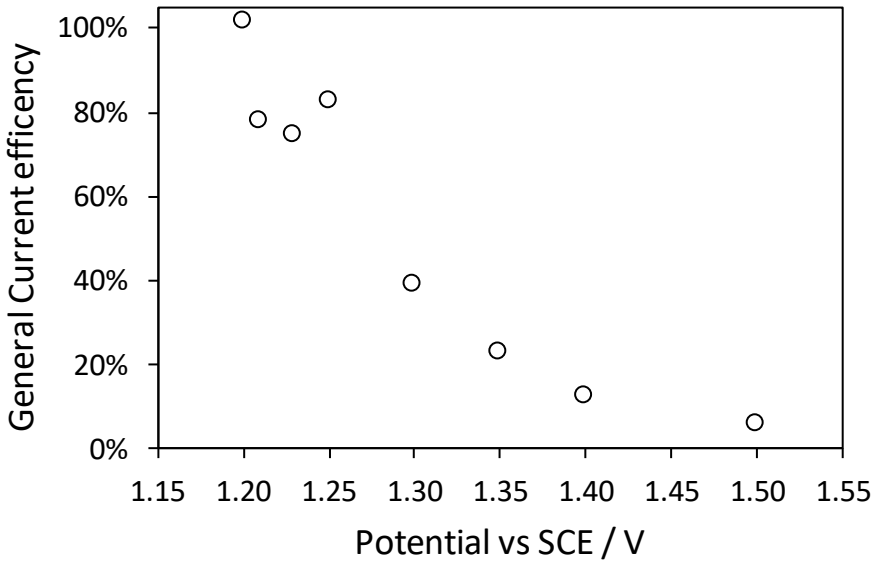

Figure 3-8 General current efficiency over 200 min of oxidation as a function of anode potential

Based on our results, some general conclusions can be reached regarding electrochemical wastewater oxidation at oxide anodes following the "active" electrode mechanism. Firstly, the oxidation should always be conducted at potentials (or current densities) below where mass transport limits the oxidation rate. Secondly, it is clear that even under conditions where mass transport does not limit the oxidation rate, the OER can still consume a significant proportion of the supplied current. Under these conditions, to improve the energy efficiency of electrochemical wastewater treatment, the anodes must promote organic oxidation over the OER. Hence, to obtain more efficient anode for organic oxidation, anode material should have the following characteristics:

• Capable of generating adsorbed hydroxyl radical fast enough at which high coverage of higher oxide (S-O) on the anode surface is obtained.

• The electrocatalytic of anode material should be in favour of fast reaction to organic oxidation or very slow for oxygen evolution reaction

• The anode coating structure should provide high active surface area, this leads to increase in the electrocatalytic performance of the anode.

3.5 Conclusions

In this study, the inherent kinetics of the 4-NP oxidation reaction at IrO_2-Sb_2O_5-SnO_2/Ti anode have been investigated. It has been shown that potential dependence of the pseudo first order oxidation rate constant is consistent with potential dependence of the S-O surface coverage, which strongly suggests that this anode follows the "active" anode mechanism. The potential range where the oxidation is limited by reaction kinetics is quite narrow (1.2-1.3 V), with the oxidation rate of 4-NP becoming limited by mass transport above 1.3 V. For anodes following the "active" anode mechanism, operating below the mass transport limiting conditions is critical to maximising the ICE for the process. Contrary to the common assumption that the organic oxidation reaction will be much faster than the OER in absence of mass transport limitations, we find that this is only true at low overpotentials and thus conclude that determining the ICE under the expected process conditions is important. By using a simple reaction model, our analysis shows that the evaluation of the ICE by using a measured rate constant is a useful method to understand the performance of electrochemical wastewater oxidation. Specifically, we show that it is possible to directly calculate the current going to 4-NP oxidation compared with the OER and thus the instantaneous and general current efficiencies can be determined as a function of time and potential. The most efficient wastewater oxidation process is when the anode potential is as low as possible due to the differences in dependences of the OER and 4-NP oxidation rate on the S-O surface coverage. Thus, it must be concluded that to improve the efficiency of electrochemical wastewater oxidation processes, the anode materials should have at high coverage of adsorbed oxygen at low potentials. It should also be noted that by operating at low anode potentials, the processes energy efficiency will also be increased due to the smaller cell potentials which would be required. While low anode potentials will improve current and energy efficiency, the net rate of 4-NP oxidation is low and thus a compromise between higher net oxidation

rates and process efficiency may be required if such a process was to be implemented in an industrial setting.

Chapter 4

Improving the stability of DSA electrodes by the addition of TiO_2 nanoparticles

This chapter can be found published as:

Kariman, Asadollah, and Aaron T. Marshall. "Improving the Stability of DSA Electrodes by the Addition of TiO2 Nanoparticles." ***Journal of The Electrochemical Society*** **166.8 (2019): E248-E251.**

4.1 Abstract

Dimensionally stable anodes (DSA) are widely used in water electrolysis, cathodic protection, wastewater treatment, metal electrowinning and chlor-alkali industry. An important parameter of these anodes is their lifetime under harsh anodic conditions. In this work, the incorporation of nanoparticles into a thermally prepared IrO_2 anode as a way of improving its service lifetime was investigated. The results show that incorporation of up to 25 wt% nanoparticles into the coating formed crack-free structure during the thermal decomposition process and thus enhances the service lifetime of modified electrode dramatically by up to 10x compared to the pure IrO_2 anode. Importantly, these nanoparticle additions have minimal

effect of the anodes performance towards the oxygen evolution reaction. Further addition of nanoparticles reduced the lifetime of the anode due to uneven distribution of the active coating over the substrate leading to electrolyte penetration to, and passivation of, the underlying titanium substrate. It is proposed that adding the right quantity of nanoparticles into the IrO_2 layer improved the anodes lifetime by minimising electrolyte penetration to the substrate while increasing the mechanical strength of the layer.

4.2 Introduction

Dimensionally stable anodes (DSA), have been widely used for water electrolysis, electro chlorination, cathodic protection, wastewater treatment, and metal electrowinning [36, 169, 205-207]. While these anodes have achieved wide-spread use in industry, they can still suffer from short service lifetimes in the strongly acidic and anodic conditions in which they often operate in. In general, the failure or deactivation of DSA is caused by a combination of substrate passivation and dissolution of the active electrocatalytic layer [208-211]. In order to overcome this problem, additional oxides such as TiO_2, Ta_2O_5, or SnO_2 are often added to the electrocatalytic oxide layer to improve the corrosion resistance of the active IrO_2 and RuO_2 materials.[212-214]. Others have used thin interlayers between the active coating and metallic substrate in order to reduce the passivation of the electrode by preventing penetration of electrolyte through the active oxide layer to the substrate [209, 211, 215-218].

As cracks in the DSA active layer facilitate electrolyte penetration to the underlying substrate [205, 211], the observations that the presence of nanoparticles within the active layer can reduce these cracks [218, 219], may suggest that adding nanoparticles to DSA can improve service lifetimes. This is partially supported by others who suggest the improved service lifetime of a IrO_2 anode when a nanoparticle-like SiO_2 interlayer was used was attributed to both the suppression of electrolyte transport to the Ti substrate and improved mechanical strength of the resulting composite layer [217]. This proposed strengthening of the nanoparticle composites has been widely investigated in other systems, with many reporting

enhanced wear resistance of the when nanoparticles are added into surface coatings [220-222]. Others have found that TiO_2 nanoparticles added into electrochemically deposited PbO_2 films can significantly change the microstructure of the film, and improves service life of the electrode under strong anodic conditions [223].

In this research, the incorporation of TiO_2 nanoparticles into IrO_2 DSA layers is investigated as a means to improve the service lifetime of these electrodes. The morphological and electrochemical properties of these nanoparticle modified IrO_2 electrodes are determined to understand and quantify the impact this nanoparticle addition has on the oxygen evolution reaction, the electrochemically active surface area and the service lifetime under accelerated testing conditions.

4.3 Experimental methods

Titanium substrates (15.5 × 17 mm) were pre-treated by etching in 10 % hydrochloric acid at room temperature for 1 h, before rinsing with deionised water and drying at room temperature. The precursor solution was prepared by mixing a solution of 0.02 M $IrCl_3$ (99.9%, American Elements) in deionised water with a suspension of 0.02 M TiO_2 nanoparticles (Degussa P25 99.9%) in isopropanol. P25 TiO_2 nanoparticles is a standard material found in applications (especially photocatalysis) and is characterised as mixture of anatase and rutile (75-84 % anatase) with a BET surface area of approximately 49 $m^2\ g^{-1}$, and average crystallite sizes of 25-29 nm (anatase phase) and 55-85 nm (rutile phase) [224, 225]. The size of the TiO_2 nanoparticles used in this work are larger than those used to stablise PbO2 films (approx. 5 nm) [223], but are smaller than the SiO_2 particle-life film used to stabilise IrO_2 films (approx. 500 nm) [217]. The mixture of $IrCl_3$ and TiO_2 nanoparticles was ultrasonicated (Alphatech) for at least 5 minutes to ensure that the TiO_2 nanoparticles were well-dispersed. This suspension was typically stable for at least 2 hours without evidence of settling or separation. To coat the titanium substrates, the suspension was sprayed over the Ti substrates which were heated at 150 °C using a small airbrush (Blackridge Professional) with a nozzle size of 0.2 mm. The

electrode was coated with 6 layers, with each layer annealed in air at 450 °C for 5 min and the final layer annealed for 1 h. Electrodes containing 0, 10, 25 and 40 wt% TiO_2 nanoparticles were prepared in this way and in all cases the total oxide loading was determined to be 0.35 $\pm$ 0.06 mg cm^{-2}.

The surface morphology of the prepared anodes was investigated using a JEOL JSM 7000F field emission, high-resolution scanning electron microscope (at 15 kV) and EDS analysis performed with the JEOL energy dispersive x-ray analysis system.

The electrochemical behaviour of the prepared anodes were assessed in 0.5 M H_2SO_4 electrolyte using a three-electrode cell system controlled by a Gamry Interface 1000 potentiostat. Electrochemical impedance spectroscopy (EIS) was used to determine the resistance between the working and reference electrode. The EIS was conducted in hybrid mode, with a DC current of Accelerated lifetime tests were performed on the TiO_2 nanoparticle + IrO_2 anodes at 50 °C using a large stainless-steel cathode (16 cm^2) and 2 M sulphuric acid as the electrolyte. In these tests, the anodes were operated at 1 A cm^{-2} until the cell potential reached 10 V at which point the anodes were deemed to have failed.

4.4 Results and discussion

4.4.1 SEM characterisation

Scanning electron microscopy revealed that the surface structure and the morphology of fabricated electrodes vary considerable as a function of the TiO_2 nanoparticles: IrO_2 ratio (Figure *4-1*). As expected, the layer of pure IrO_2 exhibits the cracked mud structure commonly observed for DSA electrodes [36, 205, 219]. For the electrode layer containing 10 wt% TiO_2 nanoparticles, a similar morphology to the pure IrO_2 anode is found, but with much smaller cracks across surface of the electrode. Quite different morphology is observed for the electrodes containing 25 and 40 wt% TiO_2 nanoparticles, with these showing pronounced roughness and a particle-like structure. While the surface morphology of electrode layer containing 25 wt% TiO_2 nanoparticles is uniform on the ~ 10 μm scale (as determined by EDS

mapping), the electrode containing 40 wt% TiO_2 nanoparticles has an uneven distribution of large agglomerates, with some regions of the substrate poorly by the IrO_2-TiO_2 composite (marked by a dashed region on the figure). EDS analysis of this electrode revealed that the poorly coated regions had Ti:Ir atomic ratios of 25:2, whereas the coated regions had Ti:Ir atomic ratios of 4:1. This suggests that the poorly coated regions were still covered with IrO_2, but as the Ti ratio was very high, it suggests that the coating in these regions were very thin. It must be noted that in all cases, the EDS revealed higher than expected Ti:Ir ratios (compared to the layer composition) as a significant fraction of the Ti signal would have originated from the underlying Ti substrate due to the penetration depth of EDS.

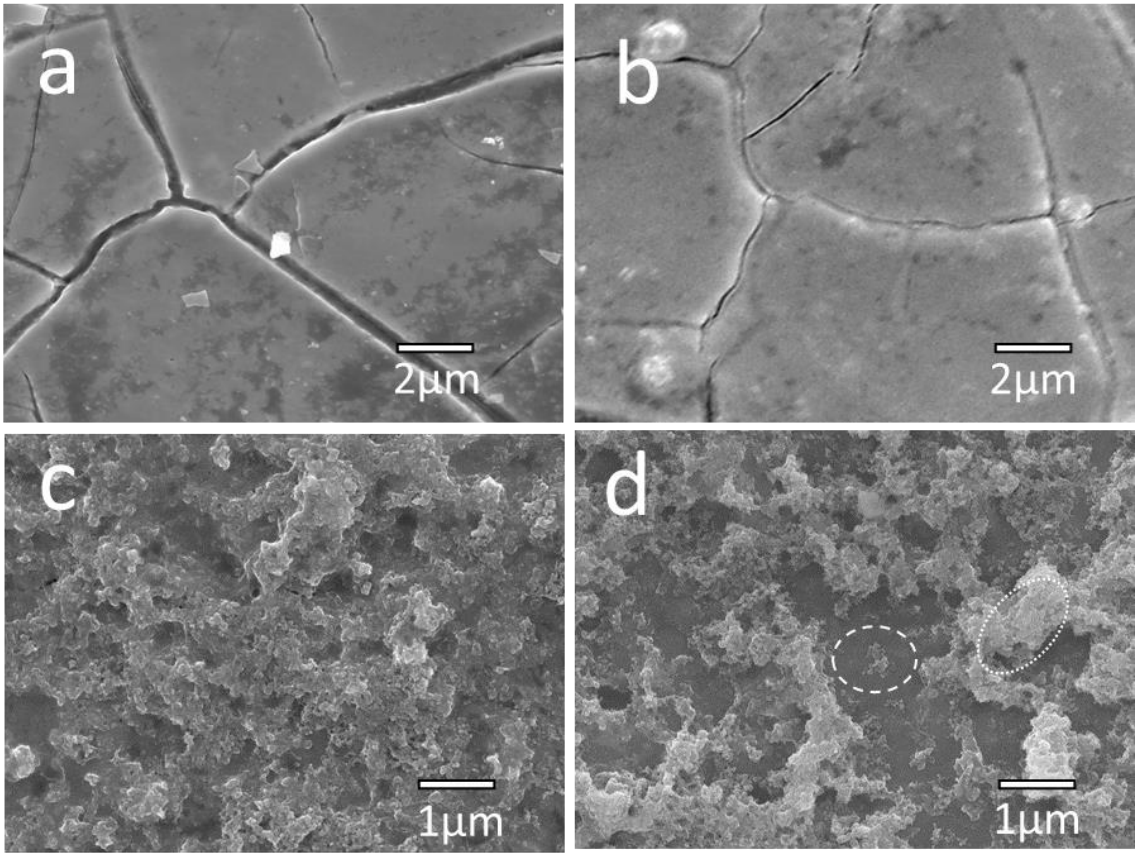

Figure 4-1 SEM micrographs of the surface morphology of IrO_2 anodes containing (a) 0, (b) 10, (c) 25 and (d) 40 wt% TiO_2 nanoparticles. In (d), the dashed region highlights a poorly coated region, where the dotted region highlights an example of an agglomerate.

We propose that the mechanism for these observed changes in morphology due to the addition of nanoparticles is related to differences in thermal expansion coefficient of composite and substrate and the improved drying characteristics of the precursor suspension. It is reported that the differences in thermal expansion coefficient of the layer and the substrate during the thermal decomposition method may be linked to the formation of cracks [211], presumably through induced mechanical stress on the coating. In our case, IrO_2 has a smaller thermal expansion coefficient (5×10^{-6} / ˚C [226]) than Ti (1×10^{-5} / ˚C [227]) which would explain the observed cracking, whereas the thermal expansion coefficient of TiO_2 (9×10^{-6} / ˚C [228, 229]) is closer to Ti, and thus the presence of the TiO_2 nanoparticles may reduce some mechanical stress. It is also possible that the composite has stronger mechanical strength as observed in some metal-ceramic composites [230]. We also speculate that the initial drying and decomposition of the precursor suspension plays a role in determining the final morphology, with many investigations revealing that the drying of suspensions leads to complex and interesting structures [231, 232]. It is also likely that the presence of the TiO_2 nanoparticles provides the $IrCl_3$ (the IrO_2 precursor) nucleation sites from which a network of IrO_2 crystallites can grow.

4.4.2 Cyclic voltammetry measurement

Cyclic voltammetry of the fabricated anodes in 0.5 M H_2SO_4 solution revealed similar electrochemical behaviour to the traditional IrO_2 DSA electrodes [233-235], which suggests that the surface electrochemistry is most likely dominated by iridium species [236, 237] (Figure *4-2*).

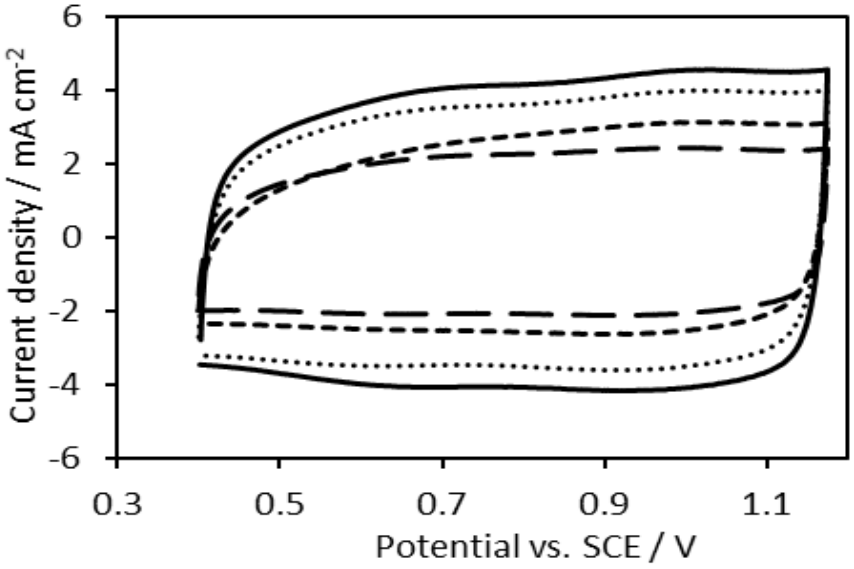

Figure 4-2 Cyclic voltammetry IrO_2 anodes containing (—) 0, (···) 10, (---) 25 and (– –) 40 wt% TiO_2 nanoparticles at 50 mV s^{-1} in 0.5 M H_2SO_4.

4.4.3 Voltammetric charge analysis

As expected, the anodic charge (a measure of the electrochemically active surface area [205, 238, 239]) was found to decrease with the addition of TiO_2 nanoparticles due to the decreasing mass of IrO_2 in the active layer (Figure *4-3*). This suggests that the TiO_2 nanoparticles do not help improve the utilisation of the IrO_2 phase within the composite layer, unlike the addition of 10 wt% Sb-doped SnO_2 nanoparticles to IrO_2 which did increase the overall electrochemically active surface area [219]. In this case, by calculating the anodic charge on an IrO_2 mass basis, it is found that the specific active area of the IrO_2 decreased upon additional of 10 wt% TiO_2 nanoparticles before increasing with further TiO_2 nanoparticle additions (Figure *4-3*). We propose that the initial decrease in IrO_2 utilisation is due to the reduced crack size, which would restrict the transport of electrolyte into the active layer [238]. Interestingly the anodic charge on an IrO_2 mass basis measured at 200 mV s^{-1} is higher for the anode containing 40 wt% TiO_2 nanoparticles compared to the pure IrO_2 anode (Figure *4-3*), which suggests that a great proportion of the Ir atoms are easily accessible [238] in this

anode, presumably due to the particle-like morphology this anode exhibits. However, it is important to note that the TiO_2 used in this work has limited electrical conductivity, and it is likely that for thicker films, this will reduce the utilisation of the IrO_2 due to ohmic losses between the film and the titanium substrate.

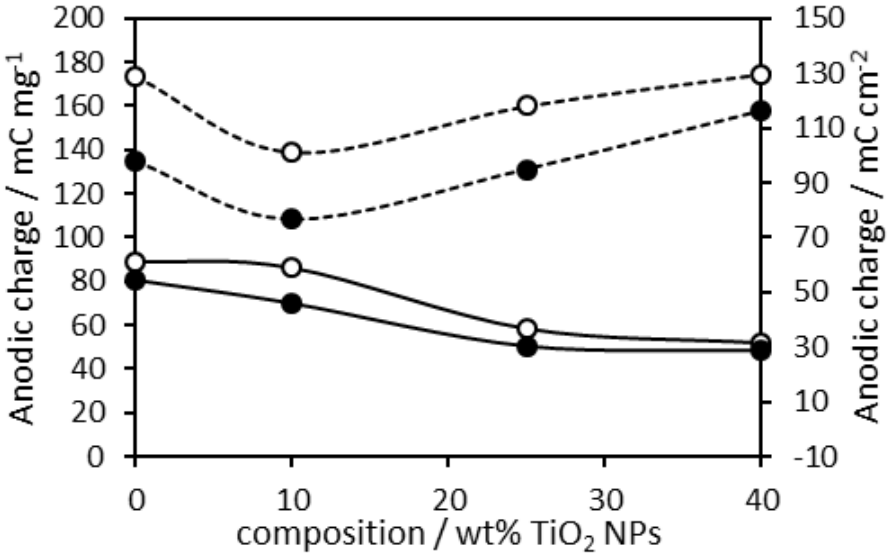

Figure 4-3 Anodic charge calculated from cyclic voltammetry measured at (○) 50 and (●) 200 mV s^{-1} in 0.5 M H_2SO_4. Solid lines = anodic charge normalised on an anode geometric area basis, Dashed lines = anodic charge normalised on an IrO_2 mass basis. Lines are guides only.

4.4.4 Steady state polarisation curve

The electrocatalytic performance of fabricated electrodes towards oxygen evolution reaction was investigated by linear sweep voltammetry in 0.5 M H_2SO_4 with a scan rate of 1 mV s^{-1} (Figure *4-4*). This shows that the onset of the oxygen evolution reaction begins at around 1.2 V vs. SCE for all electrodes, with Tafel slopes between 75-85 mV at low overpotentials, before curving upwards to Tafel slopes of 150-190 mV at higher overpotentials. The lower Tafel slope is similar to that report for IrO_2 in KOH [240] and the 60-90 mV reported on some $Ir_xTi_{(1-x)}O_2$ anodes in acid [241]. These slopes are significantly higher than that normally reported for IrO_2 in acidic electrolytes [196, 242, 243], which may suggest that the OER is operating via a

different mechanism on these anodes. This could be due to the low IrO_2 loading on the anodes used in this work (total oxide loading = 0.35 mg cm^{-2}), with some evidence suggesting that low total loadings of the active phase can increase the Tafel slope for OER [241, 244, 245]. Regardless of this, very little difference is found between the anodes, with the difference in potential between the most active anode (containing 0 wt% TiO_2 nanoparticles) and least active anode (containing 40 wt% TiO_2 nanoparticles) only around 30 mV at useful current densities (> 10 mA cm^{-2}). This shows that the OER performance can be largely maintained even with the addition of up to 40% TiO_2 nanoparticles, with any small loss in performance likely only due to fewer IrO_2 sites within the anode. We expect this loss in performance could be minimised by increasing the anode's total oxide loading as the quantity of TiO_2 nanoparticles within the layer increases, to ensure that the IrO_2 loading remains approx. constant.

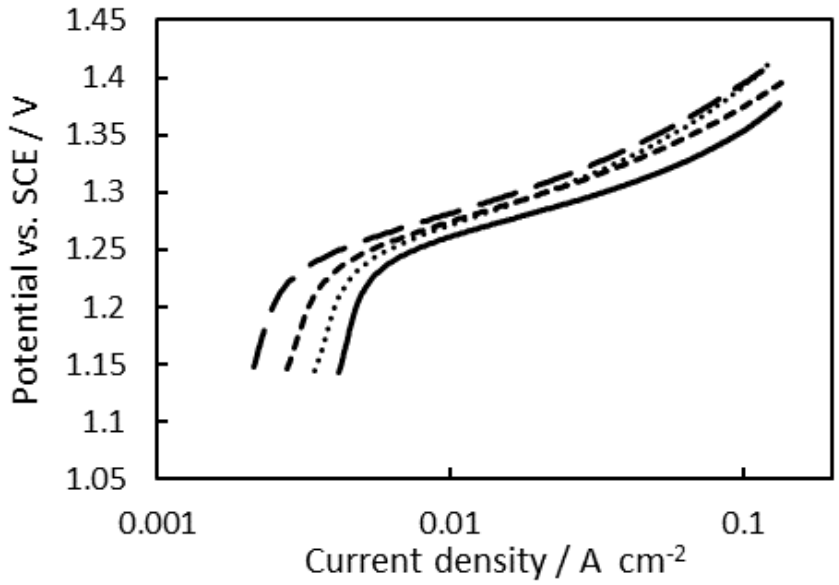

Figure 4-4 Oxygen evolution reaction polarisation curves in 0.5 M H_2SO_4 for IrO_2 anodes containing (—) 0, (···) 10, (---) 25 and (– –) 40 wt% TiO_2 nanoparticles. The data was measured at 1 mV s^{-1} and was iR corrected post-run using the resistance determined by EIS.

4.4.5 Accelerated life test

The accelerated life tests of the fabricated anodes showed that while the lifetime of the IrO_2 anode containing no TiO_2 nanoparticles was only 17 h, the addition of 10 wt% and 25 wt% TiO_2 nanoparticles increased this by two and ten times respectively (Figure *4-5*). The lifetime for the anode containing 40 wt% TiO_2 nanoparticles was much shorter at 2.7 h. This important result indicates that simply by adding an optimum amount of inert nanoparticles into a DSA layer can significantly increase the service life of these anodes. We interpret the short lifetime of the anode containing 40 wt% TiO_2 nanoparticles as being related to the poor coverage of the film over the titanium substrate which would have led to rapid passivation and possibly mechanical failure of the particle-like coating. Indeed, SEM analysis after this electrode had failed showed large regions of anode were no longer coated, suggesting that at least part of the failure mechanism was due to erosion of the coating. Given that the density of IrO_2 (11.67 g cm^{-3}) is much higher than TiO_2 (4.25 g cm^{-3}) [246], for the anode containing 40 wt% TiO_2 nanoparticles, the 60 wt% IrO_2 in the layer only corresponds to around 35 vol% IrO_2 which might not be enough to act as an effective binder for the TiO_2 nanoparticles.

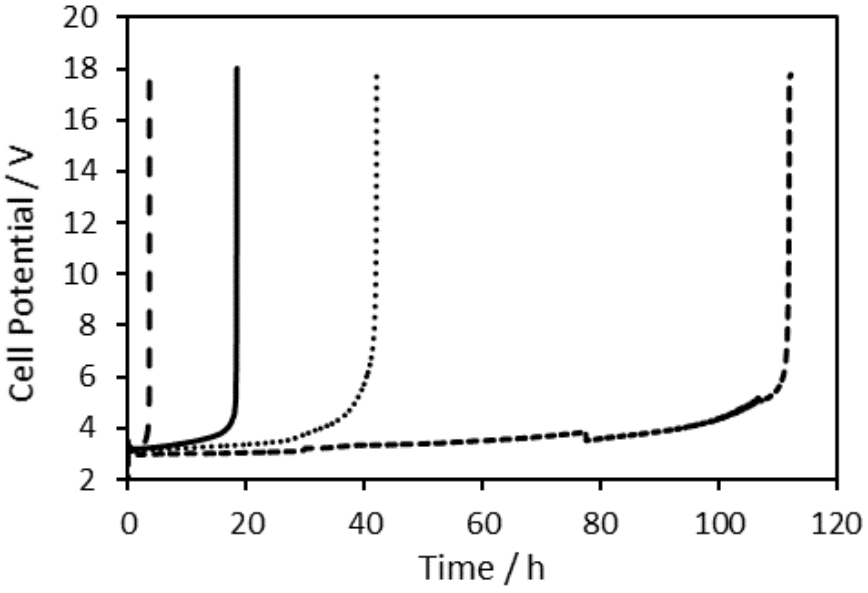

Figure 4-5 Accelerated lifetime evaluation of IrO_2 anodes containing (—) 0, (···) 10, (---) 25 and (– –) 40 wt% TiO_2 nanoparticles at 1 A cm^{-2} in 2 M H_2SO_4 at 50°C.

4.4.6 Deactivation mechanism

The deactivation of DSA electrodes is generally assumed to be due to erosion, corrosion and/or passivation of the underlying substrate [208, 247-249]. Erosion occurs when the all or part of the active layer detaches from electrode substrate due to poor adhesion of the coating or mechanical stress, resulting from bubble formation at the cracks and pores of the coating. This differs to corrosion, where the active species are anodically oxidised to a soluble or volatile species during the OER [250]. Passivation is caused by the formation of insulating layer on the (typically) titanium substrate and is widely known as final stage of DSA deactivation, and often accelerates the failure of the anodes following the partial detachment or corrosion of the coating [208, 251]. In this work, as the TiO_2 nanoparticles are unlikely to influence the corrosion rate of the active IrO_2 phase, the improved lifetime of the anodes containing 10 and 25 wt% TiO_2 nanoparticles must rise from improved mechanical strength and/or reduced electrolyte penetration through the layer leading to reduced substrate passivation. As the addition of 10 wt% TiO_2 nanoparticles resulted in noticeably smaller cracks in the layer compared to the pure IrO_2 anode, it is reasonable to propose that this anode has an improved lifetime due to less electrolyte penetration and substrate passivation. For the anode containing 25 wt% TiO_2 nanoparticles, no cracked-mud structure was found and instead the layer exhibited a particle-like morphology. While this layer is porous, the coverage of IrO_2 over the substrate was even, which suggests that electrolyte penetration to the substrate may be impeded. We also propose that the composite layer may have improved mechanical strength (similar effect to that found in other nanoparticle composites [220-222]) which reduces the erosion rate under strong oxygen evolution reaction rates.

4.5 Conclusions

This study investigated the effects of addition of TiO_2 nanoparticles on service lifetime and electrochemical behaviour of IrO_2 anodes. The accelerated service lifetime test show that the

addition of TiO_2 nanoparticles into the oxide matrix enhances the durability of the anodes, with 10 wt% and 25 wt% TiO_2 nanoparticle additions increasing the service lifetime of the electrodes by 2x and 10x respectively. When 40 wt% TiO_2 nanoparticles were added, the anodes had much lower lifetimes due in part to poor coverage of the coating on the titanium substrate. Importantly, the simplicity of embedding the oxide nanoparticles into the thermally prepared IrO_2 layers should be compatible with standard industrial DSA production methods and maybe further optimisable to improve both service lifetime and electrochemically active surface area.

Chapter 5

Incorporation of nanoparticles in DSA electrodes for organic oxidation

5.1 Abstract

The incorporation effect of antimony-doped tin oxide (ATO) nanoparticles on DSA electrode and oxidation pathway of 4-NP was investigated. Due to high energy consumption of "non-active" anodes such as BDD, a combinition of anode material with high activity towards organic oxidation and low activity towards OER at low potentials is chosen. The result indicates that an increase in nanoparticles' weight percentage leads to an increase in the electrochemical active surface area (EASA), in which anodes with 5 wt% ATO nanoparticles have the highest EASA. The complete oxidation of intermediate and products occurs at anodes with the incorporation of ATO nanoparticles, while partial oxidisation of 4-NP occurs at pure IrO_2 anode with a high accumulation of 2-hydroxy-benzoquinone (HBQ).

5.2 Introduction

Water pollution is one of the greatest challenges of the 21st century. Therefore, there has been a high demand to find a suitable eco-friendly technology to treat wastewater [166]. Advanced oxidation processes (AOPs) are an effective solution for treating various organic pollutants [252-255]. Among AOPs, electrochemical oxidation is a promising way to treat a wide range of organic compounds with high chemical toxicity and non-biodegradability, due to the ease of operation and use of electrons as a clean reagent. [5, 6, 87, 256, 257] The anode materials control the final oxidation products and the efficiency of the process [258]. Therefore, the desired electrode material for organic oxidation must have the following essential requirements: high catalytic activity towards pollutants degradation, a low production cost, and a long service life [36, 259].

The major drawback of electrochemical oxidation is the high energy consumption caused by the low current efficiency of the process [260]. The main reason for low current efficiency is the parallel competing reaction of oxygen evolution reaction (OER) at the anodes [261]. A solution for this problem is to use anodes with very high overpotentials for OER such as boron-doped diamond (BDD). [36, 262-264] These types of anodes commonly called as “non-active” anodes such as BDD, in which oxidation process occur via generation of hydroxyl radicals at the surface of the anode at high potential [1, 265, 266]. While the organic oxidation of pollutants at BDD anode can occur below the onset of OER, formation of a polymeric adhesive film on the surface of BDD anode leads rapid anode fouling [65, 267]. Thus, to oxidise the organic pollutants in this approach, high cell voltage required, which consequently leads to high energy consumption. The way out from this problem is to utilise a combination of metal oxides for anodes with high activity towards organic oxidation and low activity towards OER at low potentials. For this reason we chose antimony-doped tin oxide (ATO), which is considered to have a superior property for the oxidation of organic compounds [99, 268], to incorporate with IrO_2-based DSA electrode. Although the surface area may not be the most important factor for designing the electrode, as Yakasu et al. [269] discussed in their work, that the oxide electrodes with the larger surface area might increase the electrocatalytic

performance of the electrode. Aaron et al. [270] also found that incorporation of an optimised percentage of nanoparticles to anode coating can potentially increase the EASA. ATO nanoparticles are thus used to achieve higher EASA which result in higher electrode electrocatalytic performance. In this study, we incorporate nanoparticles form of antimony-doped tin oxide (ATO) with a combination of the IrO_2 based-DSA electrode for electro-oxidation of 4-nitrophenol. Thus, the objective of this study is to investigate the electrochemical activity of various IrO_2 based-DSA electrode and also identify the oxidation products of the 4-nitrophenol.

5.3 Experimental

The IrO_2- based DSA electrodes were prepared following the thermal decomposition method of noble metal oxide described elsewhere in details [271-273]. In brief, the titanium substrates (1.5 cm × 1.5 cm) were etched in concentrated HCl at a temperature of 50 °C for one hour, then rinsed with deionised water and acetone, before being kept at 105 °C to be dried. The precursor of ATO nanoparticles (99.5%, 10mol. % Sb_2O_5, Aldrich) and $IrCl_3$ (99.8%, Sigma Aldrich) were separately mixed in 7: 3 volume ratio of isopropanol and deionised water solution, in which the total concentration of the solution was set at an equivalent oxide concentration of 5 mg mL^{-1}. The desired ratio of 0 wt%, 5 wt%, 15 wt% and 25 wt% ATO nanoparticles suspension to the $IrCl_3$ solution was prepared. The 0.2 mL of the precursor solution was ultrasonicated and then sprayed over the surface of titanium held at 80 °C before sintering in a furnace at 400 °C for about 5 min to oxidise the precursor. This depositing process was repeated six times until the total oxide loading of 0.9 mg cm^{-2} was achieved. Finally, the solution was annealed for 1 h at 400 °C. The surface structure and composition of the coating were studied using scanning microscopy (HR-SEM JEOL JSM 7000F) coupled with energy dispersive x-ray analysis system (JOEL EDS). A working acceleration voltage of 10 kV and distance of 10 mm was used.

Cyclic voltammetry, electrochemical impedance spectroscopy, polarisation measurements and potentiostatic oxidation were performed by a Gamry Interface 1100 potentiostat in a three-electrode glass cell. Stainless steel was used as counter electrode and saturated calomel

electrode (SCE) as the reference electrode. The electrolyte used at this experiment was 0.5 M Na_2SO_4 (99.4%, Labserv) pH adjusted to pH 2 using sulphuric acid with or without 0.15 mM 4-NP (99%, BDH). All potentials reported in this article are relative to the SCE reference electrode.

The electro-oxidation experiments were conducted under the potentiostatic condition at the range between 1.125 and 1.3 V vs SCE to ensure both the kinetic and mass transport limited condition were observed. The samples were taken at regular time interval, and the change in 4-NP concentration and intermediate products were monitored by UV-Visible spectroscopy (VWR UV-1600 PC) and HPLC (Hewlett Packard series 1000 System) with a Agilent C_{18} column (250 mm × 4.6 mm, 5 μm) at a column temperature of 30 °C and flow rate of 0.5 mL min^{-1} for the separation. The mobile phase was a mixed of 55% methanol and 45% DI water. The oxidation products were detected in the HPLC using a UV-Visible detector set at 260 nm. Standard compounds used to characterise the retention time of intermediates.

5.4 Results and discussion

5.4.1 SEM characterisation

Scanning electron microscopy was employed to characterise the morphology and surface structure of the nanoparticles-modified IrO_2-based DSA electrode. The layer produced merely from $IrCl_3$ exhibited a porous cracked- mud structure, typical to DSA electrodes obtained by thermal decomposition method (Figure *5-1*) [36, 274-277]. The reasons for these crack-mud structures are the high volatility of the solvent [276] and/or stressed caused by the difference in thermal expansion coefficient between the coating and the substrate[274, 277]. However, a 5 wt% ATO nanoparticle-modified layer showed similar morphology to IrO_2-based DSA electrode layers with smaller cracks and roughness. The 25 wt% ATO nanoparticles-modified layer showed less cracking, with particles-like structure around the cracks (Figure *5-1* a).

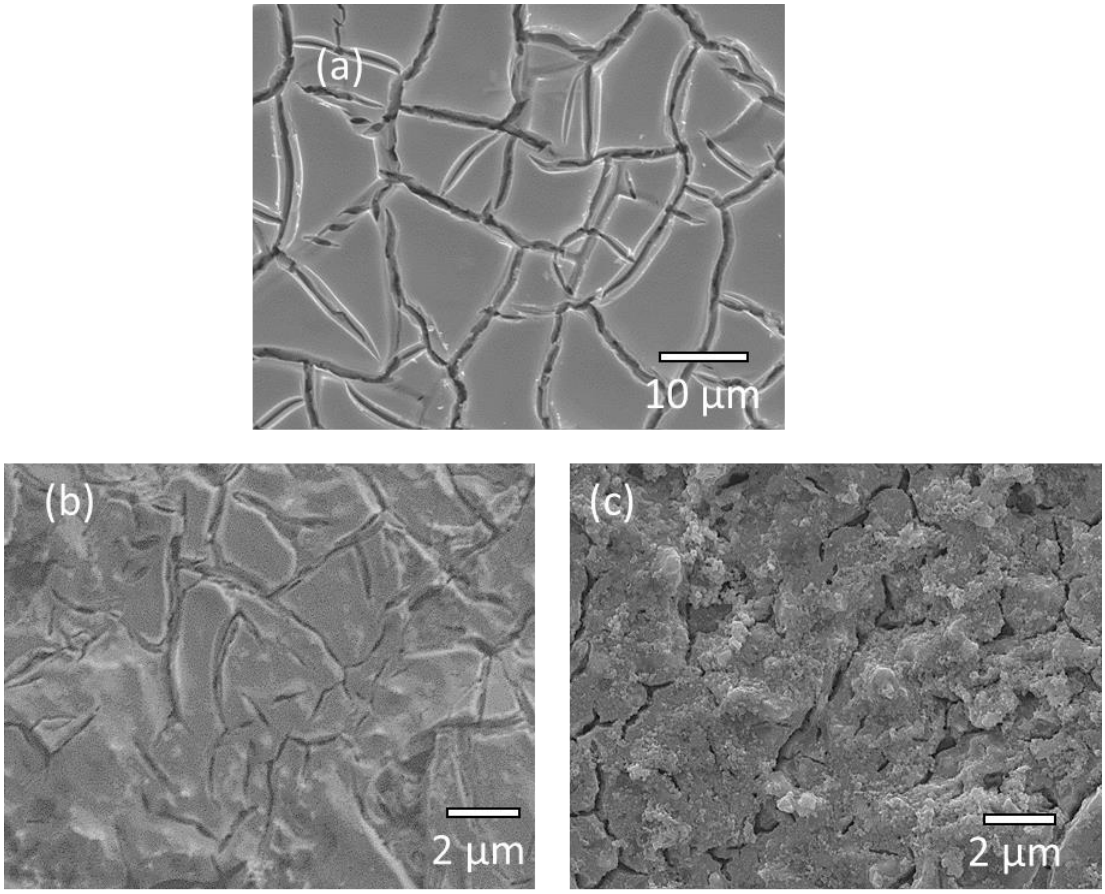

Figure 5-1 SEM images of IrO_2-based DSA electrodes containing ATO NPs (a) 0 wt% ATO NPs (b) 5 wt% ATO Nanoparticles (c) 25 wt% ATO Nanoparticles

The cracking may be caused by the stabilising effect of nanoparticles during thermal decomposition. The stabilising effect in turn was caused by high surface energy resulting from relative high surface area to volume of nanoparticles, bonds between adjacent particles form [278, 279]. Consequently, the formation of agglomerate in the composite layer eliminated and reduced the main drawback of the DSA electrode formation of crack-mud structures, which is believed to be caused by the difference in the thermal expansion coefficient of titanium substrate and iridium oxide coating [280]. We also shown in our previous study [280] that the addition of a small weight percentage of nanoparticles can potentially increase the service lifetime of DSA electrode.

5.4.2 Cyclic voltammetry measurement

Cyclic voltammetry over the potential window of water stability revealed that modified electrodes follow similar behaviour to the traditional DSA electrodes (Figure 5-2) [281-283], due to electrochemical inertness of ATO nanoparticles at this potential window. The 0 wt% ATO nanoparticles electrode does not exhibit any well-defined redox peaks as indicated by others [270]. The electrodes with the addition of 5 wt% of ATO nanoparticles have a broader peak at 0.6 V vs. SCE which related to Ir(III)/Ir(IV) solid-state redox transition of active oxides [284-286]. The Ir(III)/Ir(IV) redox reaction peak is shifted to 0.5 V as the addition of nanoparticles increase to 25 wt%, and the other redox peak is not distinguishable for 15 wt% and 25 wt% ATO nanoparticles. The proton-exchange of active surface of Ir species and solution is facilitated by redox reactions (equation 5.1) [287, 288].

$$IrO_a(OH)_b + \delta H^+ + \delta e^- \rightleftharpoons IrO_{a-\delta}(OH)_{b+\delta} \quad (5.1)$$

The redox current increases with the addition of ATO nanoparticles. The current at first increases to its highest value and then decreases when increased with the addition of ATO nanoparticles to 40 wt%. The trend in cyclic voltammetry of fabricated electrodes in this work is different from what others [270] reported for the same composition. This is mainly due to preparation by two different user as explained by Trasatti [94].

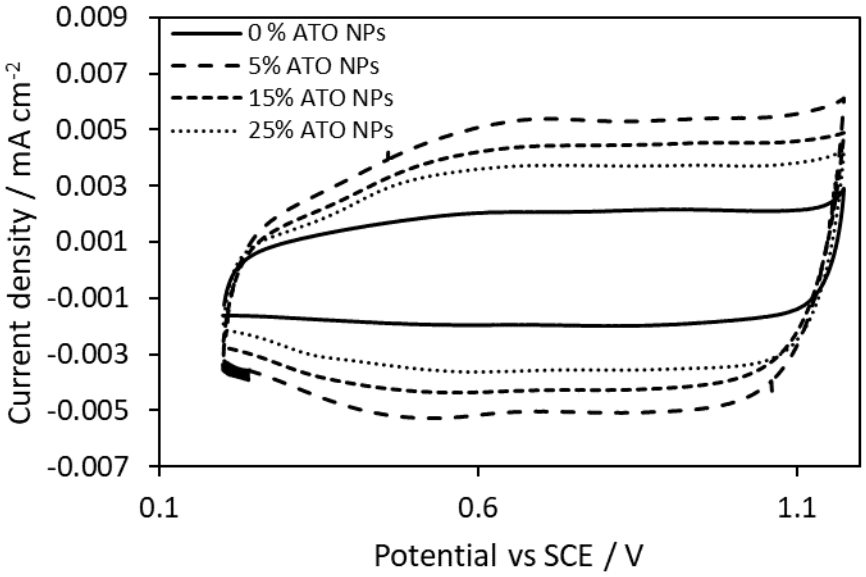

Figure 5-2 Cyclic voltammetry for different ATO nanoparticles weight percentage electrolyte 0 wt% NPs (——), 5 wt% NPs (— —) 15 wt% NPs (- - -) 25 wt% NPs (.....) at 50 mV/s, between 0.2 V and 1.15 V, in 0.5 M Na_2SO_4 adjusted to pH 2 supporting electrolyte

5.4.3 Voltammetric charge analysis

The anodic charge represents the electrochemically active surface area, also known as the real surface area [94, 289]. The measurement of anodic charge as a function of scan rate can provide useful information on the morphology of the coating [276]. In this work, the evaluation of the outer and total charge of the electrodes was conducted by methods described by others [290]. Firstly, anodic charge (Q) measured as function of sweep rate (v) then charge values at v=0 which represent Q_{total} and v=∞ which represent Q_{outer} are found by extrapolating the Q^{-1} vs. $v^{0.5}$ and Q vs. $v^{-0.5}$ data. In this experiment total and outer anodic charge was calculated for potential range between 0.2 - 1.15 V. At higher scan rate the charging process takes place only at the outer surface of the electrode coating, whereas at very low scan rate the charging process also takes place in deep pores and cracks through the diffusion of ions to the inner surface of electrode coating. The inner anodic charge that represents the less accessible surface sites of the oxide layer is calculated from the subtraction of total and outer anodic charge. The results show that the addition of a small amount (5 wt%) ATO nanoparticles to IrO_2-based DSA electrode increases the total and outer anodic charge dramatically (Figure 5-3).

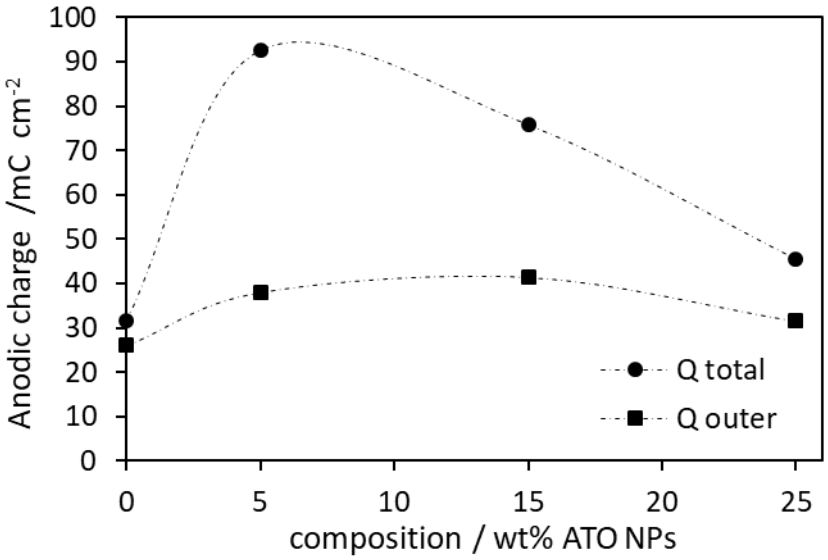

Figure 5-3 Effect of nanoparticles' addition on the total and outer anodic charge as determined from cyclic voltammetry, between 0.2 and 1.15 V vs. SCE, 0.5 M Na_2SO_4 adjusted to pH 2

A further increase of ATO nanoparticles leads to a decrease in the total and outer anodic charge. The outer anodic charge also follows a similar trend as total anodic charge but with a much smaller increase in anodic charge in comparison with the pure IrO_2 electrode. The outer anodic charge is important for electro-oxidation of organic compounds as the diffusion of organic compounds to the inner surface is poor. In this case, the proton exchange between absorbed hydroxyl radical on the electrode surface and 4-NP occur mainly at the outer surface of the electrode. This result is in a good agreement with previous SEM images, indicating that small percentage of nanoparticles improves the electrocatalytic active area which is the result of better dispersion of IrO_2 phase on ATO nanoparticles during the thermal decomposition.

5.4.4 Polarisation measurement

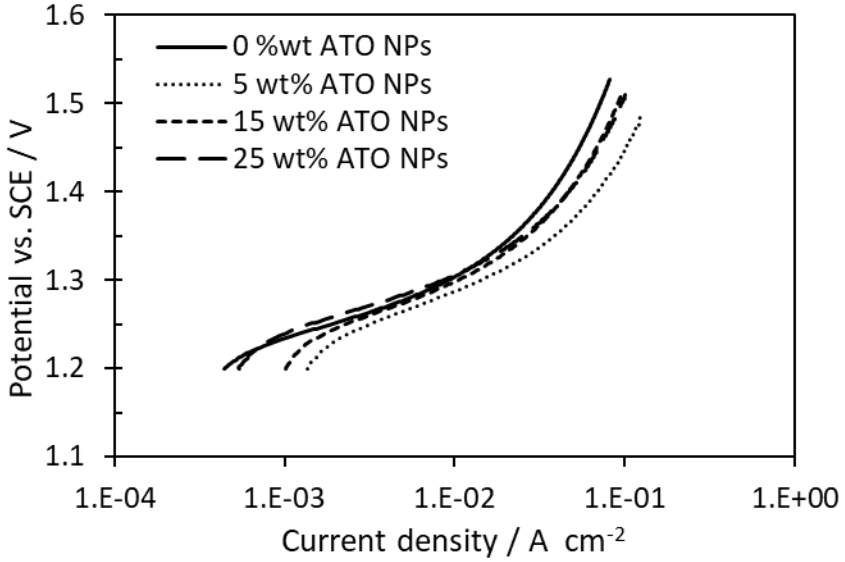

Figure 5-4 Linear sweep voltammetry of all fabricated electrode in 0.5 M Na_2SO_4 adjusted to pH 2, scan rate of 10 mV s^{-1}.

The polarisation curve shows that the electrocatalytic activity towards oxygen evolution reaction increases upon addition of ATO nanoparticles over the scanned potential range. Interestingly, the addition of 5 wt% ATO nanoparticles doubled the current density at a fixed potential of 1.3 V. With an increase in the addition of nanoparticles, the current density decreases (Figure 5-4). This pattern was also observed in cyclic voltammetry measurements, which shows that anode containing 5% ATO nanoparticles has a much higher electrochemical active surface area (EASA).

5.4.5 Activity of electrodes towards the electrochemical oxidation of 4-NP

The electrochemical activity of IrO_2-based DSA electrodes towards oxidation of 4-NP was evaluated using UV-Vis spectroscopy. The dynamic changes in the absorption of the 4-NP during the electrochemical oxidation were recorded over the wavelength range of 200-500

nm. In order to obtain the dynamic linear range of the UV calibration curves, a concentration of 0.15 mM 4-NP is chosen.

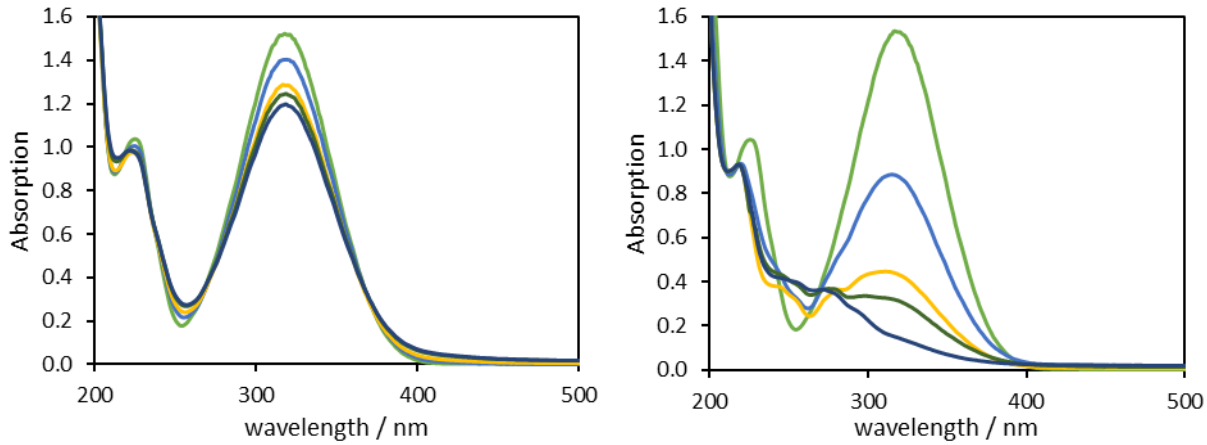

Figure 5-5 The absorption of 0.15 mM 4-NP in 0.5 M Na_2SO_4 adjusted to pH 2 over 1 h electrolysis for pure IrO_2 anode, sample interval of 15 min (a) at potential 1.125V under kinetics controlled (b) at potential 1.25 V under mass transport controlled

Figure 5-5 shows the change in the absorption of 4-NP with time at IrO_2 anode containing 5 wt% ATO nanoparticles operating at potential 1.125 V under kinetics controlled and 1.25 V under mass transport controlled. Here we presented only UV spectra of pure IrO_2 anode, since there is not much different in other anodes UV spectra. The absorption at λ_{max} (319 nm) corresponds to 4-NP compound and decreases with time and approaches to near zero after 1 h of electrolysis (Figure 5-5 b). Also, two new peaks appeared at 245 nm and 288 nm, indicating the formation of intermediate products of 1,4-benzoquinone [203] and hydroquinone [291] respectively.

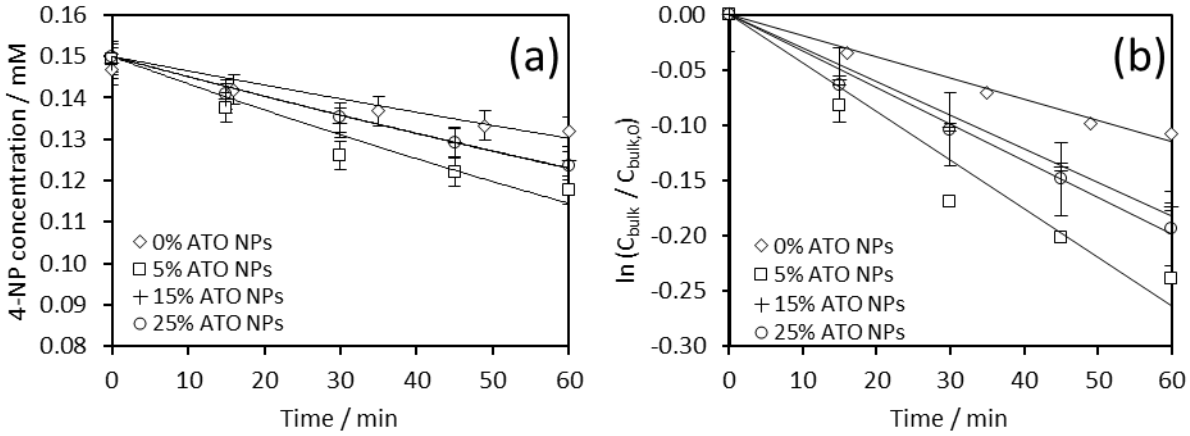

Figure 5-6 Potentiostatic electrolysis of 0.15 mM of 4-NP in a 0.5 M Na_2SO_4 solution (pH =2) at 1.125 V,(a) Concentration (C_{bulk}) vs time, (b) first-order plot of $ln(C_{bulk}/C_{(bulk,0)})$

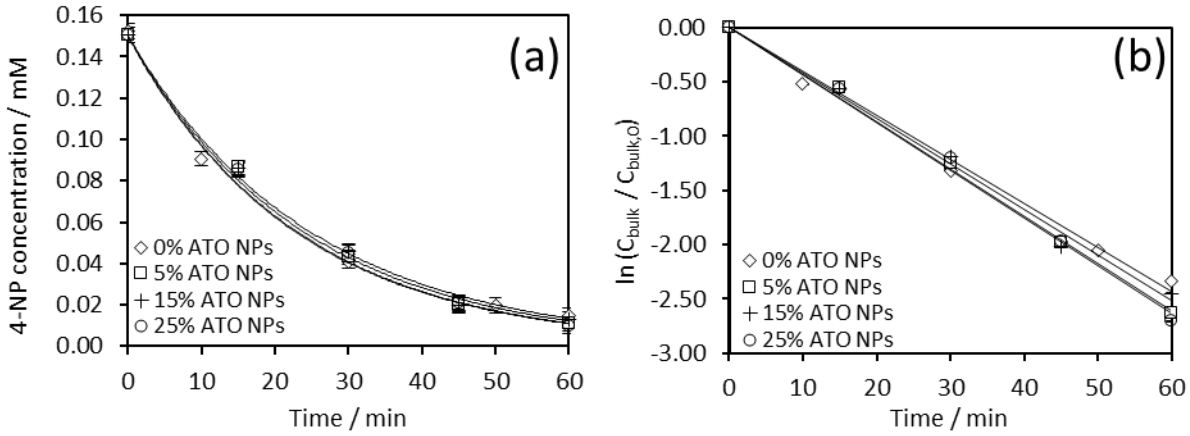

Figure 5-7 Potentiostatic electrolysis of 0.15 mM of 4-NP in a 0.5 M Na_2SO_4 solution (pH =2) at 1.25 V (a) Concentration (C_{bulk}) vs time, (b) first-order plot of $ln(C_{bulk}/C_{(bulk,0)})$

In our previous study, the oxidation rate of 4-NP was described as pseudo-first-order in respect to the 4-NP concentration with linear $ln(C_{bulk}/C_{(bulk,0)})$ vs time [234]. The rate of 4-NP oxidation is given by:

$$\frac{dC_{bulk}}{dt} = -k_{app}C_{bulk} \tag{5.2}$$

Where C_{bulk} is the concentration of 4-NP in the bulk solution and $k_{app} = k_4\theta_O$ is the apparent rate constant, with the assumption that surface coverage (θ_O) of higher oxide (S-O) is constant and k_4 is the rate constant for organic oxidation step (R4, refer to [234]).

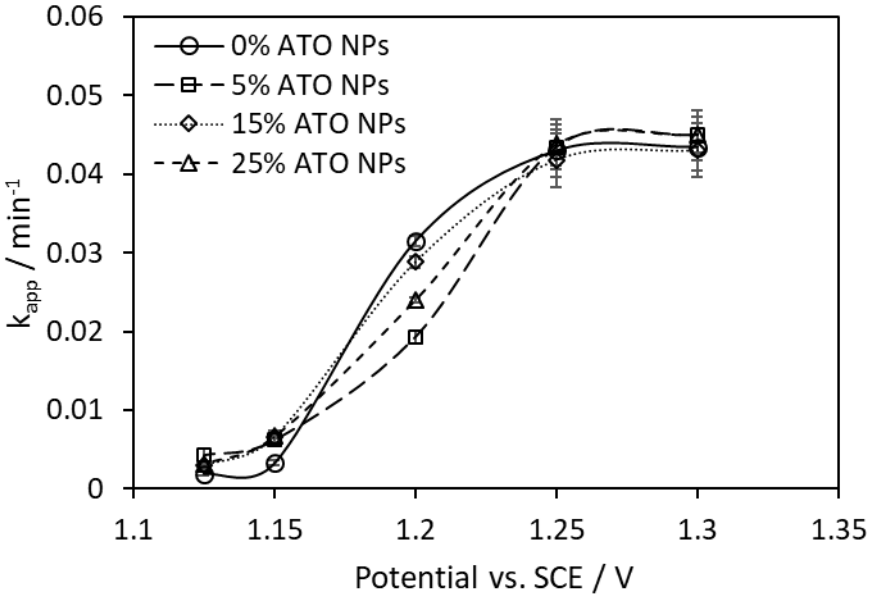

Figure 5-8 The dependence of the apparent first-order rate constant (k_{app}) on applied potential at IrO_2- based DSA electrodes

The electrochemical oxidation of 4–NP shows that there is 91% 4-NP removal in 1 h electrolysis time for all fabricated anodes at potentials 1.25 V vs SCE where the oxidation rate is controlled by mass transport (Figure 5-8). This result may be explained by the fact that electro-oxidation operated at potential below the potential at which ATO generates OH radicals [23] (1.9-2.2 V vs RHE). While, IrO_2 anode containing 0% nanoparticles at low potential where oxidation reaction is under the kinetic controlled has the lowest oxidation rate of 4-NP owing to the lowest EASA. Above 1.25 V, as no increase in the pseudo-first-order rate constant occurs. Any further additional current above that found at 1.3 V will be wasted in reactions other than 4-NP oxidation, most likely being used for oxygen evolution reaction.

5.4.6 Oxidation pathway of 4-NP

The identification of intermediates and oxidation products during the electro-oxidation of 4-NP was performed using HPLC analysis. All detected oxidation products were identified by comparing the chromatographic retention time of the standards compounds. The disappearance of 4-NP and formation of 1,2,4-Trihydroxybenzene (THB), hydroquinone (HQ), 2-hydroxy-benzoquinone (HBQ), benzoquinone (BQ) and 4-nitrocatechol (4-NC) were observed at all fabricated electrodes during 90 min electrolysis (Figure 5-9 and Figure 5-10). The main differences in measured chromatographs were found between pure IrO_2-based DSA and 5 wt% ATO nanoparticles anode, while other electrodes had similar chromatograph to that 5 wt% ATO nanoparticles anode.

Table 5-1 HPLC retention time of 4-NP and its oxidation products

Retention time / min	Intermediate products
5.8	1,2,4-Trihydroxy-benzene (THB)
6	Hydroquinone (HQ)
6.9	2-Hydroxy-benzoquinone (HBQ)
7.2	Benzoquinone (BQ)
8.2	4-Nitrocatechol (4-NC)
10.8	4-Nitrophenol (4-NP)

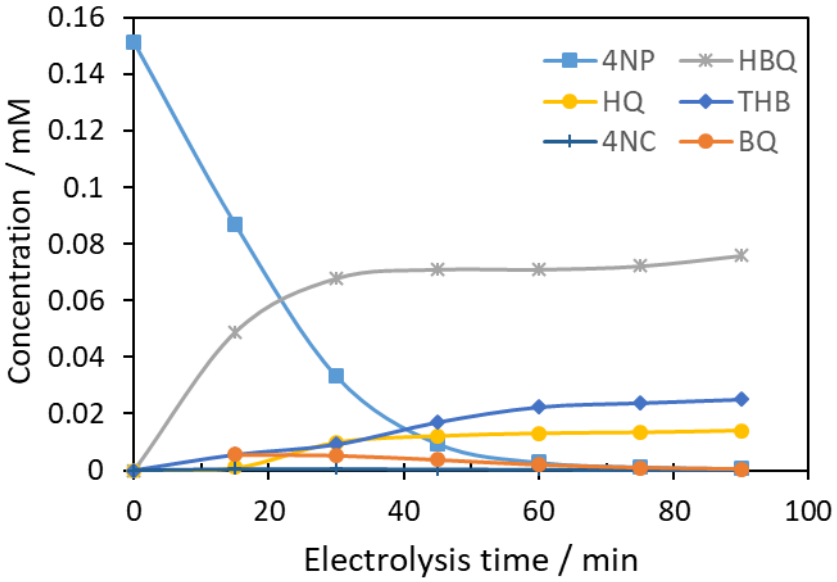

Figure 5-9 The change in concentration of 4-NP and oxidation by-products vs electrolysis time at pure IrO_2 anode for solution containing 0.15 mM 4-NP in 0.5 M Na_2SO_4 adjusted to pH 2

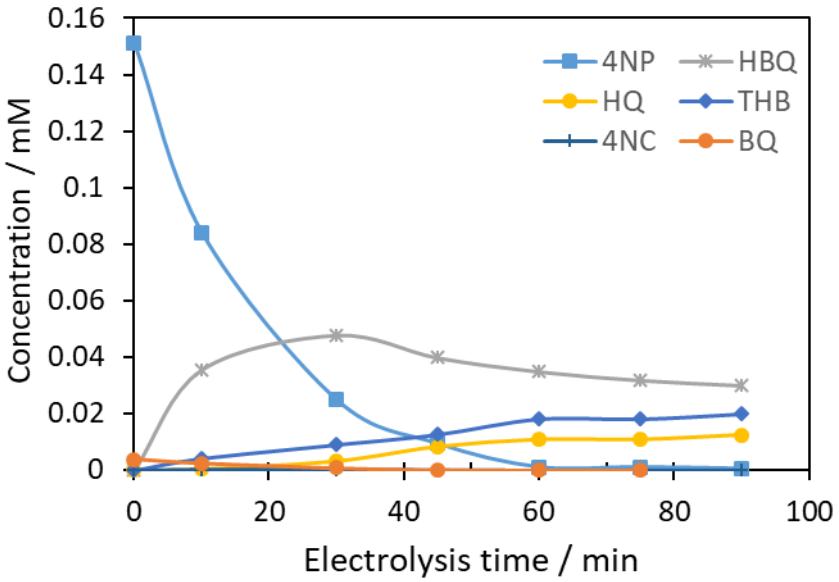

Figure 5-10 The change in concentration of 4-NP and oxidation by-products vs electrolysis time at IrO_2-based DSA 5 wt% ATO nanoparticles for solution containing 0.15 mM 4-NP in 0.5 M Na_2SO_4 adjusted to pH 2

As can be observed, The major difference between these two electrodes is the HBQ concentration, at pure IrO_2 anode the HBQ concentration increase to 0.08 mM and remain fairly constant over the electrolysis time, while at 5 wt% ATO nanoparticles anode, the HBQ concertation rises to 0.05 before decreases over the time. The overall results indicate that the electrochemical oxidation of 4-NP at pure IrO_2 anode is partial and hampered by HBQ compounds production, which no further oxidisation was observed at this anode. However, the low concentration of intermediate compounds at 5 wt% ATO nanoparticles anode indicate that the formation of aliphatic acids and CO_2 might occur from the beginning of the oxidation process and as also other [292] discussed the possible complete oxidation of all organic compounds. The minor difference observed in the chromatograms of incorporated ATO nanoparticles anodes suggest that the oxidation at these electrodes occur mainly through physiosorbed hydroxyl radicals on ATO nanoparticles. Another speculation [292] is that the chemisorbed hydroxyl radical bound which formed on IrO_2 weakens at ATO nanoparticles, where physiosorbed hydroxyl radical formed, leading to complete oxidation of organic compounds. It is noteworthy that we did not observe any cathodic compounds production in the solution, such as 4-aminophenol.

Based on the HPLC analysis, a degradation mechanism was proposed for the 4-NP oxidation at the anode with the addition of ATO nanoparticles (Figure 5-11). Generally, hydroxyl radicals attack the phenol ring at ortho-position and para-position to produce 4-NC and hydroquinone. The hydroquinone gets further oxidised to benzoquinone and THB. The THB gets further oxidised to HBQ. The HBQ and benzoquinone degrade further into aliphatic acids such as succinic acid, fumaric acid and oxalic acid, and finally, these aliphatic acids oxidised to water and carbon dioxide. The 4-NC pathway follows THB then HBQ oxidation before rings opening to aliphatic acid. The final products of complete oxidation are water and carbon dioxide.

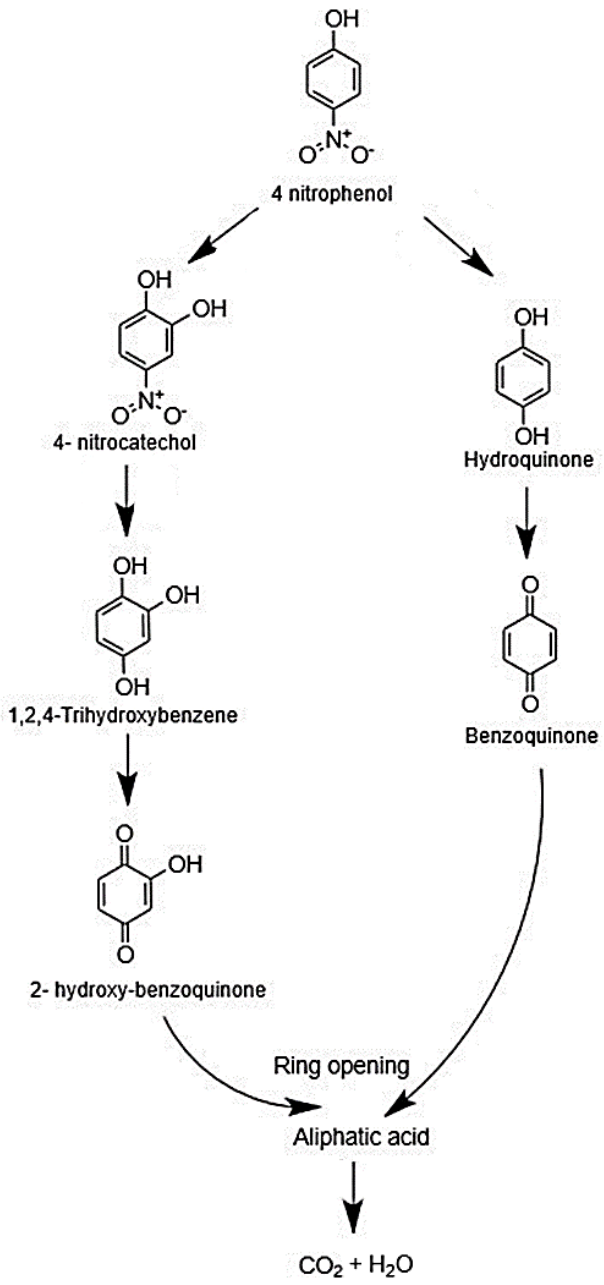

Figure 5-11 Proposed pathway of 4-nitrophenol on IrO_2-DSA anode containing ATO nanoparticles

5.5 Conclusions

In this study, the effect of addition of antimony-doped tin oxide (ATO) nanoparticles on DSA electrode and oxidation pathway of 4-NP was investigated. The result indicates that an increase in nanoparticles percentage leads to pronounced roughness and reduced cracks in the surface morphology of electrode. This can help to increase the lifetime of DSA electrode. It was also observed that anode with 5 wt% ATO nanoparticles has the highest electrochemical active surface area, which is the result of better dispersion of IrO_2 phase on ATO nanoparticles during the thermal decomposition. Investagaton of the 4-NP oxidation shows that the main differences in measured chromatographs were found between pure IrO_2-based DSA and 5 wt% ATO nanoparticles anode, while other electrodes had similar chromatograph to that 5 wt% ATO nanoparticles anode. The complete oxidation of intermediates and products occurs at anodes with the addition of ATO nanoparticles, while partial oxidisation of 4-NP occurs in pure IrO_2 anodes with a high accumulation of HBQ.

Chapter 6

Modelling the dynamics and performance of pulsed electrochemical wastewater oxidation

6.1 Abstract

The low current efficiency of electrochemical wastewater oxidation is normally caused by an unwanted parallel oxygen evolution reaction that occurs at the anode. This often occurs when the mass transport of organic species to the anode surface is insufficient to maintain the desired current. Here, pulsed electrolysis is employed to facilitate a higher flux of organic species during the short periods in which the anode is high enough to drive the desired oxidation reaction. In this study, the electrochemical oxidation of organic species using pulsed and constant potential electrolysis is investigated through numerical simulations. By comparing the pulsed potential organic oxidation with constant potential organic oxidation over a range of electrolysis, it can be concluded that the current efficiency of pulse potential organic oxidation is improved over a range of potentials compare to constant potential electrolysis. It was also found that the potential dependence of the apparent first-order oxidation rate constant is explained by this model.

6.2 Introduction

Electrochemical oxidation is a promising way to treat a wide range of wastewater, including non-biodegradable and toxic compounds in a short period compared to the conventional methods [5, 6, 16, 177, 257, 282, 293-297]. The main drawback of using electrochemical oxidation on the industrial scale is attributed to the high energy consumption and low current efficiency [170, 261]. The low current efficiency of this process is mainly due to the unwanted parallel oxygen evolution reaction that occurs at the surface of the anode [36, 298]. This happens when the mass transport of organic species to the anode surface is insufficient to maintain the desired current.

To enhance the energy consumption and facilitate a higher mass transport of reactant to the surface of the electrode, a non-steady-state technique such as pulsed voltage, pulsed current, or reverse polarity are occasionally used [299-301]. The pulsed electrolysis technique are used in various industries such as metal deposition, electro dissolution, electrochemical machining, battery and hydrogen production etc. [299, 300]. Some of these researches was conducted specifically to find out the effect of pulse on the mass transfer and current efficiency of the system. As an example hydrogen production is one of the industries that uses pulse power to produces hydrogen efficiently [302]. In similar study on effect of pulsed electrolysis on hydrogen production, the result show that using pulse potential enhances the mass transport of oxygen and hydrogen bubbles due to the pumping effect. This provides less contact with oxygen bubbles to improve corrosion resistance of anode electrodes. Moreover, decreasing mass transfer losses on the electrode surface resulted in a 20–25% lower energy consumption to produce 1 mol of hydrogen in the cell [303].

During pulsed electrolysis, a short period of high overpotential is applied, leading to a very steep concentration gradient of the reactant at the electrode surface. This steep concentration gradient results in a very high current for a short period at rates which are much higher than the equivalent mass transport limited current under normal potentiostatic conditions. Before the concentration gradient grows further into the electrolyte (leading to the mass transfer limiting current), the overpotential is stepped to a low value where the

electron transfer rate is very low. In this low overpotential pulse period, the concentration gradient reverts to a flat gradient at the bulk electrolyte concentrations due to diffusion.

In this study, a “non-active” anode oxidation pathway is investigated [5, 304, 305].

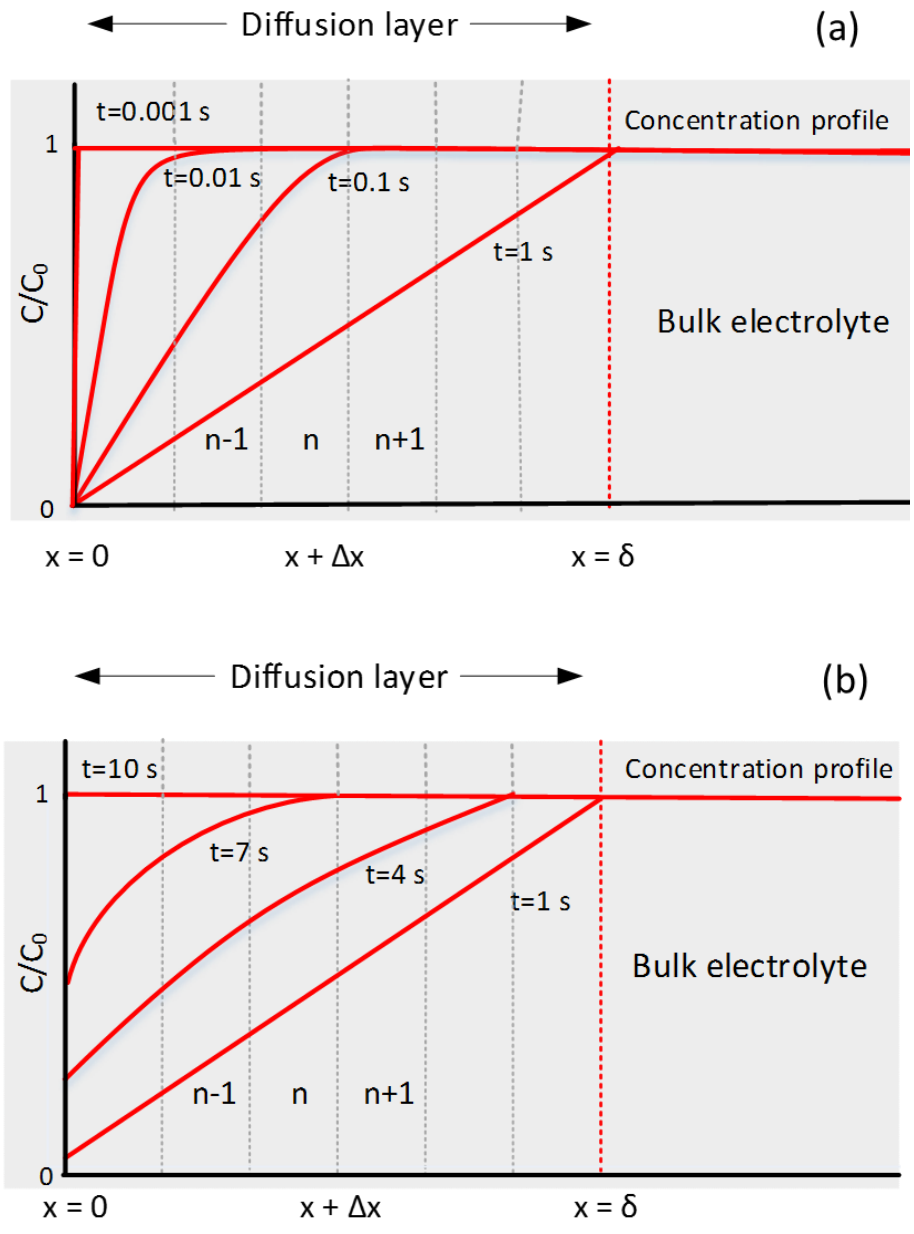

Figure 6-1 Concentration gradient in diffusion layer (a) high overpotential pulse (mass transport region) (b) low overpotential pulse (electron transfer limited region)

The mathematical models to comprehend and thus apply an optimum condition for the potentiostatic electrolysis at “non-active” anode have been proposed. Some of these models used multi-step OER [306], while others used multi-step organic oxidation reaction for the specific organic species and other variations [185, 188, 307-310].

In this study, a model on the performance of electrochemical oxidation of organics in parallel with oxygen evolution reaction using pulsed and constant potential electrolysis at “non-active” anode is developed. We hypothesise that using pulsed potential facilitates a higher flux of organic species to the surface of anode in a short period. This potentially improves the shortcoming of mass transport of organic species to the anode surface. The simulation of organic oxidation in both model; constant and pulsed potential are investigated using the kinetics parameters obtain from OER curve. The model explained the potential dependency of the apparent first-order oxidation rate constant correctly.

6.3 Mathematical model

The electrochemical oxidation of organics at the anode follows a complex reaction process. However, considering a simple model introduced by Comninellis [1] potentially enables us to study this mechanism better. In this paper the “non-active” electrode mechanism used for oxidation of organic compounds, in which the oxidation of organics species is mediated by hydroxide radicals physisorbed on the anode surface during the water discharge step (Step 1).

$$\mathrm{S} + \mathrm{H_2O} \Leftrightarrow S(\cdot OH) + H^+ + e^- \qquad \text{(Step 1)}$$

$$S(\cdot OH) \Leftrightarrow S + \frac{1}{2}O_2 + H^+ + e^- \qquad \text{(Step 2)}$$

$$S(\cdot OH) + R \rightarrow S + RO + H^+ + e^- \qquad \text{(Step 3)}$$

Where S here represents a free surface site. In this mechanism, the oxidation of organic species (step 3) competes with the generation of oxygen gas (step 3). There are more complex

reaction mechanisms for 'non-active' electrodes by others [188, 311]. For this study, however, the simple reaction mechanism shown above is sufficient.

The critical factor for this study which controls the current efficiency of the overall process is the relative rate of steps 2 and 3 while competing for the same intermediate, $S(^{\cdot}OH)$. This mechanism differs from the mechanism proposed for 'active' anodes such as Iridium oxide and platinum, where the oxidation of organic spices is mediated by the higher oxide (S-O) which chemisorbed on the anode surface at high potentials. Here, the adsorption process of the organic molecule has been ignored. Another assumption is that all steps leading the OER are considered chemically reversible, while organic oxidation process is chemically irreversible. The reaction rate for each step is given by:

$$r_1 = k_1 c_{H_2O}(1-\theta) - k_{-1} c_{H+} \theta \tag{6-1}$$

$$r_2 = k_2 \theta - k_{-2} c_{O_2}^{1/2} c_{H+}(1-\theta) \tag{6-2}$$

$$r_3 = k_3 \theta c_{R,surf} \tag{6-3}$$

Where k_1 and k_{-1} are forward and backward rate constants, c are concentrations, θ is the surface coverage of $^{\cdot}OH$ with the fraction of free sites given by $(1-\theta)$. The units of all rate equations are mol s^{-1} cm^{-2}. Note that in this model, the surface concentration of organic species used to implement the mass transport consideration into the rate equation for the organic oxidation.

The assumption for the reaction 1-3 is that their rate constant is potential dependent so that Butler-Volmer kinetics can be used. For example:

$$k_i = k_i^0 exp^{\frac{\beta F}{RT}(E-E_{rev})} \tag{6-4}$$

$$k_{-i} = k_{-i}^0 exp^{\frac{-(1-\beta)F}{RT}(E-E_{rev})} \tag{6-5}$$

where R, T, β and F are the gas constant, temperature, symmetry factor and Faraday constant respectively and E and E_{rev} are the anode and reversible potential for the OER respectively. The parameter symmetry factor (β) usually has a value of approximately 0.5 [312], although this value can differ, especially for reactions involving adsorbed species such as OER [313].

The current density (i) is calculated by summing the rates of all involved reactions in organic oxidation:

$$i = F(r_1 + r_2 + r_3) \tag{6-6}$$

6.3.1 Instantaneous current efficiency

Instantaneous current efficiency is another important parameter that reflects the fraction of the current that goes towards organic oxidation and can be calculated from the reaction rates:

$$ICE = \frac{r_3}{r_1 + r_2 + r_3} \tag{6-7}$$

6.3.2 Thermodynamic restrictions

In the above model, multiple parameters must be known or estimated before simulating the reaction. The overall OER (sum of step 1 and 2) is:

$$H_2O \rightleftharpoons \frac{1}{2}O_2 + 2H^+ + 2e^- \tag{6-8}$$

The reaction has the reversible thermodynamic potential of $E_{rev} = 1.23\ V$ vs RHE. At this potential ($\eta = E - E_{rev} = 0$) the system must be an equilibrium and thus the overall equilibrium constant is defined as:

$$K = \frac{(c_{O_2})^{0.5}(c_{H^+})^2}{c_{H_2O}} \tag{6-9}$$

As thermodynamics must be satisfied at $\eta = E - E_{rev} = 0$, this reduces the number of freely definable rate constants through:

$$K = K_1 K_2 = (\frac{k_1}{k_{-1}})(\frac{k_2}{k_{-2}}) \quad (6\text{-}10)$$

where K is the overall equilibrium constant, and K_1 and K_2 are the equilibrium constants for step 1 and 2 in the reaction. In this case, only 3 of the 4 kinetics parameters for step 1 and 2 are independent and freely definable.

6.3.3 Steady-state OER polarisation curve

The Steady-state polarisation curve under OER at the BDD electrode can be simulated by setting equation (7) to zero and ignoring step 3, the organic oxidation step. The polarisation curve i vs η can then be determined for the chosen three OER rate constants and a calculated the fourth OER rate constant from equation (14).

6.3.4 Constant potential organic oxidation in parallel with OER model

The potentiostatic organic oxidation in parallel with OER is modelled by solving equation (7) on the surface of the electrode, equations (9) and (10) at the boundary layer, and equation (8) for the diffusion layer simultaneously. The steady-state surface coverage for OER at the same potential from the previous section (**Error! Reference source not found.**) and bulk c oncentration of 15×10^{-8} mol cm^{-3} are used as initial conditions for the ODE equation (7). Then ODE is solved for a range of overpotentials for a specified time in Matlab using ODE15s function.

6.3.5 Dynamic potential organic oxidation in parallel with OER model

The dynamic potential model contains loops of two steps; a short period at high overpotential and a short period at low overpotential, which each step individually acts as a constant

potential. The initial conditions for the first step are the same as the constant potential model and the initial conditions for the second step is the last value of concentration, surface coverage and time obtained from ODE solver of the same step. Similarly, for the following loops, the last value obtained from the ODE solver of each step is used for the initial condition of the next pulse step.

6.3.6 Numerical solution

The system of mathematical equation was set up in the programming platform of MATLAB, R2016b, with ordinary differential equations solvers. The stiff solver of ODE 15s was used to calculate the solutions for a wide range of overpotential and kinetics parameter sets.

The surface coverage must be known to determine the current density passing through the anodes. This is described by ODE built from reaction steps 1-3:

$$\frac{d\theta}{dt} = (k_1 cH_2O(1-\theta) - k_{-1}c_{H+}\theta - k_2\theta + k_{-2}c_{O_2}^{1/2}c_{H+}(1-\theta) - k_3\theta c_{R,surf})/Ntot \quad (6\text{-}11)$$

Where $Ntot$ is the number of surface sites per unit electrode area (mol cm^{-2}). Finally, the concentration of organic species across the system must be determined. Here, similar to our previous work [261] the assumption of a planar diffusion across the boundary layer of the electrode is made to account for the mass transport of organic species to the electrode surface. Then according to the Fick's second law, the concentration of organic species as a function of time can be determined at any given nod, n, across the boundary layer by using the method of lines:

$$\frac{dc_{R,n}}{dt} = D_R \frac{c_{R,n+1} + c_{R,n-1} - 2c_{R,n}}{\Delta x^2} \quad (6\text{-}12)$$

where D_R is the diffusion coefficient of the organic species and Δx is the width of the segment the distance between two nodes within the boundary layer. The boundary conditions with the concentration within the bulk electrolyte found by:

$$\frac{dc_{R,bulk}}{dt} = D_R\left(\frac{A}{V_{bulk}}\right)\frac{c_{R,n=(\delta/\Delta x)} - c_{R,bulk}}{\Delta x} \quad (6\text{-}13)$$

With the concentration in the segment immediately adjacent to the electrode surface $c_{R,surf}$ found by:

$$\frac{dc_{R,surf}}{dt} = D_R\frac{c_{R,n=2} - c_{R,surf}}{\Delta x} - \frac{k_3\theta c_{R,surf}}{\Delta x} \quad (6\text{-}14)$$

The mass transport of oxygen gas (either bubbles or dissolved gas) is ignored.

6.4 Results and discussion

6.4.1 OER polarisation curve simulation

The simulated kinetic parameters of the steady-state polarisation curve for “non-active” anode were assigned to be applied in the constant and dynamic potential organic oxidation (**Error! Reference source not found.**).

Figure 6-2 simulated polarisation curve between overpotential of 0.3 V and 2 V

Based on the OER mechanism, the surface coverage of S-OH approaches 1 at high overpotentials (**Error! Reference source not found.**). This simulation model0.1 can describe t he OER of any "non-active" anode that follows similar behaviour. The kinetics of the organic oxidation at surface coverage equal to 1 (**Error! Reference source not found.**), is independent o f overpotential but dependent on surface concentration ($c_{R,surf}$) and organic rate constant (k_3). Normally when the organic oxidation rate is independent with overpotential, mass transport is considered to limit the overall oxidation rate. This has been further investigated at section 6.4.2.

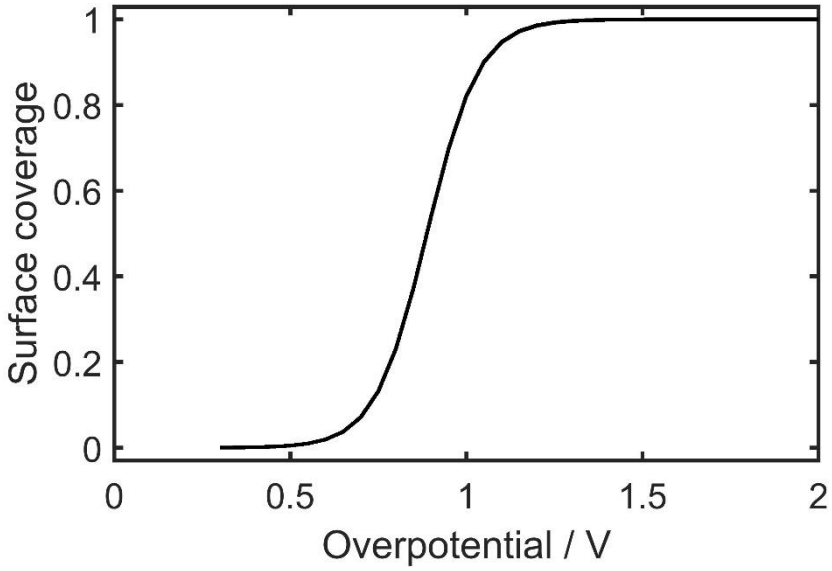

Figure 6-3 The simulated surface coverage of S-OH vs. overpotential during the oxygen evolution reaction at pH = 2

6.4.2 Constant potential organic oxidation in parallel with OER

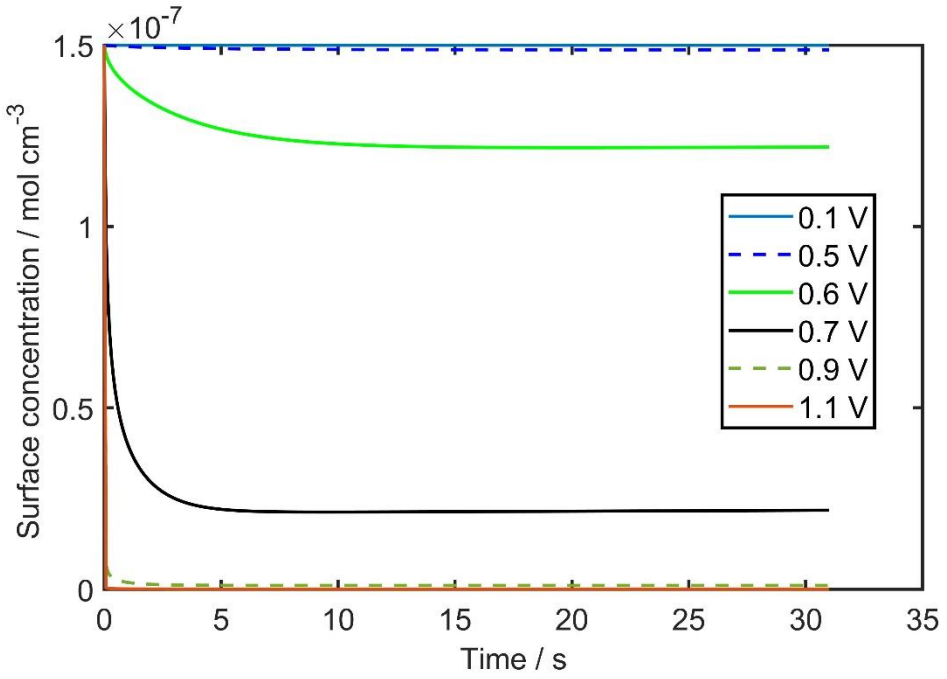

Figure 6-4 The surface concentration behavior vs time over various constant potential

The model was used to simulate and study the kinetics of the electro-oxidation of an organic compound at "non active" anode. The constant potential electrolysis was simulated at various potential, and the effect of potentials at surface concentration is investigated. The potential range was chosen to cover kinetic and mass transport limitation. The model shows that an increase in the applied anode potential leads to decrease in organic concentration at the anode surface (**Error! Reference source not found.**) and reaches zero at overpotentials where s urface coverage of S-OH is equal to 1.

Table 6-1 Parameters used to simulate the constant and pulsed electrolysis in parallel with the OER

Parameter	Value	Units
Diffusion coefficient of organics (D_R)	0.919×10^{-5} [314]	$cm^2\ s^{-1}$
Diffusion layer thickness (δ)	1×10^{-2}	cm
Bulk concentration of organic ($C_{R,bulk}$)	1.5×10^{-7}	$mol\ cm^{-3}$
Symmetry factor (β_3)	0.5	

The investigation of electrochemical wastewater oxidation involves measuring the change in organic concentration throughout electrolysis and can be simulated using the model described. The simulation of the bulk concentration of organic species revealed that the organic oxidation follows first-order kinetics (**Error! Reference source not found.**), which a grees with experimental reports by others [315, 316]. While increasing the overpotential, initially oxidation process is limited by kinetics of organic species and low coverage of hydroxyl radicals on the anode surface, but most of the current is consumed by organic oxidation reaction. Therefore, high current efficiency is expected. When operating potential exceeds the equivalent limiting current density, the rate of organic oxidation becomes independent of overpotential. At this condition, electrolysis is fast, but current efficiency decreases because the excess current is wasted to the parallel reaction of oxygen evolution [308].

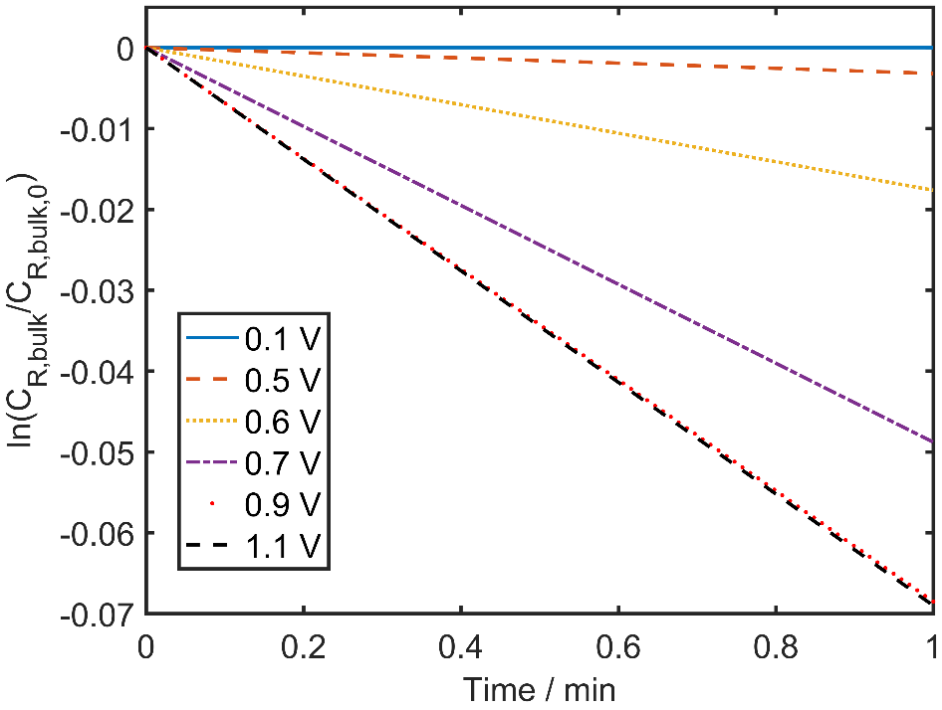

Figure 6-5 Plot of $ln(c_{R,bulk}/c_{(R,bulk,0)})$as a function of time, $c_{R,bulk} = 1.5 \times 10^{-7}\ mol\ cm^{-3}$

The determination of apparent first-order rate constant over the overpotential range also helps us to identify the kinetic and mass transport region, in which potential higher than equivalent limiting current density can be avoided to achieve higher current efficiency. Others [308] also discussed that in order to avoid fouling electrodes with polymeric adhesive products during the aromatic compounds electrolysis, the high applied potential of E > 2.0 V vs. SHE (overpotential > 0.77 V) should be applied. Our simulated apparent first-order reaction can satisfy this criterion, in which the rate of oxidation of organic compounds at around 0.8 V overpotential is fast enough (mass transport limited) that electrode fouling can be avoided.

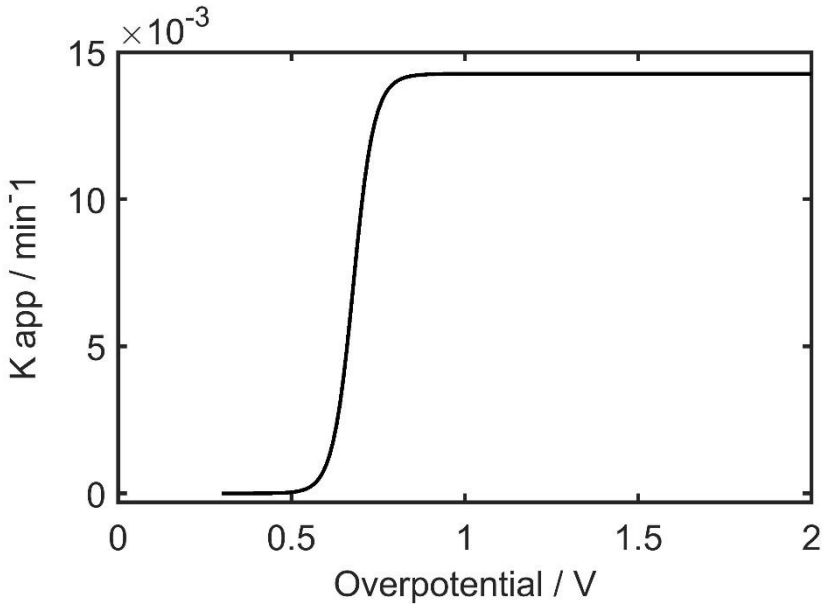

Figure 6-6 The simulated overpotential dependence of the apparent first-order rate constant (k_{app})

6.4.3 Pulsed potential organic oxidation in parallel with OER

The primary purpose of using pulsed potential is to optimise the electrolysis condition where mass transfer rate of organic compounds from the bulk solution to the surface of electrode improved by imposing a short period of high overpotential. This high overpotential oxidises the organics species immediately next to the electrode surface rapidly, leading to a very steep concentration gradient (essentially instantly after the high overpotential is applied). This steep concentration gradient means that the diffusional flux of the organic species is also very high, allowing the oxidation rate of the organic species to be much higher than what would be possible under potentiostatic conditions. This high oxidation rate will only last for a short period as the concentration profile will extend further into the electrolyte causing the diffusion rate to decrease towards the expected "steady-state" mass transfer limiting rate. Before this happens the high overpotential is switched to a low overpotential (one where the reaction rate is very low) which allows the concentration gradient of reactant species to replenish near the electrode surface (**Error! Reference source not found.**). Operating under p ulsed potential conditions results in a higher instantaneous current density, in which the

possible influences on the kinetics of different reaction can lead to change in their relative proportion of current and possibly achieving higher current efficiency. In other industry such as electroplating industry employ the pulsed electrolysis as a mean to achieve higher current efficiency [317].

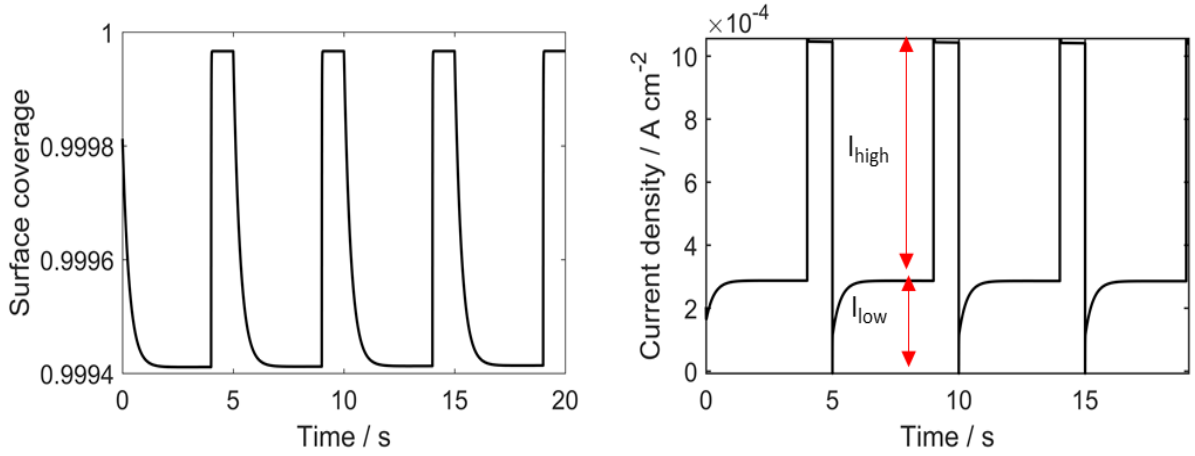

Figure 6-7 Pulsed potential electrolysis a) surface coverage b) current density over electrolysis time

The electric double layer at the electrode-solution interface can have high capacitance, and some charge requires to raise its potential to the value needed for the water discharge step at the rate corresponding to the applied pulsed potential [317]. In published literature for steady-state conditions (constant potential condition), often the effect of an electric double layer (EDL) or capacitance is neglected mainly due to activation period before running the electrolysis. In this model, the effect of electric double layer is not included.

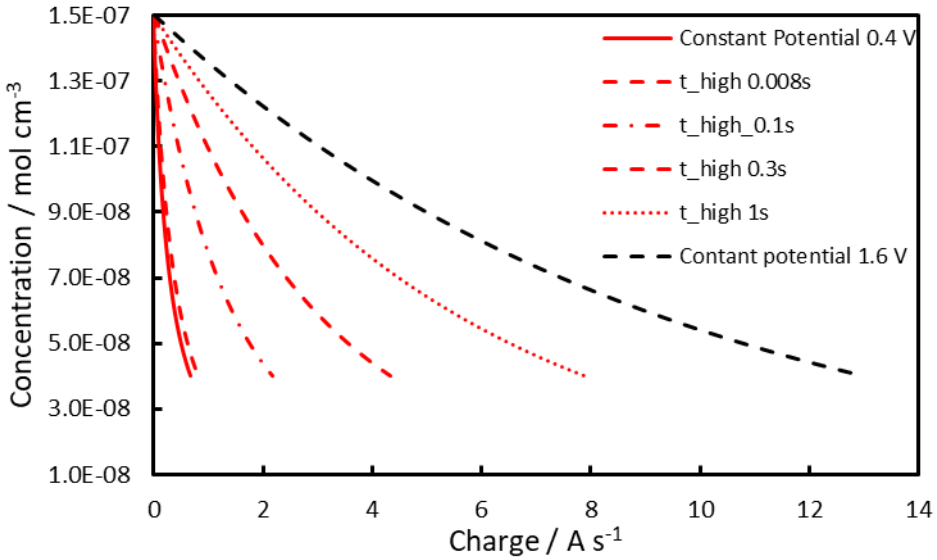

Figure 6-8 The bulk concentration as a function of charge at high pulsed overpotential of 1.6 V and low pulsed overpotential of 0.7 V for 30 minutes electrolysis

The performance of pulsed electrolysis against the constant potential electrolysis can be investigated by plotting the degradation of organic concentration vs charge consumed during the electrolysis. The result revealed that during the electrolysis the lowest charge consumed to achieve same level of organic concentration is when either electrolysis, under contant potential of 0.4 V or when pulsed potential condition at high step of 1.6 V at 8 ms and low step of 0.4 V at 1 s are applied. Further analysis on charge consumed during electrolysis for organic oxidation step (step 3) and OER step (step 2) showed that at constant potential of 0.4 V, majority of charge consumed during the electorlysis process goes towards organic oxidation. This is in agreement with previous report in litreature stated that higher current efficiency is achievable when elecrolysis operated under kinetics limitation. Although under this condition higher current efficiency is achiveable but due to generation of tiny current at this low potential, general oxidation rate is very slow.

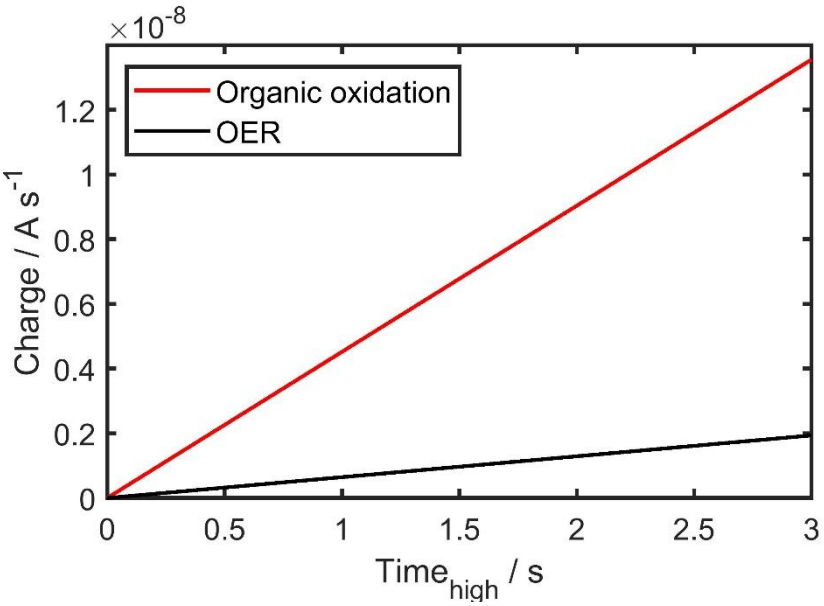

Figure 6-9 Charge consumed during the constant electrolysis at 0.4 V for OER step (black line) and Organic oxidation step (red line)

The Figure 6-10 shows that an applied high potential at very short time of 8 ms, leads to majority of charge goes towards organic oxidation step leading to achieve higher current efficiency and just before the concentration gradient grows further into electrolyte, leading to the mass transfer limiting current, the overpotential is stepped to a low value where the electron transfer rate is very low.

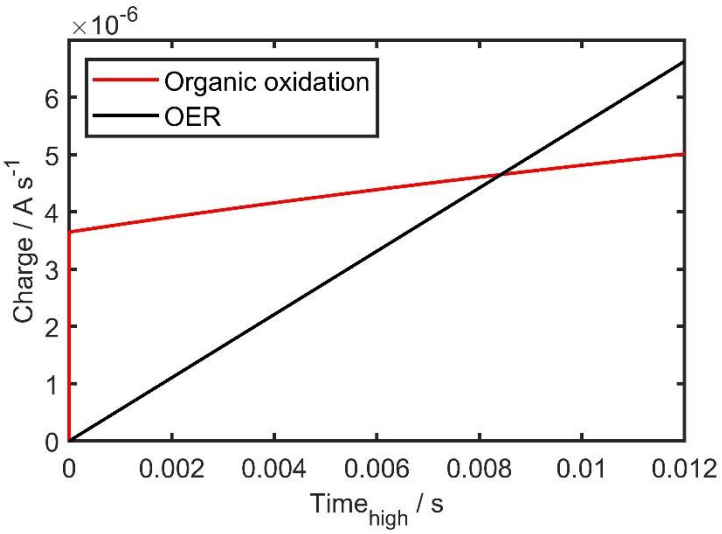

Figure 6-10 Charge consumed during the pulsed electrolysis at high step at 1.6 V for 8 ms and low step of 0.4 V for 1 s, for OER step (black line) and Organic oxidation step

Further investigation on change in concentration gradient of organic model over the electrolysis time for constant potential at 0.4 V and the pulsed electrolysis at high step of 1.6 V for 8 ms and low step of 0.4 V for 1 s revealed that although for both of this processes same amount of charge consumed but the electrolysis time is much faster, about 8 minutes, when pulsed potential electrolysis is used. Whereas to achieve the same level of organic degradation at a constant potential, electrolysis time of 25 days is required.

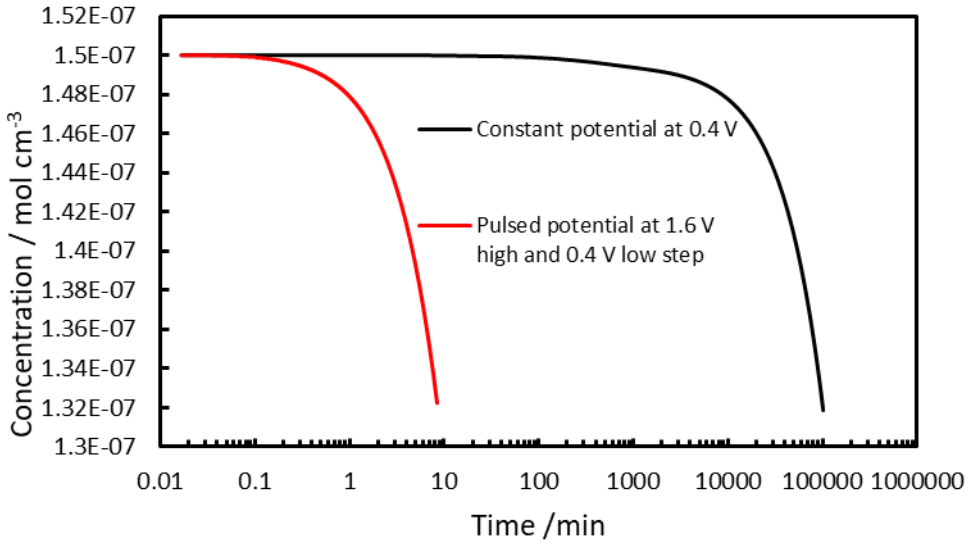

Figure 6-11 Change in concentration over the electrolysis time for constant potential of 0.4 V (black line) and pulsed electrolysis at high step of 1.6 V for 8 ms and low step of 0.4 V for 1 s (red line)

6.5 Conclusions

In this study, the electrochemical oxidation of organic species using pulsed and constant potential electrolysis is investigated through numerical simulations for "non-active" anode. The pulsed electrolysis facilitates a higher flux of organic species during the short periods in which the anode is high enough to drive the desired oxidation reaction, therefore achieving higher current efficiency. The best performance, which means lowest charge consumed for same level of of organic degradation is when pulsed potential condition at high step of 1.6 V at 8 ms and low step of 0.4 V at 1 s are applied. Further analysis on charge consumed during

electrolysis for organic oxidation step (step 3) and OER step (step 2) showed that at both cases, majority of charge consumed during the electorlysis process goes towards organic oxidation but in case of constant potential of 0.4 V due to generation of tiny current at this low potential, general oxidation rate is very slow and for the same amount of charge electrolysis time of 25 days is required, whereas in case of an applied high potenital step electrolysis time of 8 minutes is sufficent. It was also found that the potential dependence of the apparent first-order oxidation rate constant is explained by this model. In conclusion, the current efficiency of pulse potential organic oxidation is improved considerably over a range of potentials compare to constant potential electrolysis. Taking into consideration of the best step combination, the proposed pulsed electrolysis can be a breakthrough in the electrochemical wastewater treatment and in general can be implied in any other electrochemical process which follows a similar process.

Chapter 7

Conclusions and suggestion for future work

The following chapter will reiterate the key findings of this work and provide an overview of the results in terms of understanding the organic oxidation mechanism, electrocatalyst development, the identification of intermediates and products of organic oxidation, and the current efficiency of electro-oxidation of organic compounds. Finally, some suggestion on the future research are outlined briefly.

The fabrication of electrocatalyst of DSA for wastewater treatment is a complex task and requires following exact procedure and preparation, including choosing suitable solvent ratios, types of precursors, sandblasting and etching, deposition technique and synthesis method. The thermal decomposition method is used as synthesis technique for DSA electrode preparation due to its attribute superiority such as applicability to wide range of electrocatalyst compositions, high reproducibility, and controllable synthesis variable. The choice of anode material has a great impact on pollutants degradation of electrochemical oxidation. Electrochemical oxidation of pollutants is commonly divided into two oxidation mechanisms depending on the place where the overall oxidation occurs. When the oxidation occurs at or on the electrode surface the process is known as direct oxidation whereas, indirect oxidation occurs when the electrode produces a reactant which then reacts with the wastewater within the aqueous solution away from the electrode surface. Direct oxidation is

a more attractive process because it is a simpler, cleaner process; no chemical oxidant is required to be added to the solution. The anode materials control the final oxidation products and the efficiency of the direct oxidation process. The anode material must have the following properties:

- High chemical and electrochemical stability. This enables resistance to erosion and corrosion, the formation of passivation layers, and improvements in the service lifetime of the electrode;
- High electrical conductivity;
- Catalytic activity and selectivity towards organic pollutants;
- Low cost.

7.1 Kinetics and mechanism of organic oxidation

The electro-oxidation of 4-nitrophenol (4-NP) at IrO_2-Sb_2O_5-SnO_2/Ti anodes investigated to gain insight into the reaction mechanism and process efficiency. The mechanism for organic oxidation inevitably involves an oxygen evolution reaction, which happens in parallel with organic oxidation. The relative magnitude of these reactions will depend on both the inherent kinetics of the two reactions and the rate of mass transfer of the organic species into the reaction zone. For boron-doped diamond ("non-active") anodes, the literature shows that due to fast inherent reaction rate and the generated hydroxyl radicals, it is possible to balance the organic mass transfer rate with rate of the organic oxidation reaction to achieve a current efficiency of 100% with almost complete oxidation of the organic species. This balance is much more difficult for the "active" anode. The result indicate that potential dependence of the pseudo first order oxidation rate constant is consistent with potential dependence of the S-O surface coverage, which strongly suggests that this anode follows the "active" anode mechanism. This surface coverage dependent oxidation rate can only be observed at relatively low overpotentials where mass transport limitations are avoided. At high overpotentials, the rate of oxidation is completely controlled by mass transfer of 4-NP to the anode surface, with the measured and calculated rate constants agreeing closely. It is also shown that the instantaneous current efficiency can be directly calculated from the measured

pseudo first order rate constant in both the kinetic and mass transport limited regimes. Using this analytical method, it was found that the instantaneous current efficiency for 4-NP oxidation is less than 100% in both regimes and only approached 100% at very low overpotentials. This finding is important because prior literature often assumes that the instantaneous current efficiency of electrochemical wastewater oxidation will be 100%, provided that mass transfer does not limit the process. This belief stems from an underlying assumption that the rate of organic oxidation is much larger than the OER. While low anode potentials will improve current and energy efficiency, the net rate of 4-NP oxidation is low, so a compromise between higher net oxidation rates and process efficiency may be required if such a process was to be implemented in an industrial setting.

7.2 Stability of DSA electrode by addition of nanoparticles

An important parameter of DSA electrodes is their service lifetime in the strongly acidic and anodic conditions in which they often operate. The incorporation of nanoparticles into a thermally prepared IrO_2 anode as a way of improving its service lifetime was investigated. In general, the failure or deactivation of DSA is caused by a combination of substrate passivation and dissolution of the active electrocatalytic layer. In order to overcome this problem, additional oxides such as TiO_2, Ta_2O_5, or SnO_2 are often added to the electrocatalytic oxide layer to improve the corrosion resistance of the active IrO_2 and RuO_2 materials. Others have used thin interlayers between the active coating and metallic substrate in order to reduce the passivation of the electrode by preventing penetration of electrolyte through the active oxide layer to the substrate. As cracks in the DSA active layer facilitate electrolyte penetration to the underlying substrate, the observations that the presence of nanoparticles within the active layer can reduce these cracks may suggest that adding nanoparticles to DSA can improve service lifetimes. The results show that incorporation of up to 25 wt% nanoparticles into the coating formed crack-free structure during the thermal decomposition process and thus enhances the service lifetime of modified electrode dramatically by up to 10x compared to the pure IrO_2 anode. Importantly, these nanoparticle additions have minimal effect of the anodes performance towards the oxygen evolution reaction. Further addition of

nanoparticles reduced the lifetime of the anode due to uneven distribution of the active coating over the substrate leading to electrolyte penetration to, and passivation of, the underlying titanium substrate. It is proposed that adding the right quantity of nanoparticles into the IrO_2 layer improved the anodes lifetime by minimising electrolyte penetration to the substrate while increasing the mechanical strength of the layer. Importantly, the simplicity of embedding the oxide nanoparticles into the thermally prepared IrO_2 layers should be compatible with standard industrial DSA production methods and may be optimised further to improve both service lifetime and electrochemically active surface area.

7.3 Incorporation of nanoparticles in DSA electrodes for organic oxidation

The electrochemical oxidation is a promising way to treat a wide range of organic compounds with high chemical toxicity and non-biodegradability. The anode materials control the final oxidation products and the efficiency of the process. Therefore, the desired electrode material for organic oxidation must have the following essential requirements; high catalytic activity towards pollutants degradation, low production cost and long service life. Due to high energy consumption of the “non-active” anodes, the combination of metal oxide for anode with antimony-doped tin oxide (ATO) nanoparticles as high active component towards organic oxidation and iridium oxide component with low overpotential is selected. The addition of ATO nanoparticles potentially promotes the electrochemical active surface area which result in higher electrode electrocatalytic performance. The result indicates that an increase in nanoparticles percentage leads to pronounce roughness and lesser crack in the surface morphology of anode. This can help to increase the lifetime of DSA electrode. It was also observed that anode with 5 wt% ATO nanoparticles has the highest electrochemical active surface area, which is the result of better dispersion of IrO_2 phase on ATO nanoparticles during the thermal decomposition. Investagaton on the 4-NP oxidation shows that the main differences in measured chromatographs were found between pure IrO_2-based DSA and 5 wt% ATO nanoparticles anode, while other electrodes had similar chromatograph to that 5 wt% ATO nanoparticles anode. The complete oxidation of intermediates and products occurs

at anodes with the addition of ATO nanoparticles, while partial oxidisation of 4-NP occurs at pure IrO_2 anode with high accumulation of HBQ.

7.4 Modelling the dynamics and performance of pulsed electrochemical wastewater oxidation

The electrochemical oxidation of organic species using pulsed and constant potential electrolysis is investigated through numerical simulations on "non-active" anode. The main drawback of using electrochemical oxidation in the industrial scale is attributed to their high energy consumption and low current efficiency. The low current efficiency of this process is due mainly to the unwanted parallel oxygen evolution reaction that occurs at the surface of the anode. This happens when the mass transport of organic species to the anode surface is insufficient to maintain the desired current. To enhance the energy consumption and facilitate a higher mass transport of reactant to the surface of the electrode, in some industries such as electroplating, electrochemical machining and hydrogen production etc., a non-steady-state technique such as pulsed voltage, pulsed current or reverse polarity are occasionally used. The pulsing introduces a period of the pulse high-time in which the concentration gradient of reactant species steeply decreases at very short time and a pulse low-time to allow reactant species to replenish near the electrode surface.

The best performance, which means lowest charge consumed for same level of of organic degradation is when pulsed potential condition at high step of 1.6 V at 8 ms and low step of 0.4 V at 1 s are applied. Further analysis on charge consumed during electrolysis for organic oxidation step (step 3) and OER step (step 2) showed that at both cases, constant potential of 0.4 V and high step of 1.6 V at 8 ms and low step of 0.4 V at 1 s, majority of charge consumed during the electorlysis process goes towards organic oxidation but in case of constant potential of 0.4 V due to generation of tiny current at this low potential, general oxidation rate is very slow and for the same amount of charge electrolysis time of 25 days is required, whereas in case of an applied high potenital step electrolysis time of 8 minutes is sufficent. It was also found that the potential dependence of the apparent first-order oxidation rate constant is explained by this model. In conclusion, the current efficiency of pulse potential

organic oxidation is improved considerably over a range of potentials compare to constant potential electrolysis. Taking into consideration of the best step combination, the proposed pulsed electrolysis can be a breakthrough in the electrochemical wastewater treatment and in general can be implied in any other electrochemical process which follows a similar process.

7.5 Recommendations and Future work

Considering the results of this work, the electrochemical oxidation is a powerful oxidation technique, one which is relatively easy to operate and environmentally friendly, but which also involves a complex reaction mechanism. However, full control of the treatment process by a mere click of a switch is considered a major advantage of electrolysis. The biggest future challenge of electrochemical oxidation to be addressed is high treatment costs and formation of by-products with higher toxicity than initial wastewater compounds. Although this is the case for almost all advanced oxidation processes (AOPs). We have the following recommendations for further investigation and the future direction of the electrochemical oxidation of organic compounds.

7.5.1 Understanding the fundamental science

Many studies have been done on the effectiveness of electrochemical oxidation of anodes on a wide range of wastewater. To understand underlying mechanisms and performance of electrochemical oxidation better, modelling of the reaction mechanism on the surface of the electrode is essential. In this study in chapter 6, we used a simple three reaction steps model proposed by others [1] and successfully simulated the kinetics and mass transport behaviour of electro-oxidation of organics on the surface of electrode in pulsed and constant electrolysis. This shows that pulsed electrolysis can increase the efficiency of the oxidation significantly. But due to complexity the effect of phase formation such as bubble formation on the electrode, adsorption and desorption and chemical reactions has not been neglected. We used more complex model with 7 reaction steps that incorporated the adsorption and desorption effect developed by Garcia *et al. [306]* to simulate the organic oxidation on BDD

electrode, but the simulated OER polarisation curve was not a correct fit with our experimental data. Therefore, the need to develop a more comprehensive model that address all these effects is necessary so that organic oxidation behaviour in pilot or full-scale plant could be predict accurately.

7.5.2 Implementation of electrochemical oxidation

Although initial laboratory result is promising to remediate wide range of wastewater but the future development on anodes materials with specific requirement that make the process economically viable option is required. In particular, low electroactive surface area of two parallel plates prevent higher conversion rates of wastewater or induce higher electrochemical cell potential than require for treating a volume of water. The effort was made in chapters 4 and 5 to use simple method of embedding the oxide nanoparticles into the thermally prepared IrO_2 layers, which is compatible with standard industrial DSA production methods. The improvement of electroactive surface area and organic oxidation was relatively small, but the service lifetime of electrode improved significantly. Therefore, further improvement and optimisation of both service lifetime and electrochemically active surface and low cost advanced catalytic materials such as nanofiber and microporous monolete electrodes is indeed required.

7.5.3 Economic and environmental impacts

Sustainability and green remediation are utmost important to preserve and restore our environment for the future generation. To pursue this goal, scientists are investigating various strategies and technologies to minimise the human's adverse effect of the ecosystem such as carbon footprint etc. The electrochemical oxidation is a promising technique for degradation of wastewater which potentially can contribute to this goal. The advantage of electrochemical oxidation is that the primary reactant is the electron and can be produced on-site, while many of the wastewater treatment techniques require additional chemicals which involve the transportation and storage of reactants. This leads to an increase in the emission of carbon dioxide that does not generate by electrochemical oxidation. A way towards sustainability in

the near future can be the photoelectrochemical oxidation which uses both light and electricity to abatement of wastewater. Although at present, the application of photoelectrochemical oxidation is hampered due to low current delivery via visible light, so higher light intensity is provided via UV light. Another environmentally friendly strategy is to use the hydrogen evolved at the cathode in fuel cells to generate electricity and source the power requires for electrochemical oxidation or photoelectrochemical oxidation. This strategy is also beneficial to fuel cell industry – if fully developed – as relatively large energy losses are associated with producing oxygen at the anode of fuel cell [318]. In general, the feasibility of these combinations depends on several factors, such as efficiency of the processes, economic feasibility, and the development of suitable fuel cell technology are required.

Appendix 1: *HPLC parameters and calibration*

The HPLC used for 4-NP oxidation intermediates and products analysis is a Hewlett Packard 1100 series HPLC equipped with an Agilent C_{18} column with a diode array (UV/Vis). The HPLC is calibrated to detect and quantify aromatic and aliphatic compounds. The parameters used for the HPLC analysis are summarised in Table A1.1.

Table A1. 1 HPLC parameters used for the analysis of the 4-NP oxidation products inside the solution

Parameters	Setting
Column properties	Agilent C_{18} (250 mm × 4.6 mm, 5 µm)
Mobile phase	mixed of 55% methanol (HPLC grade) and 45% DI water
Flow rate	0.5 ml min^{-1}
Injection volume	10 µL
Operating pressure	Approximately 120 bar pressure at 0.5 ml min^{-1}
Operating temperature	30 °C
UV/Vis detector wavelength	260nm

The HPLC is calibrated using standards solution of aromatic compounds of 1,2,4-trihydroxy-benzene (THB), hydroquinone (HQ), 2-hydroxy-benzoquinone (HBQ), benzoquinone (BQ), 4-nitrocatechol (4-NC),4-nitrophenol (4-NP) and aliphatic compounds of oxalic acid, resorcinol, succinic acid, formic acid and acetic acid made with DI water at various concentrations. It should be mentioned that we did not identify any aliphatic compounds in the chronograms with this method and column. The external injection is enough for this HPLC method as for both calibration and measurement a fix injection of 10 µL is used.

Table A1. 2 HPLC retention time of 4-NP and its oxidation products

Retention time / min	Intermediate products
5.8	1,2,4-Trihydroxy-benzene (THB)
6	Hydroquinone (HQ)
6.9	2-Hydroxy-benzoquinone (HBQ)
7.2	Benzoquinone (BQ)
8.2	4-Nitrocatechol (4-NC)
10.8	4-Nitrophenol (4-NP)

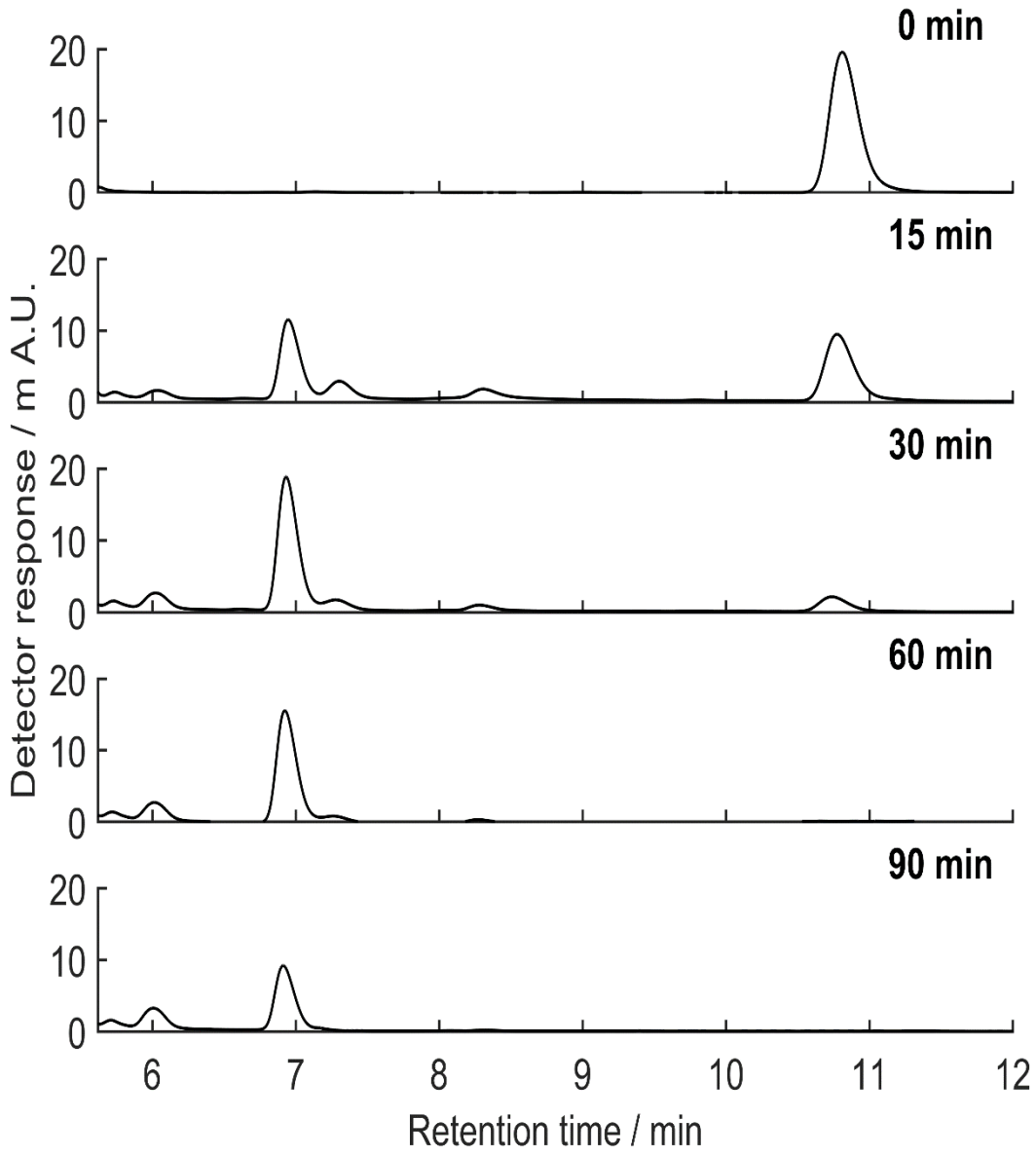

Figure A1. 1 Chromatograms of 4-NP oxidation in solution containing 0.15 mM 4-NP in 0.5 M Na_2SO_4 adjusted to pH 2 at IrO_2-based DSA 5 wt% ATO nanoparticles

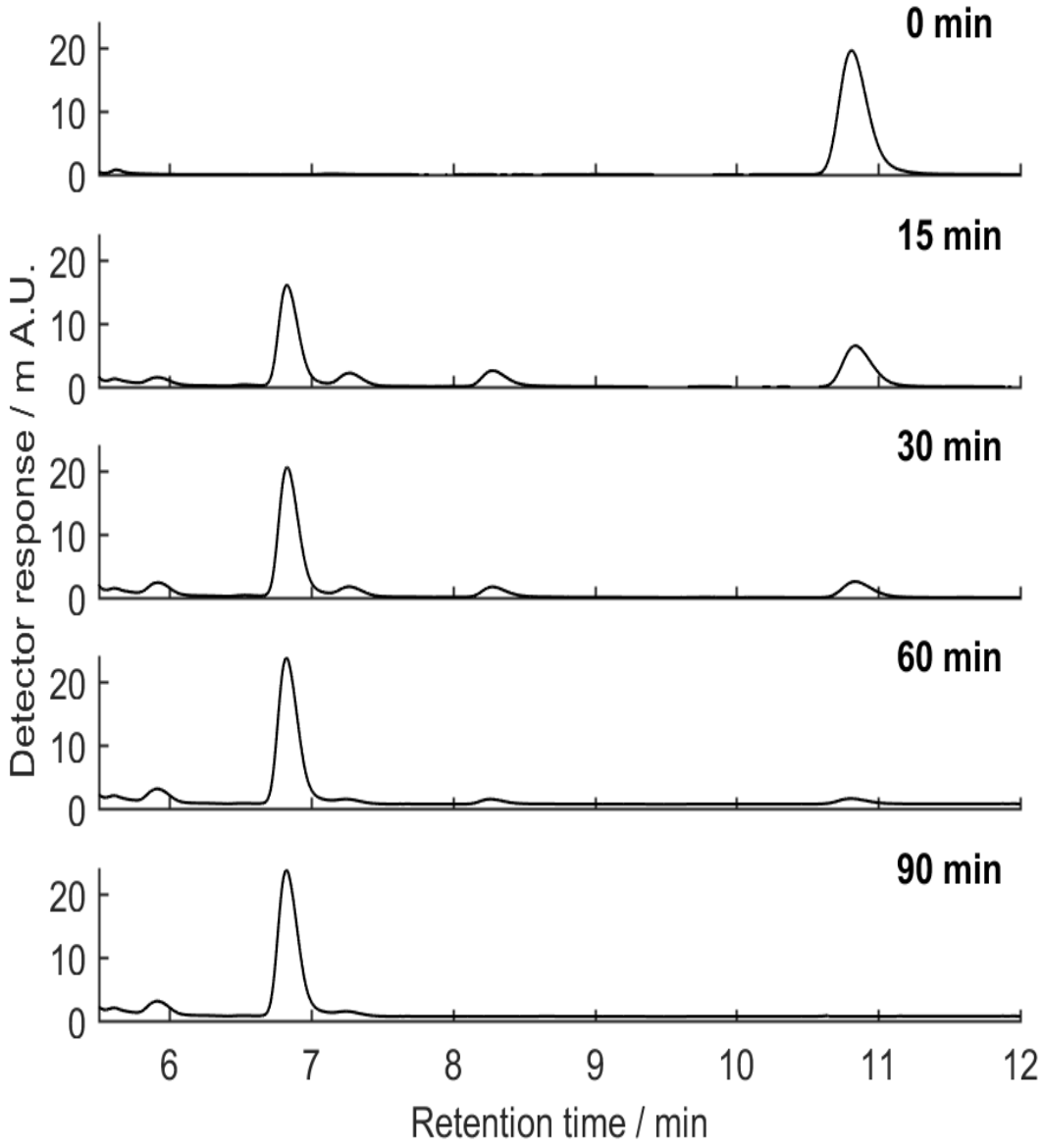

Figure A1. 2 Chromatograms of 4-NP oxidation in solution containing 0.15 mM 4-NP in 0.5 M Na_2SO_4 adjusted to pH 2 at pure IrO_2-based DSA

Appendix 2: *Modelling of pulsed electrochemical wastewater oxidation*

The following is a MATLAB script written to simulate the changes in the concentrations of species in the surface and bulk electrolyte during 4-NP oxidation at constant and pulsed electrolysis as outlined in section 6.3.

```
%=========================================
% Pulsed electrolysis model
% step 1 - define rate constants for OER and organic oxidation
% step 2 - solves steady-state polarisation curve
% step 3 - solves constant potential electrolysis with organic
% step 4 - solves pulsing electrolysis
%
%adapted by Aaron from code written by Asad Kariman, 28 June 2018
%Last modified by Asad 31/07/2019
%=========================================


%% reactions

% r1: H2O + S = S-OH + H+ + e-
% r2: S-OH = S + 1/2 O2 + H+ + e-
% r3: S-OH + R = S + RO + H+ + e-

%% assumptions

% all reactions involve Bulter-Volmer kinetics
% only r3 involves diffusion
% Langmuir isotherm behaviour of S-OH

clear all

global nodes delta D_R A F R T  V C_w C_H C_O C_R k1f_0 k1b_0 k2f_0
k2b_0 k3f_0  B1 B2 B3 x
```

```
%% Constants
C_w=0.05555;            %  mol/cm^3
pH=2;                   %  solution pH
C_H=(10^(-1*pH))/1000;  %  mol/cm^3
C_O=[2.7*10^-7];  %  mol/cm^3 from Henry's law at 1 bar O2 and 298 k

F=96485;                %  C/mol    Faraday constant
T=298;                   %  K Temperature
R=8.314;                 %  J/mol.K  Ideal gas constant

D_R = 0.919*10^-5;       %  cm^2/s     diffusion coefficient of
organic species

C_R = 15*10^-8;          %  mol/cm^3 Initial concertation of organic
species

V = 30;                  %   volume of solution / cm3
A = 1;                   %   anode area / cm2

delta =2.8E-4 ;          %   total diffusion layer thickness / cm
nodes = 20 ;             %   number of nodes used for method of
lines

x=delta/nodes;           %   thickness of each node used in method
of lines

%% rate parameters
k1f_0=10^-2;             % forward rate constant of r1, units cm/s
k2f_0=10^-4;             % forward rate constant of r2, units
mol/s.cm2
k2b_0=10^-2;             % back rate constant of r2, units
cm^2.5/s.mol^0.5

k3f_0=10^-7;             % Organic rate constant of r3, unit cm/s

K=(C_O^0.5)*(C_H^2)/C_w; % equilibrium constant, units
mol^1.5/cm^4.5

k1b_0=(k1f_0/K)*(k2f_0/k2b_0);   % calculating k_1_0 from 3 rate
constants, units cm/s

B1=0.5;                  % symmetry factor for r1
B2=0.15;                 % symmetry factor for r2
B3=0.5;                  % symmerty factor for r3
```

```
scale=0.5*10^-7;          % simple scaling factor to adjust absolute
values of k's to give sensible currents

k1f_0=k1f_0*scale;
k1b_0=k1b_0*scale;
k2f_0=k2f_0*scale;
k2b_0=k2b_0*scale;

%% calculation parameters
E_high_range = [0.5:0.2:1.4]; % overpotential for electrolysis / V
vs OER

E_low_range = [0.5:0.2:1.4];
T_loop=1;                    %number of time loop for high and low
t_high=[0.001];               % electrolysis time (pulse high) / s
t_low=[1];                    % electrolysis time (pulse low) / si3
t_end=(t_high+t_low)*T_loop   %time for electrolysis / s

for n=1:1:length(E_high_range);
    E_high=E_high_range(n);
for m=1:1:length(E_low_range);
    E_low=E_low_range(m);

=========================================================================

%% step 3 dynamic simulation of electrolysis - at E_high

if m==1               % only run once for each E_high to save time

% calculate steady-state theta at E_0
E_0=E_high;
k1f=k1f_0*exp((B1*F*E_0)/(R*T));
k1b=k1b_0*exp((-(1-B1)*F*E_0)/(R*T));
k2f=k2f_0 *exp((B2*F*E_0)/(R*T));
k2b=k2b_0*exp((-(1-B2)*F*E_0)/(R*T));
theta_0=(C_w*k1f+C_H*C_O^0.5*k2b)./(C_w*k1f+C_H*k1b+k2f+C_H*C_O^0.5*
k2b);                 % S-OH surface coverage

% define stuff for ode solver
E_ode=E_high;

t_span =linspace(0,t_end,400);     % time vector for ode

C_0 = C_R*ones(nodes,1);           % sets initial conc for each node
to the bulk value at t=0
```

```
y0 = [C_0(:); theta_0];           % sets initial conditions
options = odeset('MaxStep',10, 'RelTol',10^-12,'AbsTol',10^-12,
'InitialStep', 10^-20);
[t2,y] = ode15s(@ode_potentiostatic, t_span,y0,options,E_ode);

theta = y(:,nodes+1); %column contains theta
C_surf=y(:,1);
C = y(:,nodes);                   % bulk
C_bulkpstatic=C(end);

% calculate the rate constants at E_high
k1f=k1f_0*exp((B1*F*(E_high))/(R*T));
k1b=k1b_0*exp((-(1-B1)*F*(E_high))/(R*T));
k2f=k2f_0 *exp((B2*F*(E_high))/(R*T));
k2b=k2b_0*exp((-(1-B2)*F*(E_high))/(R*T));
k3f=k3f_0*exp((B3*F*(E_high))/(R*T));

%calculate the currents % units A/cm2
i1f=F*(C_w*k1f.*(1-theta));
i1b=F*(C_H*k1b.*theta);
i2f=F*((k2f.*theta));
i2b=F*(C_O^0.5*C_H*k2b.*(1-theta));
i3=F*(k3f.*theta.*C_surf);

%% storing the data for potentiostatic condition
c_bulk_pstatic_record(:,n)=C;
c_surf_pstatic_record(:,n)=C_surf;
theta_pstatic_record(:,n)=theta;


% store the data for all Pstat potential
i_pstatic_record(:,n)=i_pstatic(2:end,:);
i_pstatic=(i1f-i1b+i2f-i2b+i3);


% determine charge past using simple trap method.
Q1_pstatic=trapz((t2),(i1f-i1b));
Q2_pstatic=trapz(t2,(i2f-i2b));
Q3_pstatic=trapz(t2,(i3));

CE_pstatic(n)=Q3_pstatic/Q1_pstatic;

End
```

```
=====================================================================

%% step 4 simulation of pulsed electrolysis - steps from E=0 to
E_low then pulses E_high

% calculate steady-state theta at E_0
E_0=E_low;
k1f=k1f_0*exp((B1*F*E_0)/(R*T));
k1b=k1b_0*exp((-(1-B1)*F*E_0)/(R*T));
k2f=k2f_0 *exp((B2*F*E_0)/(R*T));
k2b=k2b_0*exp((-(1-B2)*F*E_0)/(R*T));
theta_0=(C_w*k1f+C_H*C_O^0.5*k2b)./(C_w*k1f+C_H*k1b+k2f+C_H*C_O^0.5*
k2b);                                % S-OH surface coverage

t_pulsed=[];
theta_pulsed=[];
C_surf_pulsed=[];
i1_pulsed=[];
i2_pulsed=[];
i3_pulsed=[];
i_pulsed_record=[];
Q1_pulsed=[];
Q2_pulsed=[];
Q3_pulsed=[];
t_0=0;
C_bulk_pulsed=[];
C_bulk_loop=[];
Qtot_loop=[];
C_bulk_pulsed_loop=[];

options = odeset('MaxStep',10, 'RelTol',10^-12,'AbsTol',10^-12,
'InitialStep', 10^-20);

C_0 = C_R*ones(nodes,1);  % sets initial conc for each node to the
bulk value at t=0
for w=1:1:T_loop;

% solve ode for first low pulse
% define stuff for ode solver
E_ode=E_low;
t_span =[0,t_low];            % time vector for ode
y0 = [C_0(:); theta_0];       % sets initial conditions

[t,y] = ode15s(@ode_potentiostatic, t_span,y0,options,E_ode);
theta = y(:,nodes+1);         %column contains theta
```

```
C_surf=y(:,1);
C_bulk = y(:,nodes);

% calculate the rate constants at E_ode
k1f=k1f_0*exp((B1*F*(E_ode))/(R*T));
k1b=k1b_0*exp((-(1-B1)*F*(E_ode))/(R*T));
k2f=k2f_0 *exp((B2*F*(E_ode))/(R*T));
k2b=k2b_0*exp((-(1-B2)*F*(E_ode))/(R*T));
k3f=k3f_0*exp((B3*F*(E_ode))/(R*T));

%calculate the currents          % units A/cm2
i1f=F*(C_w*k1f.*(1-theta));
i1b=F*(C_H*k1b.*theta);
i2f=F*((k2f.*theta));
i2b=F*(C_O^0.5*C_H*k2b.*(1-theta));
i3=F*(k3f.*theta.*C_surf);
i_pulsed=(i1f-i1b+i2f-i2b+i3);

% determine charge past using simple trap method.
Q_1=trapz(t,i1f-i1b);
Q_2=trapz(t,i2f-i2b);
Q_3=trapz(t,i3);
 Q_loop1=(Q_1+Q_2+Q_3);         % Units: Charge (A s)

%save some data
t_pulsed=[t_pulsed;t+t_0;];
theta_pulsed=[theta_pulsed; theta];
C_surf_pulsed=[C_surf_pulsed; C_surf];
i1_pulsed=[i1_pulsed; i1f-i1b];
i2_pulsed=[i2_pulsed; i2f-i2b];
i3_pulsed=[i3_pulsed; i3];
i_pulsed_record=[i_pulsed_record;i_pulsed];
Q1_pulsed=[Q1_pulsed; Q_1];
Q2_pulsed=[Q2_pulsed; Q_2];
Q3_pulsed=[Q3_pulsed; Q_3];
C_bulk_pulsed=[C_bulk_pulsed; C_bulk];

% grab final values for initial values in next step
C_0 =y(end,1:nodes);
theta_0=theta(end);
t_0=t_pulsed(end);
C_bulk_loop=[C_bulk_loop;C_0(:,end)];


%solve ode at E_high
```

```
% define stuff for ode solver
E_ode=E_high;
t_span =[0,t_high];              % time vector for ode
y0 = [C_0(:); theta_0];          % sets inital conditions
[t,y] = ode15s(@ode_potentiostatic, t_span,y0,options,E_ode);
theta = y(:,nodes+1);            %column contains theta
C_surf=y(:,1);
C_bulk = y(:,nodes);

% calculate the rate constants at E_ode
k1f=k1f_0*exp((B1*F*(E_ode))/(R*T));
k1b=k1b_0*exp((-(1-B1)*F*(E_ode))/(R*T));
k2f=k2f_0 *exp((B2*F*(E_ode))/(R*T));
k2b=k2b_0*exp((-(1-B2)*F*(E_ode))/(R*T));
k3f=k3f_0*exp((B3*F*(E_ode))/(R*T));

%calculate the currents % units A/cm2
i1f=F*(C_w*k1f.*(1-theta));
i1b=F*(C_H*k1b.*theta);
i2f=F*((k2f.*theta));
i2b=F*(C_O^0.5*C_H*k2b.*(1-theta));
i3=F*(k3f.*theta.*C_surf);
i_pulsed=(F*((C_w*k1f.*(1-theta))-(C_H*k1b.*theta)+(k2f.*theta)-
(C_O^0.5*C_H*k2b.*(1-theta))+(k3f.*theta.*C_surf)));

% determine charge past using simple trap method.
Q_1=trapz(t,i1f-i1b);
Q_2=trapz(t,i2f-i2b);
Q_3=trapz(t,i3);
Q_loop2=Q_1+Q_2+Q_3;

%save some data
t_pulsed=[t_pulsed;t+t_0;];
theta_pulsed=[theta_pulsed; theta];
C_surf_pulsed=[C_surf_pulsed; C_surf];
i1_pulsed=[i1_pulsed; i1f-i1b];
i2_pulsed=[i2_pulsed; i2f-i2b];
i3_pulsed=[i3_pulsed; i3];
i_pulsed_record=[i_pulsed_record;i_pulsed];
Q1_pulsed=[Q1_pulsed; Q_1];
Q2_pulsed=[Q2_pulsed; Q_2];
Q3_pulsed=[Q3_pulsed; Q_3];
Qtot_loop=[Q_loop1+Q_loop2;Qtot_loop+(Q_loop1+Q_loop2)];
C_bulk_pulsed=[C_bulk_pulsed; C_bulk];
C_bulk_pulsed_loop=[C_bulk_pulsed_loop;C_bulk(end)];
```

```
% grab final values for initial values in next step
C_0 =y(end,1:nodes);
theta_0=theta(end);
t_0=t_pulsed(end);
C_bulk_loop=[C_bulk_loop;C_0(:,end)];

End

C_bulk_pulsed_record(m,n)=C_bulk_pulsed(end);

Q1tot_pulsed=sum(Q1_pulsed);
Q2tot_pulsed=sum(Q2_pulsed);
Q3tot_pulsed=sum(Q3_pulsed);

Qtot_pulsed=Q1tot_pulsed+Q2tot_pulsed+Q3tot_pulsed;

CE_pulsed(m,n)=Q3tot_pulsed/Q1tot_pulsed;
%rows,columns

% plot concentration vs charge

C_bulk_pulsed_loop_record(:,m)=C_bulk_pulsed_loop;
Qtot_loop_record(:,m)=Qtot_loop;

end

end


%  log C bulk/ C initial in  bulk , 1st order reaction

lnc=log(c_bulk_pstatic_record./c_bulk_pstatic_record(1,:));

for j=1:1:length(E_high_range)

slope(j)=(-lnc(end,j)+lnc(1,j))/(t2(end,1)-t2(1,1))*60;

end

=====================================================================

%% plotting section
```

```
% The new defaults will not take effect if there are any open
figures. To
% use them, we close all figures, and then repeat the first example.
% The properties we've been using in the figures

set(0,'defaultLineLineWidth',1.5);   % set the default line width to
lw
set(0,'defaultLineMarkerSize',6); % set the default line marker size
to msz
set(0,'defaultLineLineWidth',1.5);   % set the default line width to
lw
set(0,'defaultLineMarkerSize',6); % set the default line marker size
to msz

% Set the default Size for display
defpos = get(0,'defaultFigurePosition');
width=12;
height=8;
set(0,'defaultFigurePosition', [defpos(1) defpos(2) width*40,
height*40]);

% Set the defaults for saving/printing to a file
set(0,'defaultFigureInvertHardcopy','on'); % This is the default
anyway
set(0,'defaultFigurePaperUnits','inches'); % This is the default
anyway
defsize = get(gcf, 'PaperSize');
left = (defsize(1)- width)/2;
bottom = (defsize(2)- height)/2;
defsize = [left, bottom, width, height];
set(0, 'defaultFigurePaperPosition', defsize);

figure(1);
surf(E_high_range,E_low_range,CE_pulsed)
xlabel('E_ / V','fontsize',14)
xlim([0.7 2]);
ylabel('E_ / V','fontsize',14)
ylim([0.7 2]);
zlabel('Current efficiency','fontsize',14)
zlim([0 1])
set(gca,'FontSize',14) % Creates an axes and sets its FontSize to 14

print('CE_pulsed', '-dpng', '-r300');

figure(2);
```

```
surf(E_high_range,E_low_range,C_bulk_pulsed_record)
xlabel('E_/ V','fontsize',14)
ylabel('E_ / V','fontsize',14)
zlabel('Pulsed bulk concentration','fontsize',14)
print('c_bulk_puls_record', '-dpng', '-r300');

figure (3)
plot(E_high_range,slope,'k -')
xlabel('Overpotential / V','fontsize',14)
ylabel('K_ app / min^-1','fontsize',14)
print('K_app', '-dpng', '-r300');


figure(2);
surf(E_high_range,E_low_range,C_bulk_pulsed_record)
xlabel('E_ / V','fontsize',14)
ylabel('E_ / V','fontsize',14)
zlabel('Pulsed bulk concentration','fontsize',14)
print('c_bulk_puls_record', '-dpng', '-r300');

figure (3)
plot(E_high_range,slope,'k -')
xlabel('Overpotential / V','fontsize',14)
ylabel('K_ app / min^-1','fontsize',14)
print('K_app', '-dpng', '-r300');


figure (31);
plot(t2,c_bulk_pstatic_record)
xlabel('Time / s','fontsize',14)
ylabel('Fixed potential bulk concentration','fontsize',14)
print('Fixed potential bulk concentration', '-dpng', '-r300');

figure(32);
plot(t2,c_surf_pstatic_record)
xlabel('Time / s','fontsize',14)
ylabel('surface concentration ','fontsize',14)
print('Pstat surface concentration', '-dpng', '-r300');

figure(33);
plot(t2,lnc)
xlabel('Time / s','fontsize',14)
ylabel('ln(C/C_0)','fontsize',14)
print('ln(C C_0)', '-dpng', '-r300');
```

```
figure(34);
plot(t2(2:end,:),i_pstatic_record)
xlabel('Time / s','fontsize',14)
ylabel('Pstat current density / A cm^[176]','fontsize',14)
print('i_pstatic_record_vs_t', '-dpng', '-r300');

figure(35);
plot(E_high_range,i_pstatic_record,'k -');
xlabel('E_ / V','fontsize',14)
ylabel('Pstat Current density / A cm^{-2}','fontsize',14)
print('i_pstatic_record_vs_E', '-dpng', '-r300');



 %CURVE (06082018 LSV BDD surf H2SO4.DTA)

 iBDD=[ 1.359   1.583   1.831   2.193   2.559   3.06    3.677   4.142   4.854
5.344   5.862   6.449   7.119   7.856   8.644   9.486   10.39   11.38   12.37
14.5    15.5    ];
etaBDD=[    1.013   1.086   1.149   1.234   1.289   1.339   1.374   1.394
1.419   1.434   1.449   1.464   1.479   1.494   1.509   1.524   1.539   1.554
1.569   1.597   1.612   ];


figure (36)
semilogx(i_pstatic_record(end,:),E_high_range,'r',iBDD/1000,etaBDD,'
k ')
xlabel('Current desnity / A cm^{-2}','fontsize',14)
ylabel('Overpotential / V','fontsize',14)
set(gca,'FontSize',14,'XColor','k','YColor','k') % Creates an axes
and sets its FontSize to 18
print('Polarisation', '-dpng', '-r300');

figure(37)
plot(t_pulsed,C_surf_pulsed,'k -')
xlabel('Time / s','fontsize',14)
ylabel('Surface concentration / mol cm^{-8}','fontsize',14)
print('Pulsed surface concentration ', '-dpng', '-r300');


figure(41);
plot(t_pulsed,theta_pulsed,'k -')
xlabel('Time / s','fontsize',14)
ylabel('Surface coverage','fontsize',14)
print('Pulsed_surface_coverage', '-dpng', '-r300');
```

```
figure(42)
t_e=[   0   110 165 220 330 ];
c_e=[   1.47E-07    6.96E-08    4.59E-08    2.88E-08    2.44E-08
];
plot(t_pulsed/60,C_bulk_pulsed,t_e,c_e,'r o')
hold on

t_e=[   0   10  15  20  30  ];
c_P_e=[ 1.4746E-07  8.04552E-08 5.93993E-08 4.17754E-08 1.89789E-08
];
plot(t2/60,c_bulk_pstatic_record,t_e,c_P_e,'k *')
xlabel('Time / min','fontsize',14)
ylabel('C_{R,bulk,pulsed}','fontsize',14)
print('c_pulsed_exp_model', '-dpng', '-r300');


==========================================================================


function dy=ode_potentiostatic(t,y,E_ode)

global nodes delta D_R A F R T  V C_w C_H C_O C_R k1f_0 k1b_0 k2f_0
k2b_0 k3f_0  B1 B2 B3 x

% grab the values from y
% y0=[conc...theta];

C=y(1:nodes);
theta=y(nodes+1);

% calculate the rate constants at E_ode
k1f=k1f_0*exp((B1*F*(E_ode))/(R*T));
k1b=k1b_0*exp((-(1-B1)*F*(E_ode))/(R*T));
k2f=k2f_0 *exp((B2*F*(E_ode))/(R*T));
k2b=k2b_0*exp((-(1-B2)*F*(E_ode))/(R*T));
k3f=k3f_0*exp((B3*F*(E_ode))/(R*T));

%calculate the reaction rates                    % units mol/cm^2.s
r1=C_w*k1f.*(1-theta)-C_H*k1b.*theta;
r2=(k2f.*theta)-C_O^0.5*C_H*k2b.*(1-theta);
r3=k3f.*theta*C(1);

dC=zeros(nodes,1);
dC(1)=D_R*(C(2)-C(1))/x^2-(k3f*theta*C(1)/x);     %dC_surf/dt
mol/cm^3.s
```

```
for j=2:nodes-1
    dC(j)=D_R*(C(j-1)+C(j+1)-2*C(j))/(x^2);
%dC_diffusionzone/dt mol/cm3.s

end

dC(nodes)=D_R*(A/V)*(C(nodes-1)-C(nodes))/x;         %dC_bulk/dt
mol/cm^3.s

Ntot=1E-6;      %total number of active sites mol/cm2

dtheta=(r1-r2-r3)/Ntot;

dy=[dC(:); dtheta];

end
```

Bibliography

1. Comninellis, C., *Electrocatalysis in the electrochemical conversion/combustion of organic pollutants for waste water treatment.* Electrochimica Acta, 1994. **39**(11-12): p. 1857-1862.

2. Holze, R., *Book Review: Electrochemical Methods. Fundamentals and Applications (2nd Edition). By Allen J. Bard and Larry R. Faulkner.* 2002. **41**(4): p. 655-657.

3. Bonfatti, F., S. Ferro, F. Lavezzo, M. Malacarne, G. Lodi, and A. De Battisti, *Electrochemical incineration of glucose as a model organic substrate. II. Role of active chlorine mediation.* Journal of the Electrochemical Society, 2000. **147**(2): p. 592-596.

4. Magesan, G.N. and H. Wang, *Application of municipal and industrial residuals in New Zealand forests: an overview.* Soil Research, 2003. **41**(3): p. 557-569.

5. Panizza, M. and G. Cerisola, *Direct And Mediated Anodic Oxidation of Organic Pollutants.* Chemical Reviews, 2009. **109**(12): p. 6541-6569.

6. Martinez-Huitle, C.A. and S. Ferro, *Electrochemical oxidation of organic pollutants for the wastewater treatment: direct and indirect processes.* Chemical Society Reviews, 2006. **35**(12): p. 1324-1340.

7. Lefebvre, O. and R. Moletta, *Treatment of organic pollution in industrial saline wastewater: a literature review.* Water research, 2006. **40**(20): p. 3671-3682.

8. Kolodziej, E.P., T. Harter and D.L. Sedlak, *Dairy wastewater, aquaculture, and spawning fish as sources of steroid hormones in the aquatic environment.* Environmental Science & Technology, 2004. **38**(23): p. 6377-6384.

9. Vohla, C., M. Kõiv, H.J. Bavor, F. Chazarenc and Ü. Mander, *Filter materials for phosphorus removal from wastewater in treatment wetlands—A review.* Ecological Engineering, 2011. **37**(1): p. 70-89.

10. Wakida, F.T. and D.N. Lerner, *Non-agricultural sources of groundwater nitrate: a review and case study.* Water Research, 2005. **39**(1): p. 3-16.

11. Michael, I., L. Rizzo, C. McArdell, C. Manaia, C. Merlin, T. Schwartz, C. Dagot, and D. Fatta-Kassinos, *Urban wastewater treatment plants as hotspots for the release of antibiotics in the environment: a review.* Water Research, 2013. **47**(3): p. 957-995.

12. Harrington Jr, W.M., *Hazardous solid waste from domestic wastewater treatment plants.* Environmental Health Perspectives, 1978. **27**: p. 231.

13. Chan, Y.J., M.F. Chong, C.L. Law and D. Hassell, *A review on anaerobic–aerobic treatment of industrial and municipal wastewater.* Chemical Engineering Journal, 2009. **155**(1): p. 1-18.

14. Schroeder, E.D., Book: *Water and wastewater treatment*. 1977: McGraw-Hill.

15. Oller, I., S. Malato and J. Sánchez-Pérez, *Combination of advanced oxidation processes and biological treatments for wastewater decontamination—a review.* Science of the Total Environment, 2011. **409**(20): p. 4141-4166.

16. Grady Jr, C.L., G.T. Daigger, N.G. Love and C.D. Filipe, Book: *Biological Wastewater Treatment*. 2011: CRC press.

17. Pera-Titus, M., V. Garcıa-Molina, M.A. Baños, J. Giménez and S. Esplugas, *Degradation of chlorophenols by means of advanced oxidation processes: a general review.* Applied Catalysis B: Environmental, 2004. **47**(4): p. 219-256.

18. Dorfman, L.M. and G.E. Adams, *Reactivity of the hydroxyl radical in aqueous solutions*. 1973, DTIC Document.

19. Gogate, P.R. and A.B. Pandit, *A review of imperative technologies for wastewater treatment I: oxidation technologies at ambient conditions.* Advances in Environmental Research, 2004. **8**(3): p. 501-551.

20. Andreozzi, R., V. Caprio, A. Insola and R. Marotta, *Advanced oxidation processes (AOP) for water purification and recovery.* Catalysis Today, 1999. **53**(1): p. 51-59.

21. Rajeshwar, K., J. Ibanez and G. Swain, *Electrochemistry and the environment.* Journal of Applied Electrochemistry, 1994. **24**(11): p. 1077-1091.

22. Simonsson, D., *Electrochemistry for a cleaner environment.* Chemical Society Reviews, 1997. **26**(3): p. 181-189.

23. Comninellis, C. and G. Chen, *Electrochemistry for the Environment*. 2009, New York, NY, UNITED STATES: Springer.

24. Chen, G., *Electrochemical technologies in wastewater treatment.* Separation and Purification Technology, 2004. **38**(1): p. 11-41.

25. Anglada, A., A. Urtiaga and I. Ortiz, *Contributions of electrochemical oxidation to waste-water treatment: fundamentals and review of applications.* Journal of Chemical Technology and Biotechnology, 2009. **84**(12): p. 1747-1755.

26. Chaplin, B.P., *Critical review of electrochemical advanced oxidation processes for water treatment applications.* Environmental Science: Processes & Impacts, 2014. **16**(6): p. 1182-1203.

27. Groenen-Serrano, K., E. Weiss-Hortala, A. Savall and P. Spiteri, *Role of hydroxyl radicals during the competitive electrooxidation of organic compounds on a boron-doped diamond anode.* Electrocatalysis, 2013. **4**(4): p. 346-352.

28. Jüttner, K., U. Galla and H. Schmieder, *Electrochemical approaches to environmental problems in the process industry.* Electrochimica Acta, 2000. **45**(15): p. 2575-2594.

29. Yan, L., H. Ma, B. Wang, Y. Wang and Y. Chen, *Electrochemical treatment of petroleum refinery wastewater with three-dimensional multi-phase electrode.* Desalination, 2011. **276**(1): p. 397-402.

30. Iniesta, J., E. Exposito, J. González-García, V. Montiel and A. Aldaz, *Electrochemical treatment of industrial wastewater containing phenols.* Journal of The Electrochemical Society, 2002. **149**(5): p. D57-D62.

31. Körbahtı, B.K., B. Salih and A. Tanyolaç, *Electrochemical conversion of phenolic wastewater on carbon electrodes in the presence of NaCl.* Journal of Chemical Technology and Biotechnology, 2002. **77**(1): p. 70-76.

32. Körbahti, B.K. and A. Tanyolaç, *Continuous electrochemical treatment of phenolic wastewater in a tubular reactor.* Water Research, 2003. **37**(7): p. 1505-1514.

33. Körbahti, B.K. and A. Tanyolaç, *Kinetic modeling of conversion products in the electrochemical treatment of phenolic wastewater with a NaCl electrolyte.* Industrial & Engineering Chemistry Research, 2003. **42**(21): p. 5060-5065.

34. Canizares, P., F. Martınez, M. Dıaz, J. Garcıa-Gómez and M. Rodrigo, *Electrochemical oxidation of aqueous phenol wastes using active and nonactive electrodes.* Journal of the Electrochemical Society, 2002. **149**(8): p. D118-D124.

35. Canizares, P., M. Diaz, J. Dominguez, J. Garcia-Gomez and M. Rodrigo, *Electrochemical oxidation of aqueous phenol wastes on synthetic diamond thin-film electrodes.* Industrial & Engineering Chemistry Research, 2002. **41**(17): p. 4187-4194.

36. Adams, B., M. Tian and A. Chen, *Design and electrochemical study of SnO_2-based mixed oxide electrodes.* Electrochimica Acta, 2009. **54**(5): p. 1491-1498.

37. Boye, B., M.M. Dieng and E. Brillas, *Degradation of herbicide 4-chlorophenoxyacetic acid by advanced electrochemical oxidation methods.* Environmental Science & Technology, 2002. **36**(13): p. 3030-3035.

38. Sirés, I., E. Brillas, G. Cerisola and M. Panizza, *Comparative depollution of mecoprop aqueous solutions by electrochemical incineration using BDD and PbO_2 as high oxidation power anodes.* Journal of Electroanalytical Chemistry, 2008. **613**(2): p. 151-159.

39. Polcaro, A.M., M. Mascia, S. Palmas and A. Vacca, *Electrochemical degradation of diuron and dichloroaniline at BDD electrode.* Electrochimica Acta, 2004. **49**(4): p. 649-656.

40. Brillas, E., I. Sirés, C. Arias, P.L. Cabot, F. Centellas, R.M. Rodríguez, and J.A. Garrido, *Mineralization of paracetamol in aqueous medium by anodic oxidation with a boron-doped diamond electrode.* Chemosphere, 2005. **58**(4): p. 399-406.

41. Vlyssides, A., M. Loizidou, P. Karlis, A. Zorpas and D. Papaioannou, *Electrochemical oxidation of a textile dye wastewater using a Pt/Ti electrode.* Journal of Hazardous Materials, 1999. **70**(1-2): p. 41-52.

42. Panizza, M. and G. Cerisola, *Electrocatalytic materials for the electrochemical oxidation of synthetic dyes.* Applied Catalysis B: Environmental, 2007. **75**(1-2): p. 95-101.

43. Szpyrkowicz, L., C. Juzzolino, S.N. Kaul, S. Daniele and M.D. De Faveri, *Electrochemical oxidation of dyeing baths bearing disperse dyes.* Industrial Engineering Chemistry Research, 2000. **39**(9): p. 3241-3248.

44. Mohan, N., N. Balasubramanian and C.A. Basha, *Electrochemical oxidation of textile wastewater and its reuse.* Journal of Hazardous Materials, 2007. **147**(1-2): p. 644-651.

45. Hassaan, M.A. and A. El Nemr, *Health and environmental impacts of dyes: Mini Review.* American Journal of Environmental Science Engineering, 2017. **1**(3): p. 64-67.

46. Cañizares, P., A. Gadri, J. Lobato, B. Nasr, R. Paz, M. Rodrigo, and C. Saez, *Electrochemical oxidation of azoic dyes with conductive-diamond anodes.* Industrial & Engineering Chemistry Research, 2006. **45**(10): p. 3468-3473.

47. Yi, F. and S. Chen, *Effect of activated carbon fiber anode structure and electrolysis conditions on electrochemical degradation of dye wastewater.* Journal of Hazardous Materials, 2008. **157**(1): p. 79-87.

48. Yi, F. and S. Chen, *Electrochemical treatment of alizarin red S dye wastewater using an activated carbon fiber as anode material.* Journal of Porous Materials, 2008. **15**(5): p. 565-569.

49. Wei, L., S. Guo, G. Yan, C. Chen and X. Jiang, *Electrochemical pretreatment of heavy oil refinery wastewater using a three-dimensional electrode reactor.* Electrochimica Acta, 2010. **55**(28): p. 8615-8620.

50. Al-Malack, M.H. and M. Siddiqui, *Treatment of synthetic petroleum refinery wastewater in a continuous electro-oxidation process.* Desalination Water Treatment, 2013. **51**(34-36): p. 6580-6591.

51. Gargouri, B., O.D. Gargouri, B. Gargouri, S.K. Trabelsi, R. Abdelhedi, and M. Bouaziz, *Application of electrochemical technology for removing petroleum hydrocarbons from produced water using lead dioxide and boron-doped diamond electrodes.* Chemosphere, 2014. **117**: p. 309-315.

52. Yavuz, Y., A.S. Koparal and Ü.B. Öğütveren, *Treatment of petroleum refinery wastewater by electrochemical methods.* Desalination, 2010. **258**(1-3): p. 201-205.

53. Ghanim, A. and A. Hamza, *Evaluation of Direct Anodic Oxidation Process for the Treatment of Petroleum Refinery Wastewater.* Journal of Environmental Engineering, 2018. **144**(7): p. 04018047.

54. Panizza, M., M. Zolezzi, C.J.J.o.C.T. Nicolella, E. B, Biological and electrochemical oxidation of naphthalenesulfonates. *Journal of Chemical Technology & Biotechnology: International Research in Process, Environmental & Clean Technology* 81.2 (2006): 225-232.

55. Panizza, M., M. Zolezzi and C. Nicolella, *Biological and electrochemical oxidation of naphthalenesulfonates.* Journal of Chemical Technology and Biotechnology, 2006. **81**(2): p. 225-232.

56. Pokhrel, D. and T. Viraraghavan, *Treatment of pulp and paper mill wastewater—a review.* Science of The Total Environment, 2004. **333**(1): p. 37-58.

57. Özyurt, B., Ş. Camcıoğlu and H. Hapoglu, *A consecutive electrocoagulation and electrooxidation treatment for pulp and paper mill wastewater.* Desalination Water Treatment, 2017. **93**: p. 214-228.

58. Wang, B., L. Gu and H. Ma, *Electrochemical oxidation of pulp and paper making wastewater assisted by transition metal modified kaolin.* Journal of Hazardous Materials, 2007. **143**(1): p. 198-205.

59. El-Ashtoukhy, E.S.Z., N.K. Amin and O. Abdelwahab, *Treatment of paper mill effluents in a batch-stirred electrochemical tank reactor.* Chemical Engineering Journal, 2009. **146**(2): p. 205-210.

60. Patel, U.D. and S. Suresh, *Electrochemical treatment of pentachlorophenol in water and pulp bleaching effluent.* Separation and Purification Technology, 2008. **61**(2): p. 115-122.

61. Khansorthong, S. and M. Hunsom, *Remediation of wastewater from pulp and paper mill industry by the electrochemical technique.* Chemical Engineering Journal, 2009. **151**(1): p. 228-234.

62. Wang, B., W. Kong and H. Ma, *Electrochemical treatment of paper mill wastewater using three-dimensional electrodes with Ti/Co/SnO_2-Sb_2O_5 anode.* Journal of Hazardous Materials, 2007. **146**(1): p. 295-301.

63. Sirés, I., P.L. Cabot, F. Centellas, J.A. Garrido, R.M. Rodríguez, C. Arias, and E. Brillas, *Electrochemical degradation of clofibric acid in water by anodic oxidation: comparative study with platinum and boron-doped diamond electrodes.* Electrochimica Acta, 2006. **52**(1): p. 75-85.

64. Flox, C., P.L. Cabot, F. Centellas, J.A. Garrido, R.M. Rodríguez, C. Arias, and E. Brillas, *Electrochemical combustion of herbicide mecoprop in aqueous medium using a flow reactor with a boron-doped diamond anode.* Chemosphere, 2006. **64**(6): p. 892-902.

65. Boye, B., E. Brillas, B. Marselli, P.-A. Michaud, C. Comninellis, G. Farnia, and G. Sandonà, *Electrochemical incineration of chloromethylphenoxy herbicides in*

acid medium by anodic oxidation with boron-doped diamond electrode. Electrochimica Acta, 2006. **51**(14): p. 2872-2880.

66. Carlesi Jara, C., D. Fino, V. Specchia, G. Saracco and P. Spinelli, *Electrochemical removal of antibiotics from wastewaters.* Applied Catalysis B: Environmental, 2007. **70**(1): p. 479-487.

67. Martínez-Huitle, C.A., A. De Battisti, S. Ferro, S. Reyna, M.n. Cerro-López, and M.A. Quiro, *Removal of the pesticide methamidophos from aqueous solutions by electrooxidation using Pb/PbO_2, Ti/SnO_2, and Si/BDD electrodes.* Environmental Science & Technology, 2008. **42**(18): p. 6929-6935.

68. Cortina, T. and S. Korzeniowski, *AFFF industry in position to exceed environmental goals.* Asia Pacific Fire June, 2008: p. 18-22.

69. Renner, R., *PFOS phaseout pays off*. ACS Publications, 2008, 4618-4618.

70. Mascia, M., A. Vacca, A.M. Polcaro, S. Palmas, J.R. Ruiz, and A. Da Pozzo, *Electrochemical treatment of phenolic waters in presence of chloride with boron-doped diamond (BDD) anodes: Experimental study and mathematical model.* Journal of Hazardous Materials, 2010. **174**(1): p. 314-322.

71. Sun, H., F. Li, T. Zhang, X. Zhang, N. He, Q. Song, L. Zhao, L. Sun, and T. Sun, *Perfluorinated compounds in surface waters and WWTPs in Shenyang, China: mass flows and source analysis.* Water Research, 2011. **45**(15): p. 4483-4490.

72. Giesy, J.P. and K. Kannan, *Global distribution of perfluorooctane sulfonate in wildlife.* Environmental Science Technology, 2001. **35**(7): p. 1339-1342.

73. Wang, Y., S. Beesoon, J.P. Benskin, A.O. De Silva, S.J. Genuis, and J.W. Martin, *Enantiomer fractions of chiral perfluorooctanesulfonate (PFOS) in human sera.* Environmental Science Technology, 2011. **45**(20): p. 8907-8914.

74. Niu, J., Y. Li, E. Shang, Z. Xu and J. Liu, *Electrochemical oxidation of perfluorinated compounds in water.* Chemosphere, 2016. **146**: p. 526-538.

75. Zhuo, Q., X. Li, F. Yan, B. Yang, S. Deng, J. Huang, and G. Yu, *Electrochemical oxidation of 1H, 1H, 2H, 2H-perfluorooctane sulfonic acid (6: 2 FTS) on DSA electrode: Operating parameters and mechanism.* Journal of Environmental Sciences, 2014. **26**(8): p. 1733-1739.

76. Urtiaga, A., C. Fernández-González, S. Gómez-Lavín and I. Ortiz, *Kinetics of the electrochemical mineralization of perfluorooctanoic acid on ultrananocrystalline boron doped conductive diamond electrodes.* Chemosphere, 2015. **129**: p. 20-26.

77. Zhuo, Q., S. Deng, B. Yang, J. Huang, B. Wang, T. Zhang, and G. Yu, *Degradation of perfluorinated compounds on a boron-doped diamond electrode.* Electrochimica Acta, 2012. **77**: p. 17-22.

78. Ochiai, T., Y. Iizuka, K. Nakata, T. Murakami, D.A. Tryk, A. Fujishima, Y. Koide, and Y. Morito, *Efficient electrochemical decomposition of perfluorocarboxylic acids by the use of a boron-doped diamond electrode.* Diamond Related Materials, 2011. **20**(2): p. 64-67.

79. Niu, J., H. Lin, J. Xu, H. Wu and Y. Li, *Electrochemical mineralization of perfluorocarboxylic acids (PFCAs) by Ce-doped modified porous nanocrystalline*

PbO_2 film electrode. Environmental Science Technology, 2012. **46**(18): p. 10191-10198.

80. Zhao, H., J. Gao, G. Zhao, J. Fan, Y. Wang, and Y. Wang, *Fabrication of novel SnO2-Sb/carbon aerogel electrode for ultrasonic electrochemical oxidation of perfluorooctanoate with high catalytic efficiency.* Applied Catalysis B: Environmental, 2013. **136**: p. 278-286.

81. Zhuo, Q., M. Luo, Q. Guo, G. Yu, S. Deng, Z. Xu, B. Yang, and X.J.E.A. Liang, *Electrochemical oxidation of environmentally persistent perfluorooctane sulfonate by a novel lead dioxide anode. Electrochimica Acta,* 2016. **213**: p. 358-367.

82. Carter, K.E. and J. Farrell, *Oxidative destruction of perfluorooctane sulfonate using boron-doped diamond film electrodes.* Environmental Science Technology, 2008. **42**(16): p. 6111-6115.

83. Zhuo, Q., M. Luo, Q. Guo, G. Yu, S. Deng, Z. Xu, B. Yang, and X. Liang, *Electrochemical Oxidation of Environmentally Persistent Perfluorooctane Sulfonate by a Novel Lead Dioxide Anode.* Electrochimica Acta, 2016.

84. Black, D. "Nitrophenols, ambient water quality criteria." *United State Environmental Protection Agency, Washington, DC*, 1980.

85. Polcaro, A.M., A. Vacca, M. Mascia and S. Palmas, *Oxidation at boron doped diamond electrodes: an effective method to mineralise triazines.* Electrochimica Acta, 2005. **50**(9): p. 1841-1847.

86. Polcaro, A., A. Vacca, S. Palmas and M. Mascia, *Electrochemical treatment of wastewater containing phenolic compounds: oxidation at boron-doped diamond electrodes.* Journal of Applied Electrochemistry, 2003. **33**(10): p. 885-892.

87. Feng, Y. and X.Y. Li, *Electro-catalytic oxidation of phenol on several metal-oxide electrodes in aqueous solution.* Water Research, 2003. **37**(10): p. 2399-2407.

88. Li, X.-y., Y.-h. Cui, Y.-j. Feng, Z.-m. Xie and J.-D. Gu, *Reaction pathways and mechanisms of the electrochemical degradation of phenol on different electrodes.* Water research, 2005. **39**(10): p. 1972-1981.

89. Gattrell, M. and D. Kirk, *The electrochemical oxidation of aqueous phenol at a glassy carbon electrode.* The Canadian Journal of Chemical Engineering, 1990. **68**(6): p. 997-1003.

90. Comninellis, C. and C. Pulgarin, *Anodic oxidation of phenol for waste water treatment.* Journal of applied electrochemistry, 1991. **21**(8): p. 703-708.

91. Polcaro, A.M. and S. Palmas, *Electrochemical oxidation of chlorophenols.* Industrial & Engineering Chemistry Research, 1997. **36**(5): p. 1791-1798.

92. Polcaro, A., S. Palmas, F. Renoldi and M. Mascia, *Three-dimensional electrodes for the electrochemical combustion of organic pollutants.* Electrochimica Acta, 2000. **46**(2): p. 389-394.

93. Zhuo, Q., S. Deng, B. Yang, J. Huang, B. Wang, T. Zhang, and G. Yu, *Degradation of perfluorinated compounds on a boron-doped diamond electrode.* Electrochimica Acta, 2012. **77**: p. 17-22.

94. Trasatti, S., *Physical electrochemistry of ceramic oxides.* Electrochimica Acta, 1991. **36**(2): p. 225-241.

95. Ferreira, M., H. Varela, R.M. Torresi and G. Tremiliosi-Filho, *Electrode passivation caused by polymerization of different phenolic compounds.* Electrochimica Acta, 2006. **52**(2): p. 434-442.

96. Gattrell, M. and D. Kirk, *A study of the oxidation of phenol at platinum and preoxidized platinum surfaces.* Journal of The Electrochemical Society, 1993. **140**(6): p. 1534-1540.

97. Pacheco, M., A. Morao, A. Lopes, L. Ciríaco and I. Goncalves, *Degradation of phenols using boron-doped diamond electrodes: a method for quantifying the extent of combustion.* Electrochimica Acta, 2007. **53**(2): p. 629-636.

98. Scialdone, O., A. Galia, C. Guarisco, S. Randazzo and G. Filardo, *Electrochemical incineration of oxalic acid at boron doped diamond anodes: role of operative parameters.* Electrochimica Acta, 2008. **53**(5): p. 2095-2108.

99. Kötz, R., S. Stucki and B. Carcer, *Electrochemical waste water treatment using high overvoltage anodes. Part I: Physical and electrochemical properties of SnO_2 anodes. Journal of Applied Electrochemistry,* 1991. **21**(1): p. 14-20.

100. Quiroz, M., S. Reyna, C. Martinez-Huitle, S. Ferro and A. De Battisti, *Electrocatalytic oxidation of p-nitrophenol from aqueous solutions at Pb/PbO_2 anodes.* Applied Catalysis B: Environmental, 2005. **59**(3-4): p. 259-266.

101. Hu, J.-M., J.-Q. Zhang, H.-M. Meng, J.-T. Zhang and C.-N. Cao, *Electrochemical activity, stability and degradation characteristics of IrO_2-based electrodes in*

aqueous solutions containing C1 compounds. Electrochimica Acta, 2005. **50**(27): p. 5370-5378.

102. Trasatti, S., *Electrocatalysis: understanding the success of DSA®.* Electrochimica Acta, 2000. **45**(15): p. 2377-2385.

103. Beer, H.B., *The invention and industrial development of metal anodes.* Journal of the Electrochemical Society, 1980. **127**(8): p. 303C-307C.

104. Takasu, Y., W. Sugimoto, Y. Nishiki and S. Nakamatsu, *Structural analyses of RuO_2–TiO_2/Ti and IrO_2–RuO_2–TiO_2/Ti anodes used in industrial chlor-alkali membrane processes.* Journal of Applied Electrochemistry, 2010. **40**(10): p. 1789-1795.

105. Marshall, A.T., S. Sunde, M. Tsypkin and R. Tunold, *Performance of a PEM water electrolysis cell using $Ir_xRu_yTa_zO_2$ electrocatalysts for the oxygen evolution electrode.* International Journal of Hydrogen Energy, 2007. **32**(13): p. 2320-2324.

106. Msindo, Z., V. Sibanda and J.H. Potgieter, *Electrochemical and physical characterisation of lead-based anodes in comparison to Ti–(70%) IrO_2/(30%) Ta_2O_5 dimensionally stable anodes for use in copper electrowinning.* Journal of Applied Electrochemistry, 2010. **40**(3): p. 691-699.

107. Chatzisymeon, E., A. Dimou, D. Mantzavinos and A. Katsaounis, *Electrochemical oxidation of model compounds and olive mill wastewater over DSA electrodes: 1. The case of Ti/IrO_2 anode.* Journal of Hazardous Materials, 2009. **167**(1-3): p. 268-274.

108. Chen, J., H. Shi and J. Lu, *Electrochemical treatment of ammonia in wastewater by RuO_2–IrO_2–TiO_2/Ti electrodes.* Journal of Applied Electrochemistry, 2007. **37**(10): p. 1137-1144.

109. Lei, X. and T. Maekawa, *Electrochemical treatment of anaerobic digestion effluent using a Ti/Pt–IrO_2 electrode.* Bioresource Technology, 2007. **98**(18): p. 3521-3525.

110. Gattrell, M. and D. Kirk, *A study of the oxidation of phenol at platinum and preoxidized platinum surfaces.* Journal of The Electrochemical Society, 1993. **140**(6): p. 1534-1540.

111. Bonfatti, F., S. Ferro, F. Lavezzo, M. Malacarne, G. Lodi, and A. De Battisti, *Electrochemical incineration of glucose as a model organic substrate. I. Role of the electrode material.* Journal of the Electrochemical Society, 1999. **146**(6): p. 2175-2179.

112. Brillas, E., M.A. Banos and J.A. Garrido, *Mineralization of herbicide 3, 6-dichloro-2-methoxybenzoic acid in aqueous medium by anodic oxidation, electro-Fenton and photoelectro-Fenton.* Electrochimica Acta, 2003. **48**(12): p. 1697-1705.

113. Johnson, S.K., L.L. Houk, J. Feng, R. Houk and D.C. Johnson, *Electrochemical incineration of 4-chlorophenol and the identification of products and intermediates by mass spectrometry.* Environmental Science Technology, 1999. **33**(15): p. 2638-2644.

114. Watanabe, M.a. and S. Motoo, *Electrocatalysis by ad-atoms: Part II. Enhancement of the oxidation of methanol on platinum by ruthenium ad-atoms.*

Journal of Electroanalytical Chemistry Interfacial Electrochemistry, 1975. **60**(3): p. 267-273.

115. Gao, G. and C.D. Vecitis, *Electrocatalysis aqueous phenol with carbon nanotubes networks as anodes: electrodes passivation and regeneration and prevention.* Electrochimica Acta, 2013. **98**: p. 131-138.

116. Cañizares, P., J.A. Domínguez, M.A. Rodrigo, J. Villaseñor and J. Rodríguez, *Effect of the Current Intensity in the Electrochemical Oxidation of Aqueous Phenol Wastes at an Activated Carbon and Steel Anode.* Industrial & Engineering Chemistry Research, 1999. **38**(10): p. 3779-3785.

117. Boudenne, J.L., O. Cerclier, J. Galéa and E. Van Der Vlist, *Electrochemical oxidation of aqueous phenol at a carbon black slurry electrode.* Applied Catalysis A: General, 1996. **143**(2): p. 185-202.

118. Polcaro, A.M and Palmas S, *Electrochemical oxidation of chlorophenols. Industrial & Engineering Chemistry Research,* 1997. **36**(5): p. 1791-1798.

119. Polcaro, g.A., S. Palmas, F. Renoldi and M. Mascia, *Three-dimensional electrodes for the electrochemical combustion of organic pollutants.* Electrochimica Acta, 2000. **46**(2-3): p. 389-394.

120. Boudenne, J.-L. and O. Cerclier, *Performance of carbon black-slurry electrodes for 4-chlorophenol oxidation.* Water Research, 1999. **33**(2): p. 494-504.

121. Han, Y., X. Quan, X. Ruan and W. Zhang, *Integrated electrochemically enhanced adsorption with electrochemical regeneration for removal of acid orange 7*

using activated carbon fibers. Separation Purification Technology, 2008. **59**(1): p. 43-49.

122. Fan, L., F. Yang and W. Yang, *Performance of the decolorization of an azo dye with bipolar packed bed cell.* Separation Purification Technology, 2004. **34**(1-3): p. 89-96.

123. Carey, J.J., C.S. Christ Jr and S.N. Lowery, *Method of electrolysis employing a doped diamond anode to oxidize solutes in wastewater*. 1995, Google Patents.

124. Fujishima, A., Y. Einaga, T.N. Rao and D.A. Tryk, *Diamond electrochemistry*. 2005: Elsevier.

125. Pleskov, Y.V., *Synthetic diamond in electrochemistry.* Russian chemical reviews, 1999. **68**(5): p. 381-392.

126. Rao, T. and A. Fujishima, *Recent advances in electrochemistry of diamond.* Diamond Related Materials, 2000. **9**(3-6): p. 384-389.

127. Björklund, E., B. Styrishave, G.G. Anskjær, M. Hansen and B. Halling-Sørensen, *Dichlobenil and 2,6-dichlorobenzamide (BAM) in the environment: What are the risks to humans and biota?*, Science of The Total Environment, 2011. **409**(19): p. 3732-3739.

128. Louhichi, B., M. Ahmadi, N. Bensalah, A. Gadri and M. Rodrigo, *Electrochemical degradation of an anionic surfactant on boron-doped diamond anodes.* Journal of Hazardous Materials, 2008. **158**(2-3): p. 430-437.

129. Zhuo, Q., S. Deng, B. Yang, J. Huang, B. Wang, T. Zhang, and G.J.E.A. Yu, *Degradation of perfluorinated compounds on a boron-doped diamond electrode. Electrochimica Acta,* 77 (2012): 17-22.

130. Hastie, J., D. Bejan, M. Teutli-Leon and N.J. Bunce, *Electrochemical methods for degradation of Orange II (sodium 4-(2-hydroxy-1-naphthylazo) benzenesulfonate).* Industrial Engineering Chemistry Research, 2006. **45**(14): p. 4898-4904.

131. Cañizares, P., A. Gadri, J. Lobato, B. Nasr, R. Paz, M. Rodrigo, and C. Saez, *Electrochemical oxidation of azoic dyes with conductive-diamond anodes.* Industrial Engineering Chemistry Research, 2006. **45**(10): p. 3468-3473.

132. Flox, C., S. Ammar, C. Arias, E. Brillas, A.V. Vargas-Zavala, and R. Abdelhedi, *Electro-Fenton and photoelectro-Fenton degradation of indigo carmine in acidic aqueous medium.* Applied Catalysis B: Environmental, 2006. **67**(1-2): p. 93-104.

133. Palma-Goyes, R.E., F.L. Guzmán-Duque, G. Peñuela, I. González, J.L. Nava, and R.A. Torres-Palma, *Electrochemical degradation of crystal violet with BDD electrodes: Effect of electrochemical parameters and identification of organic by-products.* Chemosphere, 2010. **81**(1): p. 26-32.

134. Zhou, M., H. Särkkä and M. Sillanpää, *A comparative experimental study on methyl orange degradation by electrochemical oxidation on BDD and MMO electrodes.* Separation and Purification Technology, 2011. **78**(3): p. 290-297.

135. Haidar, M., A. Dirany, I. Sirés, N. Oturan and M.A. Oturan, *Electrochemical degradation of the antibiotic sulfachloropyridazine by hydroxyl radicals generated at a BDD anode.* Chemosphere, 2013. **91**(9): p. 1304-1309.

136. Cañizares, P., C. Sáez, J. Lobato and M.A. Rodrigo, *Electrochemical treatment of 2,4-dinitrophenol aqueous wastes using boron-doped diamond anodes.* Electrochimica Acta, 2004. **49**(26): p. 4641-4650.

137. Cañizares, P., J. Lobato, R. Paz, M.A. Rodrigo and C. Sáez, *Electrochemical oxidation of phenolic wastes with boron-doped diamond anodes.* Water Research, 2005. **39**(12): p. 2687-2703.

138. Jiang, J., M. Chang and P. Pan, *Simultaneous Hydrogen Production and Electrochemical Oxidation of Organics Using Boron-Doped Diamond Electrodes.* Environmental Science & Technology, 2008. **42**(8): p. 3059-3063.

139. Iniesta, J., P.A. Michaud, M. Panizza, G. Cerisola, A. Aldaz, and C. Comninellis, *Electrochemical oxidation of phenol at boron-doped diamond electrode.* Electrochimica Acta, 2001. **46**(23): p. 3573-3578.

140. Sun, J., H. Lu, H. Lin, L. Du, W. Huang, H. Li, and T. Cui, *Electrochemical oxidation of aqueous phenol at low concentration using Ti/BDD electrode.* Separation and Purification Technology, 2012. **88**: p. 116-120.

141. Newkirk, A.E. and D.W. McKee, *Thermal decomposition of rhodium, iridium, and ruthenium chlorides.* Journal of Catalysis, 1968. **11**(4): p. 370-377.

142. Newkirk, A. and D. McKee, *Thermal decomposition of rhodium, iridium, and ruthenium chlorides.* Journal of Catalysis, 1968. **11**(4): p. 370-377.

143. Ardizzone, S., M. Falciola and S. Trasatti, *Effect of the nature of the precursor on the electrocatalytic properties of thermally prepared ruthenium oxide.* Journal of The Electrochemical Society, 1989. **136**(5): p. 1545-1550.

144. Gutoff, E.B. and E.D. Cohen, Water-and solvent-based coating technology. *Multilayer Flexible Packaging*. William Andrew Publishing, 2016. 205-234

145. Kakaei, K., M.D. Esrafili and A. Ehsani, Graphene and Anticorrosive Properties. *Interface Science and Technology*. Vol. 27. Elsevier, 2019. 303-337.

146. Klamklang, S., Klamklang, Songsak. *Restaurant wastewater treatment by electrochemical oxidation in continuous process*. Dissertation. 2007.

147. Dorey, R. and R. W. Whatmore, Ceramic Thick Films for MEMS. *Electroceramic-Based MEMS*. Springer, 2005. 177-197.

148. Yeniyol, S., N. Bölükbaşi, A.F. Çakir, A. Bilir and T. Özdemir, *Effects of surface modifications with oxalic acid etching and sandblasting on surface topography and biocompatibility of cpTi surfaces.* Biotechnology Biotechnological Equipment, 2013. **27**(4): p. 3995-4001.

149. Liu, Y.-C., *Electrodeposition and characterization of metals and metal oxides for energy conversion and storage.* Dissertation. 2016.

150. M., Eric, Vanessa F.C., and Tulio Matencio. “Metallic and Oxide Electrodeposition.” *Modern Surface Engineering Treatments*. InTech, 2013. *Modern Surface Engineering Treatments*. Web.

151. Wang, Q., Q. Cao, X. Wang, B. Jing, H. Kuang, and L. Zhou, *A high-capacity carbon prepared from renewable chicken feather biopolymer for supercapacitors.* Journal of Power Sources, 2013. **225**: p. 101-107.

152. Asano, Y., T. Komatsu, K. Murashiro and K. Hoshino, Capacitance studies of cobalt compound nanowires prepared via electrodeposition. *Journal of Power Sources* 196.11 (2011): 5215-5222.

153. Charles, U.A., M.A. Ibrahim and M.A.M. Teridi, *Electrodeposition of organic–inorganic tri-halide perovskites solar cell.* Journal of Power Sources, 2018. **378**: p. 717-731.

154. Ge, J. and Y. Yan, Controllable multinary alloy electrodeposition for thin-film solar cell fabrication: a case study of kesterite Cu2ZnSnS4. *iScience* 1 (2018): 55-71.

155. Shi, L., C. Sun, P. Gao, F. Zhou and W. Liu, *Mechanical properties and wear and corrosion resistance of electrodeposited Ni–Co/SiC nanocomposite coating.* Applied Surface Science, 2006. **252**(10): p. 3591-3599.

156. Gavrila, M., J. Millet, H. Mazille, D. Marchandise and J. Cuntz, *Corrosion behaviour of zinc–nickel coatings, electrodeposited on steel.* Surface Coatings Technology, 2000. **123**(2-3): p. 164-172.

157. El Abedin, S.Z., N. Borissenko and F. Endres, *Electrodeposition of nanoscale silicon in a room temperature ionic liquid.* Electrochemistry Communications, 2004. **6**(5): p. 510-514.

158. Endres, F., *Ionic liquids: solvents for the electrodeposition of metals and semiconductors.* ChemPhysChem, 2002. **3**(2): p. 144-154.

159. Morent, R. and N. De Geyter, *1 - Improved textile functionality through surface modifications*, in *Functional Textiles for Improved Performance, Protection and Health*, N. Pan and G. Sun, Editors. 2011, Woodhead Publishing. p. 3-26.

160. Pierson, Hugh O. *Handbook of chemical vapor deposition: principles, technology and applications*. William Andrew, 1999.

161. Parsons, S. Book: *Advanced oxidation processes for water and wastewater treatment*. 2004: IWA. xii, 356 p.-xii, 356 p.

162. Sonune, A. and R. Ghate, *Developments in wastewater treatment methods.* Desalination, 2004. **167**: p. 55-63.

163. Helmer, R. and I. Hespanhol, *Water pollution control : a guide to the use of water quality management principles*. 1997: E&FN Spon. xvi, 510 p.-xvi, 510 p.

164. Comninellis, C., A. Kapalka, S. Malato, S.A. Parsons, L. Poulios, and D. Mantzavinos, *Advanced oxidation processes for water treatment: advances and trends for R&D.* Journal of Chemical Technology and Biotechnology, 2008. **83**(6): p. 769-776.

165. Sires, I., E. Brillas, M.A. Oturan, M.A. Rodrigo and M. Panizza, *Electrochemical advanced oxidation processes: today and tomorrow. A review.* Environmental Science and Pollution Research, 2014. **21**(14): p. 8336-8367.

166. Oturan, M.A. and J.J. Aaron, *Advanced Oxidation Processes in Water/Wastewater Treatment: Principles and Applications. A Review.* Critical Reviews in Environmental Science and Technology, 2014. **44**(23): p. 2577-2641.

167. Murphy, O.J., G.D. Hitchens, L. Kaba and C.E. Verostko, *Direct Electrochemical Oxidation of Organics for Waste-Water Treatment.* Water Research, 1992. **26**(4): p. 443-451.

168. Comninellis, C., *Electrocatalysis in the electrochemical conversion/combustion of organic pollutants for waste water treatment.* Electrochimica Acta, 1994. **39**(11–12): p. 1857-1862.

169. Martínez-Huitle, C.A. and S. Ferro, *Electrochemical oxidation of organic pollutants for the wastewater treatment: direct and indirect processes.* Chemical Society Reviews, 2006. **35**(12): p. 1324-1340.

170. Anglada, Á., A. Urtiaga and I. Ortiz, *Contributions of electrochemical oxidation to waste-water treatment: fundamentals and review of applications.* Journal of Chemical Technology and Biotechnology, 2009. **84**(12): p. 1747-1755.

171. Adams, B., M. Tian and A. Chen, *Design and electrochemical study of SnO_2-based mixed oxide electrodes.* Electrochimica Acta, 2009. **54**(5): p. 1491-1498.

172. Hernlem, B.J., *Electrolytic destruction of urea in dilute chloride solution using DSA electrodes in a recycled batch cell.* Water Research, 2005. **39**(11): p. 2245-2252.

173. Martínez-Huitle, C.A., S. Ferro and A. De Battisti, *Electrochemical incineration of oxalic acid - Role of electrode material.* Electrochimica Acta, 2004. **49**(22-23): p. 4027-4034.

174. Panizza, M., P.A. Michaud, G. Cerisola and C. Comninellis, *Anodic oxidation of 2-naphthol at boron-doped diamond electrodes.* Journal of Electroanalytical Chemistry, 2001. **507**(1-2): p. 206-214.

175. Polcaro, A.M., A. Vacca, S. Palmas and M. Mascia, *Electrochemical treatment of wastewater containing phenolic compounds: oxidation at boron-doped diamond electrodes.* Journal of Applied Electrochemistry, 2003. **33**(10): p. 885-892.

176. Simond, O. and C. Comninellis, *Anodic oxidation of organics on Ti/IrO_2 anodes using Nafion® as electrolyte.* Electrochimica Acta, 1997. **42**(13–14): p. 2013-2018.

177. Tian, M., L. Bakovic and A.C. Chen, *Kinetics of the electrochemical oxidation of 2-nitrophenol and 4-nitrophenol studied by in situ UV spectroscopy and chemometrics.* Electrochimica Acta, 2007. **52**(23): p. 6517-6524.

178. Cañizares, P., C. Saez, J. Lobato and M.A. Rodrigo, *Electrochemical Treatment of 4-Nitrophenol-Containing Aqueous Wastes Using Boron-Doped Diamond Anodes.* Industrial & Engineering Chemistry Research, 2004. **43**(9): p. 1944-1951.

179. Andrade, L.S., T.T. Tasso, D.L. da Silva, R.C. Rocha, N. Bocchi, and S.R. Biaggio, *On the performances of lead dioxide and boron-doped diamond electrodes in the anodic oxidation of simulated wastewater containing the Reactive Orange 16 dye.* Electrochimica Acta, 2009. **54**(7): p. 2024-2030.

180. Bock, C. and B. MacDougall, *The electrochemical oxidation of organics using tungsten oxide based electrodes.* Electrochimica Acta, 2002. **47**(20): p. 3361-3373.

181. Bonfatti, F., S. Ferro, F. Lavezzo, M. Malacarne, G. Lodi, and A. De Battisti, *Electrochemical incineration of glucose as a model organic substrate - II. Role of active chlorine mediation.* Journal of the Electrochemical Society, 2000. **147**(2): p. 592-596.

182. Fierro, S., L. Ouattara, E.H. Calderon, E. Passas-Lagos, H. Baltruschat, and C. Comninellis, *Investigation of formic acid oxidation on Ti/IrO_2 electrodes.* Electrochimica Acta, 2009. **54**(7): p. 2053-2061.

183. Watts, R.J., M.S. Wyeth, D.D. Finn and A.L. Teel, *Optimization of Ti/SnO_2-Sb_2O_5 anode preparation for electrochemical oxidation of organic contaminants in water and wastewater.* Journal of Applied Electrochemistry, 2008. **38**(1): p. 31-37.

184. Cañizares, P., J. García-Gómez, J. Lobato and M.A. Rodrigo, *Modeling of Wastewater Electro-oxidation Processes Part I. General Description and Application to Inactive Electrodes.* Industrial & Engineering Chemistry Research, 2004. **43**(9): p. 1915-1922.

185. Mascia, M., A. Vacca, S. Palmas and A.M. Polcaro, *Kinetics of the electrochemical oxidation of organic compounds at BDD anodes: modelling of surface reactions.* Journal of Applied Electrochemistry, 2007. **37**(1): p. 71-76.

186. Simond, O., V. Schaller and C. Comninellis, *Theoretical model for the anodic oxidation of organics on metal oxide electrodes.* Electrochimica Acta, 1997. **42**(13-14): p. 2009-2012.

187. Cañizares, P., J. García-Gómez, J. Lobato and M.A. Rodrigo, *Modeling of Wastewater Electro-oxidation Processes Part II. Application to Active Electrodes.* Industrial & Engineering Chemistry Research, 2004. **43**(9): p. 1923-1931.

188. Scialdone, O., *Electrochemical oxidation of organic pollutants in water at metal oxide electrodes: A simple theoretical model including direct and indirect oxidation processes at the anodic surface.* Electrochimica Acta, 2009. **54**(26): p. 6140-6147.

189. Rodrigo, M.A., P.A. Michaud, I. Duo, M. Panizza, G. Cerisola, and C. Comninellis, *Oxidation of 4-chlorophenol at boron-doped diamond electrode for wastewater treatment.* Journal of the Electrochemical Society, 2001. **148**(5): p. D60-D64.

190. Beer, H.B., *The Invention and Industrial-Development of Metal Anodes.* Journal of the Electrochemical Society, 1980. **127**(8): p. C303-C307.

191. Gil, A.F., L. Galicia and I. Gonzalez, *Diffusion coefficients and electrode kinetic parameters of different Fe(III)-sulfate complexes.* Journal of Electroanalytical Chemistry, 1996. **417**(1-2): p. 129-134.

192. Klaning, U.K., K. Sehested and J. Holcman, *Standard Gibbs energy of formation of the hydroxyl radical in aqueous solution. Rate constants for the reaction* $ClO_2^- + O_3 <=> O_3^- + ClO_2$. The Journal of Physical Chemistry, 1985. **89**(5): p. 760-763.

193. De Pauli, C. and S. Trasatti, *Composite materials for electrocatalysis of O_2 evolution: IrO_2 + SnO_2 in acid solution.* Journal of Electroanalytical Chemistry, 2002. **538-539**: p. 145-151.

194. Bockris, J.O.M., *Kinetics of Activation Controlled Consecutive Electrochemical Reactions: Anodic Evolution of Oxygen.* The Journal of Chemical Physics, 1956. **24**(4): p. 817-827.

195. De Pauli, C. and S. Trasatti, *Electrochemical Surafce Characterization of IrO_2 + SnO_2 Mixed Oxide Electrodes.* Journal of Electroanalytical Chemistry, 1995. **396**: p. 161-168.

196. Marshall, A.T. and L. Vaisson-Béthune, *Avoid the quasi-equilibrium assumption when evaluating the electrocatalytic oxygen evolution reaction mechanism by Tafel slope analysis.* Electrochemistry Communications, 2015. **61**: p. 23-26.

197. Gileadi, E., *Problems in interfacial electrochemistry that have been swept under the carpet.* Journal of Solid State Electrochemistry, 2011. **15**(7-8): p. 1359-1371.

198. Niesner, R. and A. Heintz, *Diffusion coefficients of aromatics in aqueous solution.* Journal of Chemical and Engineering Data, 2000. **45**(6): p. 1121-1124.

199. Kapalka, A., G. Foti and C. Comninellis, *Kinetic modelling of the electrochemical mineralization of organic pollutants for wastewater treatment.* Journal of Applied Electrochemistry, 2008. **38**(1): p. 7-16.

200. Lea, J. and A.A. Adesina, *Oxidative degradation of 4-nitrophenol in UV-illuminated titania suspension.* Journal of Chemical Technology and Biotechnology, 2001. **76**(8): p. 803-810.

201. Chaliha, S., K.G. Bhattacharyya and P. Paul, *Oxidation of 4-nitrophenol in water over Fe(III), Co(II), and Ni(II) impregnated MCM41 catalysts.* Journal of Chemical Technology and Biotechnology, 2008. **83**(10): p. 1353-1363.

202. Cornard, J., Rasmiwetti and J. Merlin, *Molecular structure and spectroscopic properties of 4-nitrocatechol at different pH: UV–visible, Raman, DFT and TD-DFT calculations.* Chemical Physics, 2005. **309**(2–3): p. 239-249.

203. Sirajuddin, M.I. Bhanger, A. Niaz, A. Shah and A. Rauf, *Ultra-trace level determination of hydroquinone in waste photographic solutions by UV–vis spectrophotometry.* Talanta, 2007. **72**(2): p. 546-553.

204. Oturan, M.A., J. Peiroten, P. Chartrin and A.J. Acher, *Complete Destruction of p-Nitrophenol in Aqueous Medium by Electro-Fenton Method.* Environmental Science & Technology, 2000. **34**(16): p. 3474-3479.

205. Trasatti, S., *Physical electrochemistry of ceramic oxides.* Electrochimica Acta, 1991. **36**: p. 225-241.

206. Wyatt, B.S., *Cathodic protection of steel in concrete.* Corrosion Science, 1993. **35**(5): p. 1601-1615.

207. Zeng, K. and D.K. Zhang, *Recent progress in alkaline water electrolysis for hydrogen production and applications.* Progress in Energy and Combustion Science, 2010. **36**(3): p. 307-326.

208. Profeti, D., T.A.F. Lassali and P. Olivi, *Preparation of $Ir_{0.3}Sn_{(0.7-x)}Ti_xO_2$ Electrodes by the Polymeric Precursor Method: Characterization and Lifetime Study.* Journal of Applied Electrochemistry, 2006. **36**(8): p. 883-888.

209. Correa-Lozano, B., C. Comninellis and A.D. Battisti, *Service life of Ti/SnO_2–Sb_2O_5 anodes.* Journal of Applied Electrochemistry, 1997. **27**(8): p. 970-974.

210. Mazhari Abbasi, H., K. Jafarzadeh and S.M. Mirali, *An investigation of the effect of RuO_2 on the deactivation and corrosion mechanism of a Ti/IrO_2+Ta_2O_5 coating in an OER application.* Journal of Electroanalytical Chemistry, 2016. **777**: p. 67-74.

211. Shao, D., X. Li, H. Xu and W. Yan, *An improved stable Ti/Sb–SnO_2 electrode with high performance in electrochemical oxidation processes.* RSC Advances, 2014. **4**(41): p. 21230-21237.

212. De Battisti, A., A. Barbieri, A. Giatti, G. Battaglin, S. Daolio, and A.B. Boscoletto, *Depth profiles and electrochemical properties of IrO_2 electrocatalysts stabilized with TiO_2.* Journal of Materials Chemistry, 1991. **1**(2): p. 191-195.

213. Ardizzone, S., C.L. Bianchi, G. Cappelletti, M. Ionita, A. Minguzzi, S. Rondinini, and A. Vertova, *Composite ternary SnO_2–IrO_2–Ta_2O_5 oxide electrocatalysts.* Journal of Electroanalytical Chemistry, 2006. **589**(1): p. 160-166.

214. Roginskaya, Y.E., O.V. Morozova, E.N. Loubnin, A.V. Popov, Y.I. Ulitina, V.V. Zhurov, S.A. Ivanov, and S. Trasatti, *X-ray diffraction, transmission electron microscopy and X-ray photoelectron spectroscopic characterization of IrO_2+ Ta_2O_5 films.* Journal of the Chemical Society, Faraday Transactions, 1993. **89**(11): p. 1707-1715.

215. Chen, A. and S. Nigro, *Influence of a Nanoscale Gold Thin Layer on Ti/SnO_2-Sb_2O_5 Electrodes.* The Journal of Physical Chemistry B, 2003. **107**(48): p. 13341-13348.

216. Kamegaya, Y., K. Sasaki, M. Oguri, T. Asaki, H. Kobayashi, and T. Mitamura, *Improved durability of iridium oxide coated titanium anode with interlayers for oxygen evolution at high current densities.* Electrochimica Acta, 1995. **40**(7): p. 889-895.

217. Wu, L.-K., X.-Y. Liu and J.-M. Hu, *Electrodeposited SiO_2 film: a promising interlayer of a highly active Ti electrode for the oxygen evolution reaction.* Journal of Materials Chemistry A, 2016. **4**(30): p. 11949-11956.

218. Xu, H.-B., Y.-H. Lu, C.-H. Li and J.-Z. Hu, *A novel IrO_2 electrode with iridium–titanium oxide interlayers from a mixture of TiN nanoparticle and H_2IrCl_6 solution.* Journal of Applied Electrochemistry, 2010. **40**(4): p. 719-727.

219. Marshall, A. and R. Haverkamp, *Nanoparticles of IrO_2 or Sb–SnO_2 increase the performance of iridium oxide DSA electrodes.* Journal of Materials Science, 2012. **47**(3): p. 1135-1141.

220. Shokouhfar, M. and S.R. Allahkaram, *Effect of incorporation of nanoparticles with different composition on wear and corrosion behavior of ceramic coatings developed on pure titanium by micro arc oxidation.* Surface and Coatings Technology, 2017. **309**: p. 767-778.

221. Baghery, P., M. Farzam, A.B. Mousavi and M. Hosseini, *Ni–TiO_2 nanocomposite coating with high resistance to corrosion and wear.* Surface and Coatings Technology, 2010. **204**(23): p. 3804-3810.

222. Roknian, M., A. Fattah-alhosseini, S.O. Gashti and M.K. Keshavarz, *Study of the effect of ZnO nanoparticles addition to PEO coatings on pure titanium substrate: Microstructural analysis, antibacterial effect and corrosion behavior of coatings*

in Ringer's physiological solution. Journal of Alloys and Compounds, 2018. **740**: p. 330-345.

223. Amadelli, R., L. Samiolo, A.B. Velichenko, V.A. Knysh, T.V. Luk'yanenko, and F.I. Danilov, *Composite PbO_2-TiO_2 materials deposited from colloidal electrolyte: Electrosynthesis, and physicochemical properties.* Electrochimica Acta, 2009. **54**(22): p. 5239-5245.

224. Chen, W.-T., A. Chan, V. Jovic, D. Sun-Waterhouse, K.-i. Murai, H. Idriss, and G.I.N. Waterhouse, *Effect of the TiO_2 Crystallite Size, TiO_2 Polymorph and Test Conditions on the Photo-Oxidation Rate of Aqueous Methylene Blue.* Topics in Catalysis, 2015. **58**(2): p. 85-102.

225. Ohno, T., K. Sarukawa, K. Tokieda and M. Matsumura, *Morphology of a TiO_2 Photocatalyst (Degussa, P-25) Consisting of Anatase and Rutile Crystalline Phases.* Journal of Catalysis, 2001. **203**(1): p. 82-86.

226. Bayer, G. and H.G. Wiedemann, *Formation, dissociation and expansion behavior of platinum group metal oxides (PdO, RuO_2, IrO_2).* Thermochimica Acta, 1975. **11**(1): p. 79-88.

227. Hidnert, P., *Thermal expansion of titanium.* Journal of Research of the National Bureau of Standards, 1943. **30**(2): p. 101-105.

228. Shackelford, J.F., Y.-H. Han, S. Kim and S.-H. Kwon, *CRC Materials Science and Engineering Handbook*. 2016: CRC Press.

229. Kirby, R.K., *Thermal Expansion of Rutile from 100 to 700 °K.* Journal of Research of the National Bureau of Standards, 1967. **71A**(5): p. 363-369.

230. Neralla, S., D. Kumar, S. Yarmolenko and J. Sankar, *Mechanical properties of nanocomposite metal–ceramic thin films.* Composites Part B: Engineering, 2004. **35**(2): p. 157-162.

231. Deegan, R.D., *Pattern formation in drying drops.* Physical Review E, 2000. **61**(1): p. 475-485.

232. Shmuylovich, L., A.Q. Shen and H.A. Stone, *Surface Morphology of Drying Latex Films: Multiple Ring Formation.* Langmuir, 2002. **18**(9): p. 3441-3445.

233. de Oliveira-Sousa, A., M. de Siliva, S. Machado, L. Avaca and P. de Lima-Neto, *Influence of the preparation method on the morphological and electrochemical properties of Ti/IrO_2-coated electrodes.* Electrochim. Acta, 2000. **45**: p. 4467-4473.

234. Kariman, A. and A.T. Marshall, *Investigating the kinetics and mechanism of organic oxidation in parallel with the oxygen evolution reaction.* Electrocatalysis, 2018. **9**: p. 31-39.

235. Ardizzone, S., A. Carugati and S. Trasatti, *Properties of thermally prepared iridium dioxide electrodes.* Journal of Electroanalytical Chemistry, 1981. **126**: p. 287-292.

236. De Pauli, C. and S. Trasatti, *Electrochemical Surafce Characterization of IrO_2 + SnO_2 Mixed Oxide Electrodes.* Journal of Electroanalytical Chemistry, 1995. **396**: p. 161-168.

237. Angelinetta, C., L. Atanasoska, R. Atanasoski and S. Trasatti, *Surface properties of RuO_2 + IrO_2 mixed oxide electrodes.* Journal of Electroanalytical Chemistry, 1986. **214**: p. 535-546.

238. Ardizzone, S., G. Fregonara and S. Trasatti, *"Inner" and "Outer"' Active Surface of RuO_2 Electrodes.* Electrochimica Acta, 1990. **35**: p. 263-267.

239. Da Silva, L.M., L.A. De Faria and J.F.C. Boodts, *Determination of the morphology factor of oxide layers.* Electrochimica Acta, 2001. **47**(3): p. 395-403.

240. Wan, J., W. Chen, C. Chen, Q. Peng, D. Wang, and Y. Li, *Facile synthesis of CoNix nanoparticles embedded in nitrogen–carbon frameworks for highly efficient electrocatalytic oxygen evolution.* Chemical Communications, 2017. **53**(90): p. 12177-12180.

241. Endo, K., Y. Katayama, T. Miura and T. Kishi, *Composition dependence of the oxygen-evolution reaction rate on $Ir_xTi_{1-x}O_2$ mixed-oxide electrodes.* Journal of Applied Electrochemistry, 2002. **32**: p. 173-178.

242. Hu, J.-M., J.-Q. Zhang and C.-N. Cao, *Oxygen evolution reaction on IrO_2-based DSA® type electrodes: kinetics analysis of Tafel lines and EIS.* International Journal of Hydrogen Energy, 2004. **29**(8): p. 791-797.

243. De Pauli, C. and S. Trasatti, *Composite materials for electrocatalysis of O_2 evolution: IrO_2 + SnO_2 in acid solution.* Journal of Electroanalytical Chemistry, 2002. **538-539**: p. 145-151.

244. Marshall, A.T. and R.G. Haverkamp, *Electrocatalytic activity of IrO_2-RuO_2 supported on Sb-doped SnO_2 nanoparticles.* Electrochimica Acta, 2010. **55**(6): p. 1978-1984.

245. Bernt, M., A. Siebel and H.A. Gasteiger, *Analysis of Voltage Losses in PEM Water Electrolyzers with Low Platinum Group Metal Loadings.* Journal of The Electrochemical Society, 2018. **165**(5): p. F305-F314.

246. Trasatti, S. and G. Lodi, Properties of conductive transition metal oxides with rutile-type structure. *Electrodes of conductive metallic oxides Part A, Elsevier Scientific Publishing Company* (1980): 301-358.

247. Xu, L.K. and J.D. Scantlebury, *A study on the deactivation of an IrO_2–Ta_2O_5 coated titanium anode.* Corrosion Science, 2003. **45**(12): p. 2729-2740.

248. Panić, V., A. Dekanski, V.B. Mišković-Stanković, S. Milonjić and B. Nikolić, *On the deactivation mechanism of RuO_2–TiO_2/Ti anodes prepared by the sol–gel procedure.* Journal of Electroanalytical Chemistry, 2005. **579**(1): p. 67-76.

249. Hoseinieh, S., F. Ashrafizadeh and M. Maddahi, *A comparative investigation of the corrosion behavior of RuO_2–IrO_2–TiO_2 coated titanium anodes in chloride solutions.* Journal of the Electrochemical Society, 2010. **157**(4): p. E50-E56.

250. Kötz, R. and S. Stucki, *Stabilization of RuO_2 by IrO_2 for anodic oxygen evolution in acid media.* Electrochimica Acta, 1986. **31**: p. 1311-1316.

251. Shao, D., X. Li, H. Xu and W.J.R.A. Yan, *An improved stable Ti/Sb–SnO_2 electrode with high performance in electrochemical oxidation processes. RSC advances*, 2014. **4**(41): p. 21230-21237.

252. Amor, C., L. Marchão, M.S. Lucas and J.A. Peres, *Application of Advanced Oxidation Processes for the Treatment of Recalcitrant Agro-Industrial Wastewater: A Review.* Water Research, 2019. **11**(2): p. 205.

253. Parsons, S., *Advanced oxidation processes for water and wastewater treatment*. 2004: IWA publishing.

254. Wang, J.L. and L.J. Xu, *Advanced oxidation processes for wastewater treatment: formation of hydroxyl radical and application.* Critical Reviews in Environmental Science and Technology, 2012. **42**(3): p. 251-325.

255. Oturan, M.A. and J.-J. Aaron, *Advanced oxidation processes in water/wastewater treatment: principles and applications. A review.* Critical Reviews in Environmental Science Technology, 2014. **44**(23): p. 2577-2641.

256. Cañizares, P., M. Díaz, J.A. Domínguez, J. Lobato and M.A. Rodrigo, *Electrochemical treatment of diluted cyanide aqueous wastes.* Journal of Chemical Technology Biotechnology: International Research in Process, Environmental Clean Technology, 2005. **80**(5): p. 565-573.

257. Sirés, I., E. Brillas, M.A. Oturan, M.A. Rodrigo and M. Panizza, *Electrochemical advanced oxidation processes: today and tomorrow. A review.* Environmental Science and Pollution Research, 2014. **21**(14): p. 8336-8367.

258. Comninellis, C. and A. De Battisti, *Electrocatalysis in anodic oxidation of organics with simultaneous oxygen evolution.* Applied Catalysis B: Environmental, 1996. **93**: p. 673-679.

259. Montilla, F., E. Morallon and J. Vázquez, *Evaluation of the electrocatalytic activity of antimony-doped tin dioxide anodes toward the oxidation of phenol in aqueous solutions.* Journal of the Electrochemical Society, 2005. **152**(10): p. B421-B427.

260. Anglada, A., A. Urtiaga and I. Ortiz, *Contributions of electrochemical oxidation to waste-water treatment: fundamentals and review of applications.* Journal of Chemical Technology Biotechnology, 2009. **84**(12): p. 1747-1755.

261. Marshall, A.T. and A. Herritsch, *Understanding how the oxygen evolution reaction kinetics influences electrochemical wastewater oxidation.* Electrochimica Acta, 2018. **282**: p. 448-458.

262. Fugivara, C.S., P. Sumodjo, A.A. Cardoso and A.V. Benedetti, *Electrochemical decomposition of cyanides on tin dioxide electrodes in alkaline media.* Analyst, 1996. **121**(4): p. 541-545.

263. Panizza, M., P. Michaud, G. Cerisola and C. Comninellis, *Anodic oxidation of 2-naphthol at boron-doped diamond electrodes.* Journal of Electroanalytical Chemistry, 2001. **507**(1): p. 206-214.

264. Rodrigo, M., P. Michaud, I. Duo, M. Panizza, G. Cerisola, and C. Comninellis, *Oxidation of 4-chlorophenol at boron-doped diamond electrode for wastewater treatment.* Journal of the Electrochemical Society, 2001. **148**(5): p. D60-D64.

265. Kapałka, A., G. Fóti and C. Comninellis, *Basic principles of the electrochemical mineralization of organic pollutants for wastewater treatment*, in *Electrochemistry for the Environment*. 2010, Springer. p. 1-23.

266. Kapałka, A., G. Fóti and C. Comninellis, *The importance of electrode material in environmental electrochemistry: formation and reactivity of free hydroxyl radicals on boron-doped diamond electrodes.* Electrochimica Acta, 2009. **54**(7): p. 2018-2023.

267. Cañizares, P., J. García-Gómez, C. Sáez and M.A. Rodrigo, *Electrochemical oxidation of several chlorophenols on diamond electrodes Part I. Reaction mechanism.* Journal of Applied Electrochemistry, 2003. **33**(10): p. 917-927.

268. Correa-Lozano, B., C. Comninellis and A. De Battisti, *Service life of Ti/SnO_2–Sb_2O_5 anodes.* Journal of Applied Electrochemistry, 1997. **27**(8): p. 970-974.

269. Takasu, Y. and Y. Murakami, *Design of oxide electrodes with large surface area.* Electrochimica acta, 2000. **45**(25-26): p. 4135-4141.

270. Marshall, A.T. and R.G. Haverkamp, *Nanoparticles of IrO_2 or Sb–SnO_2 increase the performance of iridium oxide DSA electrodes.* Journal of Materials Science, 2012. **47**(3): p. 1135-1141.

271. Yi, Z., C. Kangning, W. Wei, J. Wang and S. Lee, *Effect of IrO_2 loading on RuO_2–IrO_2–TiO_2 anodes: A study of microstructure and working life for the chlorine evolution reaction.* Ceramics International, 2007. **33**(6): p. 1087-1091.

272. Zhou, X.-L., Z.-G. Ye, X.-Z. Hua, A.-H. Zou and Y.-H. Dong, *Electrocatalytic activity and stability of Ti/IrO_2 + MnO_2 anode in 0.5 M NaCl solution.* Journal of Solid State Electrochemistry, 2010. **14**(7): p. 1213-1219.

273. Mousty, C., G. Fóti, C. Comninellis and V. Reid, *Electrochemical behaviour of DSA type electrodes prepared by induction heating.* Electrochimica Acta, 1999. **45**(3): p. 451-456.

274. Montilla, F., E. Morallón, A. De Battisti and J.L. Vázquez, *Preparation and Characterization of Antimony-Doped Tin Dioxide Electrodes. Part 1. Electrochemical Characterization.* The Journal of Physical Chemistry B, 2004. **108**(16): p. 5036-5043.

275. Shieh, D.T. and B.J. Hwang, *Oxygen evolution on PTFE-modified ruthenium oxide electrodes investigated by CV techniques.* Journal of Electroanalytical Chemistry, 1995. **391**(1): p. 77-91.

276. De Pauli, C.P. and S. Trasatti, *Electrochemical surface characterization of IrO_2 + SnO_2 mixed oxide electrocatalysts.* Journal of Electroanalytical Chemistry, 1995. **396**(1): p. 161-168.

277. Ren, Z., S. Quan, J. Gao, W. Li, Y. Zhu, Y. Liu, B. Chai, and Y. Wang, *The electrocatalytic activity of IrO_2–Ta_2O_5 anode materials and electrolyzed oxidizing water preparation and sterilization effect.* RSC Advances, 2015. **5**(12): p. 8778-8786.

278. Borm, P.J., D. Robbins, S. Haubold, T. Kuhlbusch, H. Fissan, K. Donaldson, R. Schins, V. Stone, W. Kreyling, and J. Lademann, *The potential risks of nanomaterials: a review carried out for ECETOC.* Particle Fibre Toxicology, 2006. **3**(1): p. 11.

279. Bantz, C., O. Koshkina, T. Lang, H.-J. Galla, C.J. Kirkpatrick, R.H. Stauber, and M. Maskos, *The surface properties of nanoparticles determine the agglomeration*

state and the size of the particles under physiological conditions. Beilstein journal of nanotechnology, 2014. **5**: p. 1774.

280. Kariman, A. and A.T. Marshall, *Improving the Stability of DSA Electrodes by the Addition of TiO_2 Nanoparticles.* Journal of The Electrochemical Society, 2019. **166**(8): p. E248-E251.

281. de Oliveira-Sousa, A., M.A.S. da Silva, S.A.S. Machado, L.A. Avaca and P. de Lima-Neto, *Influence of the preparation method on the morphological and electrochemical properties of Ti/IrO_2-coated electrodes.* Electrochimica Acta, 2000. **45**(27): p. 4467-4473.

282. Kariman, A. and A.T. Marshall, *Investigating the Kinetics and Mechanism of Organic Oxidation in Parallel with the Oxygen Evolution Reaction.* Electrocatalysis, 2017. **9**(1): p. 31-39.

283. Fierro, S., L. Ouattara, E.H. Calderon, E. Passas-Lagos, H. Baltruschat, and C. Comninellis, *Investigation of formic acid oxidation on Ti/IrO_2 electrodes.* Electrochimica Acta, 2009. **54**(7): p. 2053-2061.

284. Birss, V.I., C. Bock and H. Elzanowska, *Hydrous Ir oxide films: the mechanism of the anodic prepeak reaction.* Canadian journal of chemistry, 1997. **75**(11): p. 1687-1693.

285. Felix, C., T. Maiyalagan, S. Pasupathi, B.J. Bladergroen and V. Linkov, *Synthesis, characterisation and evaluation of IrO_2 based binary metal oxide electrocatalysts for oxygen evolution reaction. International. Journal of Electrochemmical Science, 7(2012)12064 -12077.*

286. Alves, P.D., M. Spagnol, G. Tremiliosi-Filho and A.R.d. Andrade, *Investigation of the influence of the anode composition of DSA-type electrodes on the electrocatalytic oxidation of phenol in neutral medium.* Journal of the Brazilian Chemical Society, 2004. **15**(5): p. 525-533.

287. Wu, L.-K., X.-Y. Liu and J.-M. Hu, *Electrodeposited SiO_2 film: a promising interlayer of a highly active Ti electrode for the oxygen evolution reaction.* Journal of Materials Chemistry A, 2016. **4**(30): p. 11949-11956.

288. Wen, T.C. and C.C. Hu, *Hydrogen and Oxygen Evolutions on Ru-Ir Binary Oxides.* Journal of the Electrochemical Society, 1992. **139**(8): p. 2158-2163.

289. Berenguer, R., C. Quijada and E. Morallon, *Electrochemical characterization of SnO_2 electrodes doped with Ru and Pt.* Electrochimica Acta, 2009. **54**(22): p. 5230-5238.

290. Ardizzone, S., G. Fregonara and S. Trasatti, *"Inner" and "outer" active surface of RuO2 electrodes.* Electrochimica Acta, 1990. **35**(1): p. 263-267.

291. Arora, P.K. and R.K. Jain, *Metabolism of 2-chloro-4-nitrophenol in a Gram negative bacterium, Burkholderia sp. RKJ 800.* PloS one, 2012. **7**(6): p. e38676.

292. Zanta, C.L., P.-A. Michaud, C. Comninellis, A.R. De Andrade and J.F. Boodts, *Electrochemical oxidation of p-chlorophenol on SnO_2–Sb_2O_5 based anodes for wastewater treatment.* Journal of Applied Electrochemistry, 2003. **33**(12): p. 1211-1215.

293. Comninellis, C., A. Kapalka, S. Malato, S.A. Parsons, I. Poulios, and D. Mantzavinos, *Advanced oxidation processes for water treatment: advances and*

trends for R&D. Journal of Chemical Technology Biotechnology, 2008. **83**(6): p. 769-776.

294. Oturan, M.A. and J.-J. Aaron, *Advanced oxidation processes in water/wastewater treatment: principles and applications. A review.* Critical Reviews in Environmental Science Technology, 2014. **44**(23): p. 2577-2641.

295. Murphy, O.J., G.D. Hitchens, L. Kaba and C.E. Verostko, *Direct electrochemical oxidation of organics for wastewater treatment.* Water Research, 1992. **26**(4): p. 443-451.

296. Polcaro, A., A. Vacca and S. Palmas, *Electrochemical treatment of wastewater containing phenolic compounds: oxidation at boron-doped diamond electrodes.* Journal of Applied Electrochemistry, 2003. **33**(10): p. 885-892.

297. Panizza, M. and G. Cerisola, *Electrochemical oxidation of 2-naphthol with in situ electrogenerated active chlorine.* Electrochimica Acta, 2003. **48**(11): p. 1515-1519.

298. Kötz, R., S. Stucki and B. Carcer, *Electrochemical waste water treatment using high overvoltage anodes. Part I: Physical and electrochemical properties of SnO_2 anodes.* Journal of Applied Electrochemistry, 1991. **21**(1): p. 14-20.

299. Rajurkar, K.P., J. Kozak, B. Wei and J. McGeough, *Study of pulse electrochemical machining characteristics.* CIRP annals, 1993. **42**(1): p. 231-234.

300. Chandrasekar, M. and M. Pushpavanam, *Pulse and pulse reverse plating—Conceptual, advantages and applications.* Electrochimica Acta, 2008. **53**(8): p. 3313-3322.

301. Khosla, N., S. Venkatachalam and P. Somasundaran, *Pulsed electrogeneration of bubbles for electroflotation.* Journal of Applied Electrochemistry, 1991. **21**(11): p. 986-990.

302. Monk, N. and S. Watson, *Review of pulsed power for efficient hydrogen production.* International Journal of Hydrogen Energy, 2016. **41**(19): p. 7782-7791.

303. Demir, N., M.F. Kaya and M.S. Albawabiji, *Effect of pulse potential on alkaline water electrolysis performance.* International Journal of Hydrogen Energy, 2018. **43**(36): p. 17013-17020.

304. Iniesta, J., P. Michaud, M. Panizza, G. Cerisola, A. Aldaz, and C. Comninellis, *Electrochemical oxidation of phenol at boron-doped diamond electrode.* Electrochimica Acta, 2001. **46**(23): p. 3573-3578.

305. Alfaro, M.A.Q., S. Ferro, C.A. Martínez-Huitle and Y.M. Vong, *Boron doped diamond electrode for the wastewater treatment.* Journal of the Brazilian Chemical Society, 2006. **17**(2): p. 227-236.

306. García-Osorio, D., R. Jaimes, J. Vazquez-Arenas, R. Lara and J. Alvarez-Ramirez, *The kinetic parameters of the oxygen evolution reaction (OER) calculated on inactive anodes via EIS transfer functions:•OH formation.* Journal of The Electrochemical Society, 2017. **164**(11): p. E3321-E3328.

307. Cañizares, P., J. García-Gómez, J. Lobato and M.A. Rodrigo, *Modeling of wastewater electro-oxidation processes part I. General description and application to inactive electrodes.* Industrial Engineering Chemistry Research, 2004. **43**(9): p. 1915-1922.

308. Panizza, M., A. Kapalka and C. Comninellis, *Oxidation of organic pollutants on BDD anodes using modulated current electrolysis.* Electrochimica Acta, 2008. **53**(5): p. 2289-2295.

309. Kapałka, A., G. Fóti and C. Comninellis, *Kinetic modelling of the electrochemical mineralization of organic pollutants for wastewater treatment.* Journal of Applied Electrochemistry, 2008. **38**(1): p. 7-16.

310. Spasojević, M., N. Krstajić, P. Spasojević and L. Ribić-Zelenović, *Modelling current efficiency in an electrochemical hypochlorite reactor.* Chemical Engineering Research and Design, 2015. **93**: p. 591-601.

311. García-Osorio, D., R. Jaimes, J. Vazquez-Arenas, R. Lara and J. Alvarez-Ramirez, *The kinetic parameters of the oxygen evolution reaction (OER) calculated on inactive anodes via EIS transfer functions:•OH formation.* Journal of The Electrochemical Society, 2017. **164**(11): p. E3321-E3328.

312. Wüthrich, R. and J.D. Abou Ziki, *Preface*, in *Micromachining Using Electrochemical Discharge Phenomenon (Second Edition)*, William Andrew Publishing: Boston. 2015,. p. ix-x.

313. Gileadi, E., *Problems in interfacial electrochemistry that have been swept under the carpet.* Journal of Solid State Electrochemistry, 2011. **15**(7-8): p. 1359.

314. Niesner, R. and A. Heintz, *Diffusion coefficients of aromatics in aqueous solution.* Journal of Chemical & Engineering Data, 2000. **45**(6): p. 1121-1124.

315. Lan, Y., C. Coetsier, C. Causserand and K.G. Serrano, *An experimental and modelling study of the electrochemical oxidation of pharmaceuticals using a*

boron-doped diamond anode. Chemical Engineering Journal, 2018. **333**: p. 486-494.

316. Körbahti, B.K. and P. Demirbüken, *Electrochemical oxidation of resorcinol in aqueous medium using boron-doped diamond anode: Reaction kinetics and process optimization with response surface methodology.* Frontiers in chemistry, 2017. **5**: p. 75.

317. Ibl, N., *Some theoretical aspects of pulse electrolysis.* Surface Technology, 1980. **10**(2): p. 81-104.

318. Li, T., T. Kasahara, J. He, K.E. Dettelbach, G.M. Sammis, and C.P. Berlinguette, *Photoelectrochemical oxidation of organic substrates in organic media.* Nature Communications, 2017. **8**(1): p. 390.